Review

The Future of Bone Prosthetic Design: A Comparative Analysis of Materials for Smart Integration in Implants and Grafts

David J. Herzog , Nitsa J. Herzog * , Alexander Zhak

Posted Date: 11 May 2026

doi: 10.20944/preprints202605.0674.v1

Keywords: smart prosthetics; bone graft; bone implant; bioceramics; bioglass; sensors; smart materials; composites; biocompatibility; signal processing

 doi:10.20944/preprints202605.0674.v1

Review

The Future of Bone Prosthetic Design: A Comparative Analysis of Materials for Smart Integration in Implants and Grafts

David J. Herzog [1], Nitsa J. Herzog [2],* and Alexander Zhak [3]

[1] Ulster University
[2] Northumbria University
[3] Independent Researcher
* Correspondence: nitsa.herzog@northumbria.ac.uk

Abstract

This paper presents a comprehensive comparative analysis of recent advances in smart bone prosthetics. The emphasis is made on the integration of embedded sensors, adaptive control systems, and wireless monitoring into metallic, carbon-based and bioceramic materials. The evaluation of essential characteristics of mechanical strength, durability, and biocompatibility is combined with its integration of smart functionality. The key mechanical properties, such as tensile strength, Young's modulus, and fatigue life, are reviewed to assess how each material supports long-term prosthetic performance. Concurrently, biocompatibility factors, tissue integration and inflammatory response are examined to ensure safe and effective clinical application. The integrative approach can help clinicians and biomedical engineers to fine-tune the selection of the optimal material-smart system and provide individually tailored combinations to specific patient needs and surgical-operative contexts.

Keywords: smart prosthetics; bone graft; bone implant; bioceramics; bioglass; sensors; smart materials; composites; biocompatibility; signal processing

1. Introduction

1.1. Contextual Background

Orthopedic and bone prosthetics have been documented since antiquity. It has significantly evolved over the past few decades. Industry 4.0 is described as "physical, digital and biological convergence" [1] . In bone prosthetics and osseous implants, this is reflected in the introduction of new materials with specific properties and in digitalization. Historically, materials used for prosthetics were mostly metals, wood, and leather, with little attention to biocompatibility, durability or wear resistance. The introduction of lightweight metals such as titanium in the mid-20th century, bioceramics [2], and carbon fiber composites [3] offered bone prosthetics with higher strength-to-weight ratios. AI-enabled design opens up possibilities for the complex integration of other elements, such as sensors and actuators [4]. Advancements in prosthetic sensing capabilities added a dynamic informational dimension. Modern bone prosthetics and osseous implants can incorporate a variety of embedded sensors that measure force, motion, position, chemical properties, and electromyographic signals, enabling real-time monitoring and adaptive control [5]. Smart materials with sensor-like properties, such as piezoelectric polymers, shape-memory alloys [6], and carbon nanotube- or polymer-based composites with unique properties [7], can also be incorporated. Active responses to environmental stimuli like pressure, temperature, or electrical signals enable nuanced follow-up and necessary intervention. Continuous flow of data from sensors can be analyzed by AI applications for adaptation, personalization and optimization of prosthetic function, often in real

 doi:10.20944/preprints202605.0674.v1

time. Reinforcement learning techniques allow smart prosthetic devices to self-improve, enhance mobility and improve user experience. AI and ML tools are also actively used for material and structural design, including 4D printing [8], and sensor data is important in this context.

1.2. Problem Statement

Research into bone prostheses and osseous implants has achieved considerable advances in the development of metallic, carbon-based and bioceramic materials. Significant improvements have been made in prosthetics, mechanical properties and clinical performance. Metallic alloys, such as titanium, cobalt-chromium, and zirconium, offer exceptional strength and durability compared to stainless steel, making them appropriate for high-load applications, while magnesium and zinc alloys are suitable for biodegradable applications [9]. Carbon-based composites, such as carbon fiber-reinforced polymers, provide lightweight alternatives that enhance patient mobility [10]. Bioceramic prosthetics show unique strength, high biocompatibility and osseointegration [11]. A significant number of studies also reported on bioglass biocompatibility and clinical outcomes [12]. Metallic alloys, bioceramics, bioglasses and carbon-based composites exhibit exceptional mechanical strength, durability, and weight efficiency. However, their distinct contributions and limitations within the rapidly evolving domain of smart prosthetic systems remain only partially elucidated, with nuanced interactions yet to be fully explored [13].

However, integrating new materials into smart prosthetic systems, incorporating advanced features such as embedded sensors, adaptive actuators, and real-time biomechanical feedback loops, introduces complex challenges that must be fully addressed. A comprehensive comparative analysis integrating materials science, smart functionality, and clinical applicability is essential for further development of bone prosthetics and osseous implants. This nuanced approach has to elucidate the trade-offs among metallic alloys, bioceramics, and carbon-based composites.

1.3. Comprehensive Review Aims

This review seeks to:

1. Analyze and align data on material properties of metallic alloys, bioceramics, and carbon-based composites in smart orthopedic prosthetics. Comparative evaluation includes key characteristics such as tensile strength, Young's modulus, fatigue life, density, and corrosion resistance.
2. Analyze the application of these materials in smart prosthetic designs for osseous implants and bone prosthetics, to assess their impact on functional performance. The focus is on integrating advanced functionalities: real-time biomechanical feedback, adaptive joint control, and sensor systems.
3. Evaluate the biocompatibility of these materials within intelligent prosthetic systems: aseptic inflammatory responses, immune and other potential adverse reactions.
4. Identify and compare the clinical contexts in which metallic alloys, bioceramics, and carbon-based composites are most effective in smart prosthetics. Patient-specific factors such as activity level, body weight, anatomical requirements, and lifestyle are considered to guide the development of potential personalized prosthetic solutions.
5. Identify possible gaps in the current state of intelligent prosthetic systems and propose directions for future studies to enhance the functionality and patient-centered outcomes.

2. Biological and Mechanical Properties of the Bone

Bone, an organ composed of specialized tissues, is a load-bearing and protective structure. It supports body or body-part weight, facilitates movements and shields vital organs from potential mechanical damage. Bone, as an organ and tissue, also participates in calcium and phosphate metabolism and serves as a hematopoietic structure. It actively interacts with the immune system through cytokines. Interleukin-6 (IL-6) and Tumor Necrosis Factor alpha (TNF-α) regulate

 doi:10.20944/preprints202605.0674.v1

inflammatory processes and bone remodeling. Both are produced by osteoblasts and other cell types [14].

2.1. Biological Structure and Function

Bone is primarily a composite tissue. It consists of an osteoid, a mineralized extracellular matrix, and an interspersed cellular network. The extracellular matrix is composed primarily of collagen type I (30%) and hydroxyapatite crystals (60%) [15]. Bone provides mechanical strength against applied forces and resistance to elastic deformation, while preserving functional geometry and architectural integrity.

Bone matrix is produced and remodeled by cells differentiated from Mesenchymal Stem Cells (MSCs) [16]. Osteoblasts are lineage-committed, pre-terminally differentiated cells responsible for the synthesis of type I collagen and the deposition of hydroxyapatite crystals. Osteocytes are terminally differentiated cells responsible for bone remodeling through mechanosensory functions and paracrine signaling. Osteoclasts are multinucleated resorptive cells that degrade bone matrix via their acidification and proteolysis [17]. Bone morphology and microarchitecture are determined by the dynamics of osteoblast-osteoclast coupling coordinated by osteocytes. Repair is initiated by the initial inflammatory response, soft callus formation, and finalizes with hard callus mineralization. Bone is immunologically active. IL-6 and TNF-α link immune signals to bone resorption via the Receptor Activator of Nuclear Factor kappa-B Ligand (RANK/RANKL/NF-κB) pathway [18].

Dense cortical bone tissue is organized into osteons. A central Haversian canal of the osteon is surrounded by concentric matrix lamellae with embedded cellular lacunae. Haversian canal houses blood vessels and nerves. They are connected to traverse Volkmann's canals and smaller canaliculi. Interstitial lamellae occupy spaces between osteons. The bone tissue is extensively vascularized. Blood vessels penetrate the cortical bone through canals and trabecular bone via marrow spaces. [19,20]. Figure 1 presents the structure of the bone.

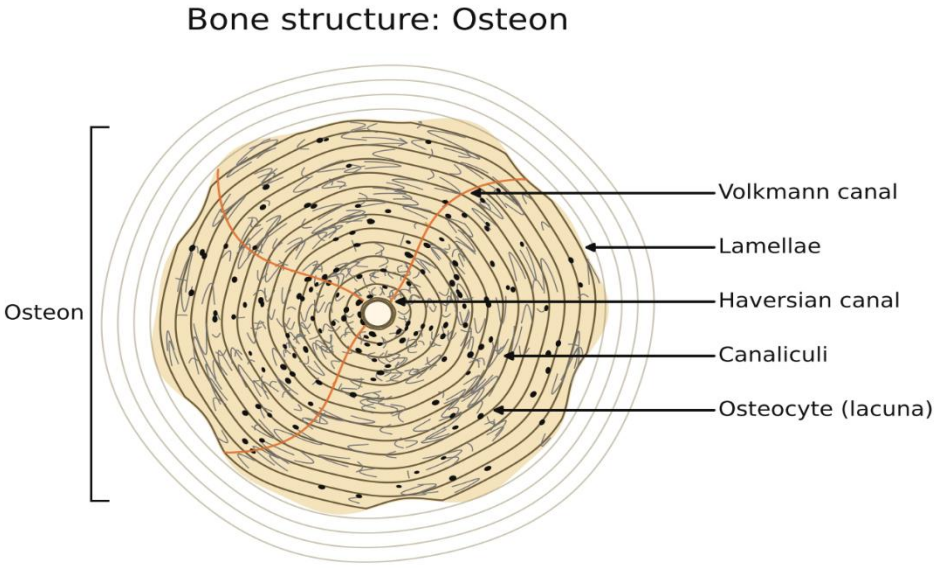

Figure 1. Bone microstructure: Osteon (created by authors).

2.2. Bone Development as Tissue and Organ

The bone morphology at the macroscopic level is determined by a combination of developmental, genetic, and functional factors (Figure 2). Homeobox (HOX) genes encode transcription factors that guide embryonic patterning and skeletal development [21]. They establish patterns and assign positional identity of bones along the anterior–posterior body axis. Bone Morphogenetic Protein Growth Factors (BMP GFs) induce osteoblast differentiation and consequent

 doi:10.20944/preprints202605.0674.v1

bone matrix formation with a certain shape and density [22]. Fibroblast Growth Factors (FGFs) stimulate cell proliferation and differentiation in specific bone-forming regions. The activity is reflected in cortical thickness and growth plate activity. Wnt/β-catenin regulates gene expression, responsible for the trabecular orientation and overall bone geometry [23]. Postnatal adaptation is done by mechanotransduction. Osteocytes sense strain and refine the macro shape to optimize load distribution and functional performance in accordance with Wolff's law.

Long bone (e.g., femur, humerus) ossification geometry is acquired through endochondral ossification [24]. Chondroblasts create a cartilage template with excretion of type II collagen and proteoglycans. Chondroblasts then mature into chondrocytes, proliferate, become hypertrophic, calcify extracellular matrix and undergo apoptosis. Subsequent vascularization brings MSC osteoprogenitors from bone marrow or periosteum. MSCs differentiate into osteoblasts, which produce bone matrix and induce mineralization [25]. In endochondral ossification cartilage is progressively replaced by mineralized bone along a prepatterned growth axis. In this process length, curvature, and diaphyseal–epiphyseal proportions of the bone are established. Flat bones (e.g., cranial vault, sternum) are produced through intramembranous ossification [24]. Bone is directly generated from MSCs.

In the postnatal period, during childhood and adolescence, long bones grow from the physis, or the cartilage epiphyseal plate, located between the metaphysis (shaft) and epiphysis [25]. During this period, new cartilage is produced on the epiphyseal side. Then it undergoes endochondral ossification on the metaphyseal side. In adulthood, the ossified epiphyseal line remains as a remnant.

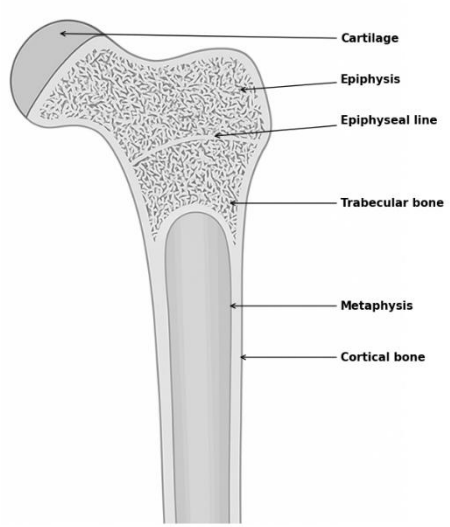

Figure 2. Femoral bone macrostructure: Epiphysis and upper part of diaphysis (created by authors).

2.3. Biophysical Structure and Function

The bone morphology at the macroscopic level is determined by a combination of developmental, genetic, and functional factors (Figure 2). Homeobox (HOX) genes encode.

Table 1. Hierarchical scales of bone organization.

Scale	Cortical Bone	Trabecular Bone	Cartilage
Molecular (0.1–2 nm)	Protein–mineral interactions; collagen–hydroxyapatite composite	Collagen–hydroxyapatite composite, but less dense	Collagen–proteoglycan interactions, highly hydrated glycosaminoglycan matrix

 doi:10.20944/preprints202605.0674.v1

Nanoscale (2–200 nm)	Collagen type I fibrils reinforced with hydroxyapatite crystals	Collagen type I fibrils with hydroxyapatite, lower mineral density	Collagen type II fibrils; generally non-mineralized (except calcified zones).
Sub-micro (0.2–10 μm)	Lamellar collagen fibril orientation alternating between layers	Lamellar or woven arrangement in trabecular rods and plates	Dense collagen II fibril mesh with proteoglycan aggregates
Micro-scale (10–500 μm)	Osteons (Haversian systems), concentric lamellae	Trabeculae (rod- and plate-like struts) aligned to mechanical loading	Chondrocytes in lacunae are dispersed in the extracellular matrix
Macro-scale (mm–cm)	Dense outer shell; defines bone shape, stiffness, and main load-bearing capacity	Porous lattice; contributes to lightness, shock absorption, and adaptive remodeling	Smooth articular surfaces; flexible support and shock absorption in joints

Cortical or compact bone forms the dense outer layer. It provides necessary mechanical rigidity, compressive strength, and resistance to bending and torsion. Cortical bone comprises approximately 80% of total skeletal mass. It is mainly responsible for primary load-bearing capacity [26]. Trabecular, cancellous (spongy) bone has a porous, three-dimensional lattice structure. It reduces bone weight and provides shock absorption through optimized energy dissipation. Porous structure facilitates metabolic exchange. Trabecular bones have a higher surface area-to-volume ratio. It facilitates enhanced bone remodeling rate, efficient oxygen and nutrient transport, and robust hematopoietic activity [27].

The extracellular matrix is composed of collagen type I (30%) and hydroxyapatite crystals (60%). The volume fraction of the mineral phase is 33-43% due to its compactness (Figure 3a).

The Voigt bound for the cortical bond assumes uniform strain across phases, yielding an upper bound on stiffness. V_i reflects a volume fraction of phase i, E_i is the elastic modulus of phase i, and N is the total number of phases:

$$E_V = \sum_{i=1}^{N} V_i E_i \quad (1)$$

The Reuss bound assumes uniform stress across phases and provides a lower bound for stiffness, where V_i/E_i is the compliance contribution:

$$E_R = 1/(\sum_{i=1}^{N} (V_i / E_i)) \quad (2)$$

Hill's average is a simple form:

$$E_H = \frac{E_V + E_R}{2} \quad (3)$$

The mechanical behavior of cellular solids, such as trabecular bone, is better described by the Gibson–Ashby power-law model (Figure 3b).

Extending this two-framework analysis to all five bone classifications reveals a broader principle governing skeletal mechanical behavior (Figure 4). Sometimes bones are classified according to shape and length. However, Figure 4 shows that bones are mostly cortical or trabecular.

 doi:10.20944/preprints202605.0674.v1

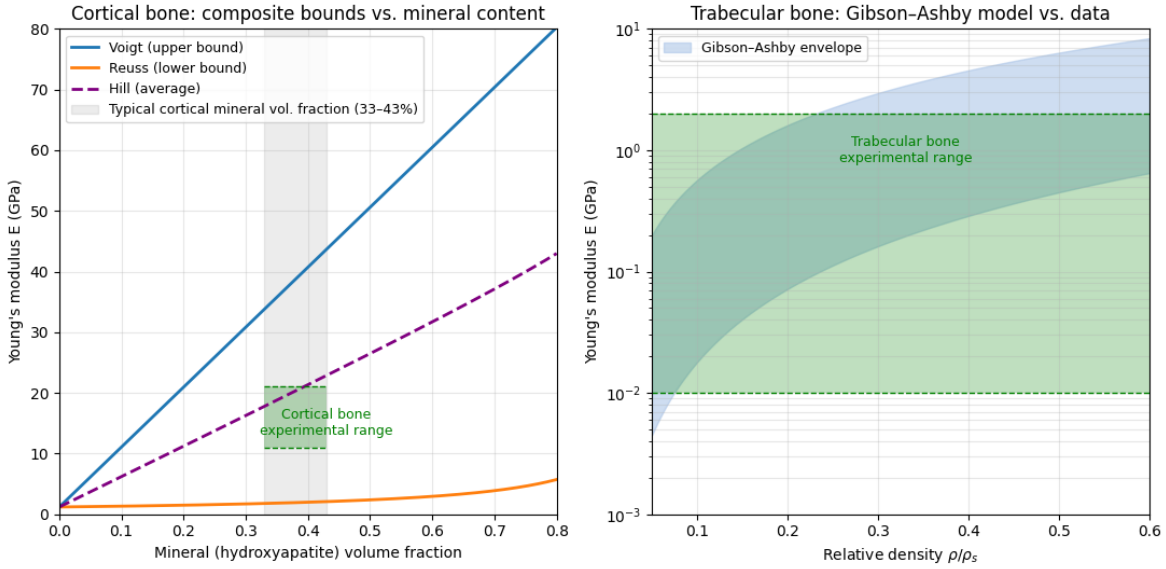

(**a**) (**b**)

Figure 3. Micromechanical modelling of cortical and trabecular bone stiffness. (**a)** Voigt (upper) and Reuss (lower) bounds for cortical bone Young's modulus as a function of hydroxyapatite volume fraction, with the Hill average as an intermediate estimate. The shaded region indicates the physiological mineral fraction (33–43%), within which predicted moduli correspond to reported cortical stiffness values (15–25 GPa). (**b)** Gibson–Ashby model predictions for trabecular bone Young's modulus versus relative density (ϱ/ϱ_s), shown alongside the experimental range. The model envelope captures the observed stiffness variation, underscoring relative density as the primary determinant of trabecular mechanical behavior.

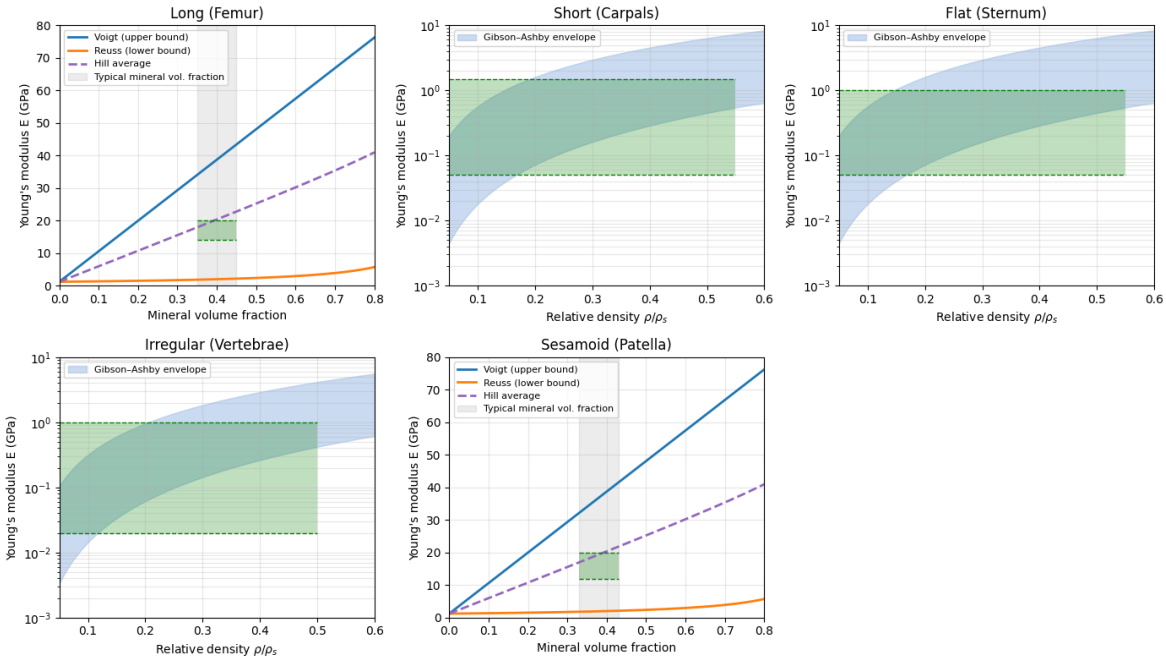

Figure 4. Young's modulus predictions across five bone classifications using two micromechanical models. Long and sesamoid bones (femur, patella) are evaluated using Voigt–Reuss bounds as a function of mineral volume fraction, whereas short, flat, and irregular bones (carpals, sternum, vertebrae) are modelled using the Gibson–Ashby framework as a function of relative density (ϱ/ϱ_s). In all categories, predicted moduli fall within experimentally reported ranges, indicating that microstructural composition, rather than anatomical form, primarily governs skeletal stiffness.

 doi:10.20944/preprints202605.0674.v1

The mechanical behavior of bone exhibits significant variation between its cortical and trabecular compartments, reflecting their specialized structural and functional roles (Table 2).

Cortical bone, constituting the dense outer layer, demonstrates remarkable compressive strength, ranging from 75.9 to 136.6 MPa [28] and tensile strength from roughly 100 to 150 MPa [29]. Young's modulus, $E=\sigma/\varepsilon$, is approximately 15 to 20 GPa [30]. The ratio of stress $\sigma=F/A$ measured in Pascals, where F is the applied force, and A is the cross-sectional area, to strain $\varepsilon=\Delta L/L0$, where ΔL is the length change, and L0 is the original length.

Table 2. Key mechanical properties of bone and cartilage tissue.

Property	Cortical Bone	Trabecular Bone	Cartilage
Tensile Strength	100–150 MPa	2–12 MPa	10–25 MPa (depends on type and hydration level)
Young's Modulus	15–20 GPa	0.1–2 GPa	0.5–1 MPa
Fracture Toughness	2–7 MPa·m$^{1/2}$; enhanced by collagen	0.5–3 MPa·m$^{1/2}$, depends on density and trabecular orientation.	Very low, easily deformed
Fatigue Life	Withstands cyclic loading; microdamage accumulates under repeated stress	Shorter fatigue life; microdamage accumulates faster	Not applicable; viscoelastic damping absorbs energy

Cortical bone tissue has the capacity to withstand deformation under substantial mechanical loads [28]. In contrast, trabecular bone tissue is characterized by its porous, lattice-like architecture. It exhibits considerably lower tensile strength of 2–12 MPa, but can be up to 30 MPa and a Young's modulus as low as 0.1–2 GPa, but can be up to 8.8 GPa [30]. It is an effective shock absorber. Cartilage, a compliant and viscoelastic tissue, possesses an intermediate tensile strength of 10–25 MPa, depending on hydration levels, and a markedly lower Young's modulus of 0.5–1 MPa [31,32]. Collagen and HA fractions create a clear correlation with cortical and transverse Young`s modulus (Figure 5).

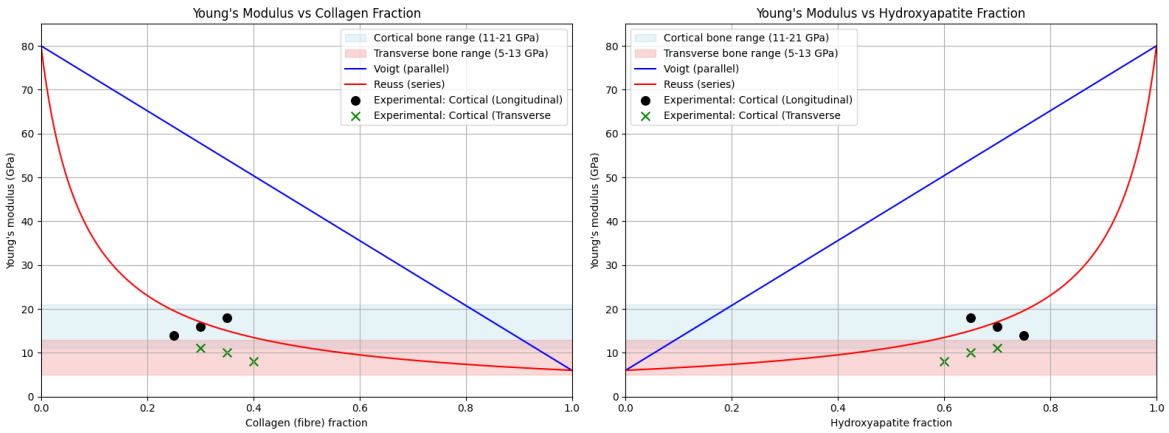

Figure 5. Cortical and transverse Young`s modulus vs hydroxyapatite/collagen fractions.

Anisotropic property of cortical bone with Haversian system running in longitudinal or transverse direction. It can influence the direction of fraction lines.

Cortical bone has a fracture toughness of 2–7 MPa·m$^{1/2}$ [33]. Trabecular bone, however, displays reduced toughness of 0.5–3 MPa·m$^{1/2}$, making it more susceptible to microfractures under load. This property is enhanced by collagen-mediated energy dissipation, which can mitigate crack propagation

 doi:10.20944/preprints202605.0674.v1

[34]. Cartilage exhibits minimal fracture resistance, with its integrity heavily reliant on the viscoelastic properties of its extracellular matrix. The matrix effectively dissipates energy but offers little inherent toughness [35]. Cortical bone endures cyclic loading through gradual microdamage accumulation, while trabecular bone fatigues more rapidly. Cartilage relies entirely on viscoelastic deformation for energy dissipation rather than on conventional fatigue resistance.

Bone stress–strain behavior comprises elastic deformation, yield, and plastic flow prior to fracture. This biomechanical profile provides the basis for considerations in prosthetic design. Ideally, it should replicate the native bone stiffness of approximately 20 GPa to prevent stress shielding. Stress shielding is a well-known phenomenon in which overly rigid implants redistribute loads, often inducing localized bone resorption due to reduced stress. Prosthetic materials must possess sufficient toughness to ensure long-term durability. Alignment of implant mechanical properties and biochemical compatibility with native tissue is essential in preventing loosening, microdamage, and early failure [36].

Bone tissue condition is dynamic. It is influenced by age, mechanical load, nutritional habits, and acquired or inherited disease (Table 3). Ageing is reflected in bone mass decline, progressing to osteopenia or osteoporosis, due to reduced osteoblast activity and increased resorption by still-active osteoclasts. Gravity and physical activity maintain structural integrity, while lower gravity or reduced activity also lead to bone tissue decline. Nutritional deficiencies, particularly of calcium and vitamin D, can significantly impair mineralization. Inherited or acquired disorders, hormonal imbalances, chronic inflammation, medications, or metabolic diseases can significantly alter bone density and architecture. Repeated microtrauma can induce cumulative structural and cellular changes in bone tissue condition [35].

Table 3. Main factors of bone tissue pathology.

Factor	Effect on Bone Tissue
Age (osteopenia, osteoporosis)	Decline in bone mass due to reduced osteoblast activity and stable resorption by osteoclasts
Mechanical load; Gravity	Maintains structural integrity; reduced load or inactivity accelerates bone decline
Nutrition (calcium, vitamin D deficiency, malnutrition)	Impaired mineralization, reduced bone strength, and increased susceptibility to fractures
Inherited conditions (osteogenesis imperfecta, osteopetrosis)	Alters bone density and architecture; predisposition to fractures and deformities
Hormonal disorders (hyperparathyroidism, thyroid disorders, diabetes)	Dysregulated remodeling: can increase resorption or reduce formation
Immune-mediated diseases (rheumatoid arthritis, lupus, chronic inflammation)	Chronic inflammation promotes osteoclast activation, microarchitectural deterioration
Renal and metabolic diseases (chronic kidney disease, chronic metabolic acidosis)	Alters bone mineralization and strength due to disrupted calcium-phosphate balance
Repeated microtrauma	Causes cumulative structural and cellular changes, leading to microfractures and deformities
Medications (glucocorticoids, proton pump inhibitors, heparin, loop diuretics, phenytoin)	Impair bone formation or increase resorption

2.4. Bone–Implant Mechanical and Biocompatibility

Osseointegration of the bone implant is influenced by surface texture, structure, chemistry, and bioactivity. Rough or porous surfaces enhance osteoblast adhesion and matrix deposition. Some alloys, such as titanium Ti-6Al-4V, are coated with hydroxyapatite for cementless implantation [37]. Rapid cell adhesion and proliferation within 7–14 days is desirable. Bioactive coatings can also be used to promote immune acceptance and minimize potential aseptic inflammation. Inadequate

 doi:10.20944/preprints202605.0674.v1

biocompatibility can lead to fibrous tissue formation, encapsulation, hindered integration, loosening, or fracture [38].

There are other potential incompatibility problems, such as differences in the mechanical properties of the bone and implant (Figure 6). The mismatch, especially in high-stiffness synthetic implants, can cause stress shielding (Figure 7). Most of the load is taken by the implant, and reduced bone tissue load leads to resorption [39]. Young`s modulus of the material ideally has to be matched to that of the bone. It is also important for bone prostheses to distribute loads evenly. Energy absorption with 10–20% energy dissipation is acceptable. Fatigue resistance, for example, in a femoral implant, must exceed 10^6 cycles.

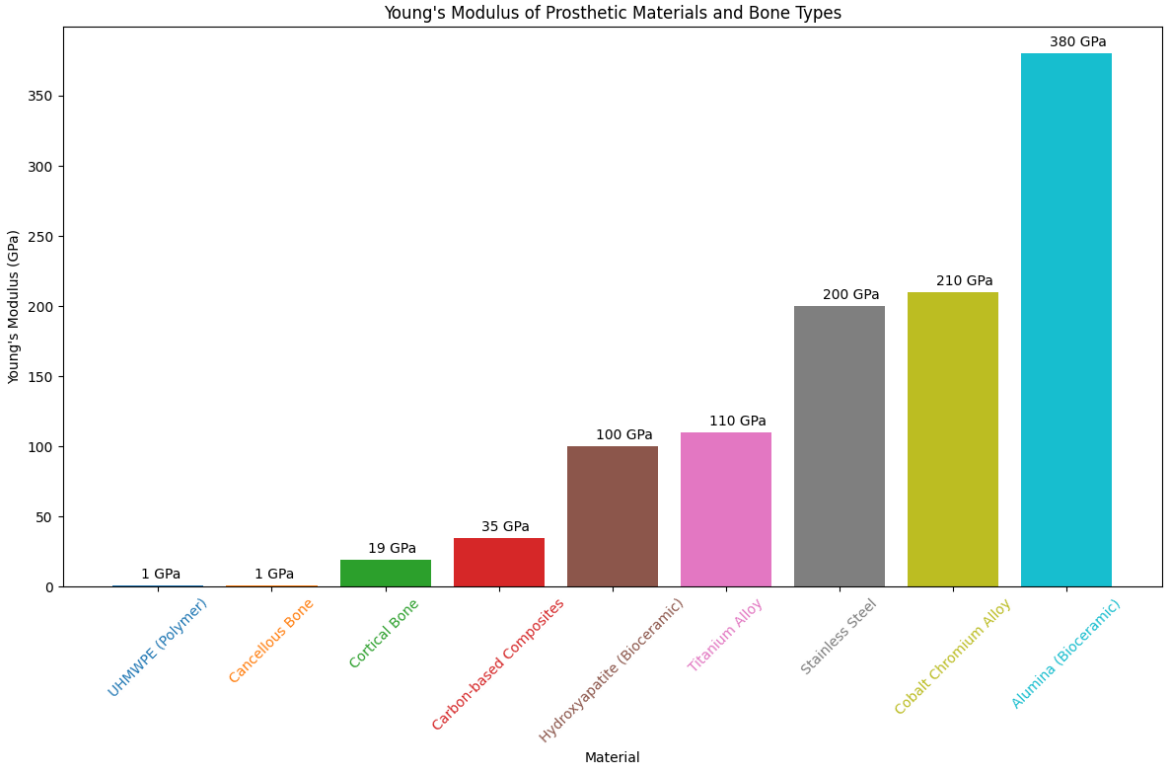

Figure 6. Young's modulus of common prosthetic materials compared with cortical and cancellous bone. Metallic implants (stainless steel, cobalt–chromium alloy, titanium alloy) and bioceramics (alumina, hydroxyapatite) exhibit stiffness values far exceeding those of native bone (1–19 GPa), underscoring the mechanical mismatch at the bone–implant interface.

 doi:10.20944/preprints202605.0674.v1

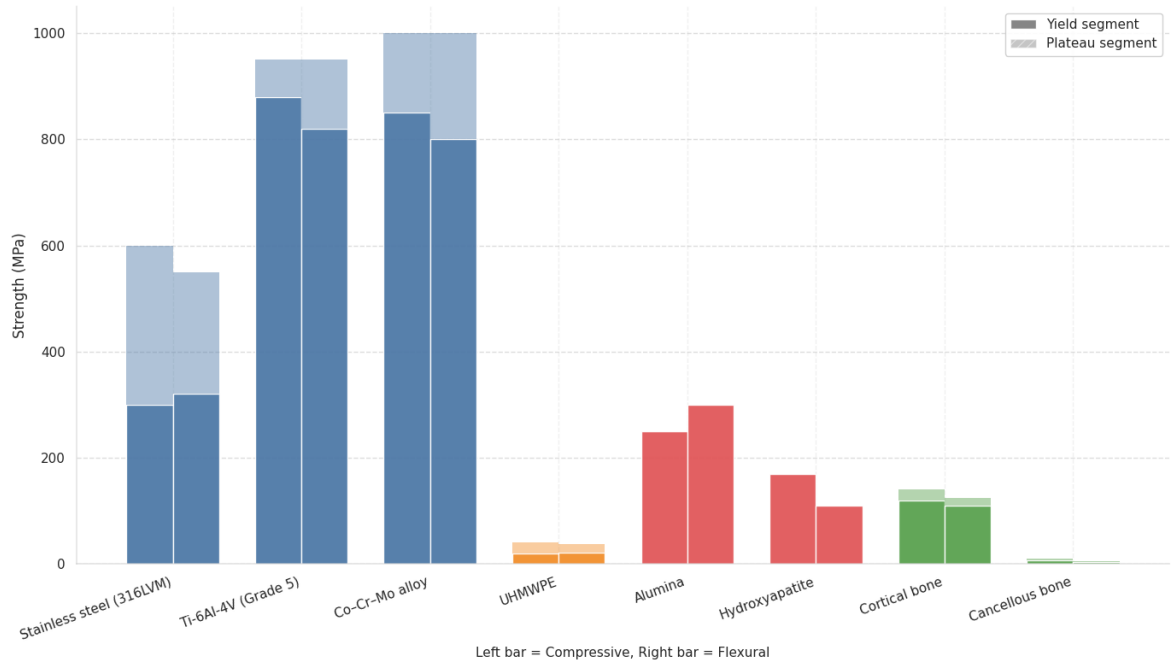

Figure 7. Compressive and flexural strength of selected material classes compared with bone tissues. Metallic alloys (316LVM stainless steel, Ti-6Al-4V, Co-Cr-Mo) exhibit strengths of 300–1000 MPa, far exceeding cortical bone (5–150 MPa), while UHMWPE and cancellous bone show comparatively low strength. This pronounced mismatch contributes to uneven load transfer and stress shielding at the implant–bone interface.

Prosthetic design has to match these mechanical and biological criteria to ensure durability, functional performance, and patient-specific compatibility [40,41]. There are a number of biocompatibility standards applicable to synthetic implants and grafts (Table 4). Materials are tested for local genotoxicity, carcinogenicity, reproductive toxicity, hemocompatibility, cytotoxicity, and implantation histology (ISO 10993-3, -4, -5, -6) [42], toxicokinetics (ISO 10993-13, -14, -15, -16), chemical characterization (ISO 10993-17, -18) and possible immunotoxicity. In turn, contact between biological liquids and tissues and metallic implants and graft materials can lead to material corrosion, so ASTM standards apply.

Table 4. Main biocompatibility standards for synthetic implants and grafts.

Metric	Governing Standards	What It Covers	Use
Biological response tests	ISO 10993-3, -4, -5, -6	Genotoxicity, carcinogenicity, reproductive toxicity, hemocompatibility, cytotoxicity, implantation histology	Baseline biocompatibility; selected by device type or contact type
Skin sensitization	ISO 10993-10:2021	Sensitization assays (in vitro or in chemico)	Skin, mucosal contact
Systemic toxicity	ISO 10993-11	Acute, sub-chronic, chronic systemic effects	Devices with potential systemic exposure
Degradation of products and toxicokinetics	ISO 10993-13, -14, -15, -16	Identification and quantification of polymer, ceramic, metal degradation and toxicokinetics	Applied for degradable, corrosive devices

 doi:10.20944/preprints202605.0674.v1

Chemical characterization	ISO 10993-17, -18	Extractables, leachables allowed limits	Biological evaluation
Immunotoxicology	ISO/TS 10993-20	Immunotoxicity principles and methods	Optional, if immune concerns exist
Nanomaterial guidance	ISO/TR 10993-22	Evaluation guidance for nano-structured materials	Optional for nano-enabled devices
Irritation	ISO 10993-23:2021	Standalone irritation assays (skin, mucosa)	Contact-type dependent
Metallic implant corrosion (small devices)	ASTM F2129	Potentiodynamic polarization	Small metallic implants
Corrosion of dental metals/alloys	ISO 10271:2020	Corrosion behavior in oral environment	Dental implants
General metal corrosion	ASTM G31, ASTM G59	Immersion mass loss (G31), polarization resistance (G59)	Supplemental metal/ alloy testing

3. Material Properties of Metallic Alloys, Bioceramics, and Carbon-Based Composites

Bone prostheses and osseous implants have specific physical and chemical properties that depend on the materials used (Table 5). Strength, weight, wear resistance, biocompatibility, and osseointegration can be tailored to different types of bone replacement. Main prosthetic functionality must be accompanied by the ability to integrate with smart systems or to demonstrate specific properties that can be utilized in smart bone prostheses [43].

Metals and metallic alloys possess high tensile strength, ductility, fatigue resistance, moderate to high weight, moderate to high wear resistance, and generally good sensor-integration potential. Titanium and cobalt-chromium alloys are widely used due to their mechanical robustness and corrosion resistance, although long-term ion leaching remains a concern [44].

Bioceramics and bioglasses, such as alumina, ZrO_2, and hydroxyapatite, have high compressive strength but are brittle in tension. Their weight is moderate, and wear resistance is high. These materials exhibit excellent biocompatibility and osseointegration, though their insulating nature limits smart integration capabilities [45].

Carbon-based composites, such as carbon fiber (CF), carbon nanotubes (CNT), and graphene, have exceptional strength-to-weight ratios. They are ultra-lightweight with tunable wear resistance. Most demonstrate good biocompatibility and are ideal for sensor integration due to their electrical conductivity and inherent smart properties [43].

Table 5. Properties of materials used for bone prostheses.

Property	Metallic Alloys (316LVM steel, Ti, Co–Cr, Zr, Mg)	Bioceramics (Alumina, ZrO_2, SiO, HA)	Carbon-Based (CF, CNT, Graphene)	Combinations of Materials
Strength	High tensile strength, ductile, fatigue resistant	High compressive strength, brittle in tension	Very high strength-to-weight ratio	Hybrid and composite systems (bioceramic-coated Ti, CF-reinforced Ti), PMMA: combine high compressive and tensile strengths, brittleness and

 doi:10.20944/preprints202605.0674.v1

				ductility Composites (CF with Ti or bioceramic coatings) reduce weight while maintaining structural integrity
Weight	Higher (Ti lighter, Co–Cr heavier)	Moderate (heavier than carbon-based)	Low (ultra-lightweight)	
Wear resistance	Moderate–High (Co–Cr excels, Ti moderate)	High (Al_2O_3, ZrO_2 ideal for articulating surfaces)	Good, tunable with matrix modifications	Bioceramic coatings on metallic or carbon-based substrates enhance wear resistance
Biocompatibility	High (Ti, Zr High; Co–Cr moderate due to ion release risks)	High (bioinert Al_2O_3, ZrO_2; bioactive HA)	Good (CF reliable; CNT, graphene biocompatibility is debated	Hybrid and composite systems (HA-coated Ti or CF) have bioactive properties of bioceramics to enhance biocompatibility
Osseointegration	High (Ti, Zr facilitate strong bone integration)	High (HA, bioactive glass promotes bone bonding)	Limited (dependent on matrix, e.g., polymer coatings)	Bioceramic-metallic composites (HA-coated Ti) optimize osseointegration, strength with bioactive surfaces
Prosthetic use	Structural load-bearing, osseointegration components	Bearings, coatings, articulating surfaces	Lightweight limbs, embedded sensor platforms	Hybrid and composite applications (bioceramic-coated Ti for load-bearing joints, CF-Ti for lightweight smart limbs)
Smart integration	High (conductive, supports sensors and actuators, adaptive alloys)	Limited (insulation properties require coatings for sensor compatibility)	High (inherently conductive, ideal for sensors)	Hybrid and composite systems (Ti with CNT/graphene coatings) enhance conductivity and sensor integration
Smart sensors or sensor-like properties	High (Ti, Zr support embedded sensors; Mg offers bioresorbable sensor potential)	Limited (minimal conductivity; sensor-like properties via coatings, e.g., piezoelectric HA)	High (CNTs/graphene are highly conductive, enabling strain and pressure sensors, bioelectrical signal detection)	Combinations (CNT-coated Ti, bioceramic-CF hybrids) enable advanced sensor functionalities;

 doi:10.20944/preprints202605.0674.v1

Every type and subtype of material has particular mechanical and physical properties that make it more compatible with certain bone tissues. Cortical bones are usually grafted with metallic alloys for load-bearing due to their high tensile strength and fatigue resistance [44]. Specific subchondral bone areas can be mapped with bioceramics due to compressive forces and wear stresses at joints. These materials, such as alumina and zirconia, offer high biocompatibility and wear resistance but are brittle under tension [46]. Trabecular bones match with carbon-based materials, which are lightweight, potentially porous, and offer excellent strength-to-weight ratios and conductivity for smart integration [43].

Composite and hybrid implants and grafts often include several materials. Coatings and significant inclusions are used in composites, while hybrids are mixed on the molecular or nanoscale. Metamaterials are usually designed by combining smart properties and sensor functions.

There are additional types of bone tissue (Table 6) that can influence the feasibility of synthetic materials' application. Woven bone is usually found in areas of rapid development, such as a fractured callus or the embryonic skeleton. Other forms of bone tissue are pathological -- osteoporotic, osteomalacic, rickets bone, or Paget's disease bone. Due to low density and poor organization, there is little to no possibility of synthetic implants and grafts.

Polymer materials such as CF-PMMA and CFR-PEEK can be used as fixators in cases of fracture, mostly as plates or rods, with limited potential for macro-scaffolding or full implants or grafts. Recent studies show that nanofiber-coated CF-PEEK composites improve hydrophilicity and osteogenesis, making them promising for orthopedic applications despite their bioinert base [47]. Calcium Phosphate Cement (CPC), based on hydroxyapatite or brushite, can be used as an osteoinductive filler, but has limited mechanical abilities and is often used for osteoplasty and filling in non-load-bearing areas [48].

Table 6. Normal and pathological types of bone tissue compatible with synthetic implants and graft material.

Bone Type and Synthetic Analogue	Bone Structure and Density	Material Strength and Function	Bone Locations and Examples
Cortical bone: metallic alloys; CF-PMMA	Compact osteons, high density	High tensile & compressive; structural load-bearing	Slow, lifelong turnover; diaphysis of long bones, flat bone cortex (femoral shaft, tibial shaft, humeral diaphysis)
Trabecular bone: bioceramics; porous Ti and Mg alloys	Porous trabecular lattice, low density	Moderately compressive, low tensile; lightweight support, energy absorption and dissipation	Rapid, stress-adaptive; epiphyses, vertebral bodies, pelvis (vertebrae, femur epiphysis, calcaneus bone)
Woven bone: HA composites, PLGA, Mg scaffolds	Random collagen, immature, low density	Low tensile, moderate compressive; rapid temporary support in repair and growth	Very fast turnover; fracture callus, fetal skeleton (healing fracture, embryonic skeleton)
Subchondral bone: HA-Bioglass Composites	Dense layer beneath cartilage, high density	Very high compressive; shock absorption, load distribution	Moderate turnover; joint surface (distal femur, tibial plateau, humeral head)
Osteoporotic bone:	Cortical thinning, trabecular loss,	Reduced strength, fracture-prone	Altered remodeling; vertebrae, hip, wrist

 doi:10.20944/preprints202605.0674.v1

CPC, CFR-PEEK, CF-PMMA (vertebroplasty)	porous, low density		(compression fractures, hip fractures)
Osteomalacic or rickets bone: limited CFR-PEEK fixation	Poor mineralization, soft, low density	Weak, deforms under load	Defective mineralization; long bones, vertebrae, ribs (bowing legs, fragility fractures)
Pagetic bone: limited CFR-PEEK fixation	Disorganized mosaic lamellae, enlarged, variable density	Structurally irregular, locally weak	Excessive turnover; pelvis, skull, femur, tibia (bowed femur, skull thickening)

3.1. Physical and Mechanical Properties of Synthetic Implant and Graft Materials

Physico-mechanical parameters of synthetic materials are essential metrics for the functionality of bone implants. Mechanical loads and mechanical stresses' sustainability influence structural integration and usability (Table 7).

Table 7. Main physico-mechanical features of synthetic bone implants and grafts.

Metric	Description	Relevance and examples
Tensile strength (MPa)	Maximum stress material can withstand while being stretched	Load-bearing capability in tension-dominated regions: femoral shaft, ulna, tendon insertions
Compressive strength (MPa)	Resistance to compressive forces	Weight-bearing structures: vertebrae, femoral head, tibial plateau, calcaneus
Fatigue life (cycles)	Number of load cycles before failure	Long-term durability in repeatedly loaded sites: hip and knee joints, lumbar spine, femoral diaphysis
Young's modulus (GPa)	Stiffness vs. elasticity of the material	Stress distribution and compatibility with cortical bone: diaphyses, subchondral bone at joints
Density (g/cm³)	Material weight	Prosthesis mass, mobility in large reconstructions: femur, pelvis, long bones
Wear and Abrasion Resistance	Material degradation under friction	Long-term performance in articulating sites: hip, knee, temporomandibular joint
Fracture Toughness (MPa·m½)	Resistance to crack propagation	High-stress locations: femoral neck, acetabulum, vertebral arches

Tensile strength is the maximum stress the material can sustain when subjected to elongation. It dictates the load-bearing capacity of long bones under bending or at tendon insertion sites. *Compressive strength* reflects the ability to withstand compressive loads and is important in weight-bearing sites such as the vertebrae, femoral condyles, and tibial plateau. *Fatigue life* is the number of cycles of repeated load that the material can withstand before failure [49]. *Young's modulus* is a measure of stiffness related to elasticity. The modulus can be matched to that of the host bone (Figure 8). Excessive material stiffness leads to stress shielding, resulting in bone tissue resorption. Insufficient stiffness may lead to mechanical collapse or implant loosening [50]. Fracture toughness is a metric of resistance to material crack initiation and crack propagation.

The *weight* of the material is related to density. Lightweight materials reduce musculoskeletal energy expenditure. It enhances mobility, improves usability while maintaining safety. *Wear and abrasion resistance* are important in joint replacements. Insufficiently smooth surfaces may exacerbate

 doi:10.20944/preprints202605.0674.v1

cartilage degradation and joint loosening, leading to further mechanical damage. Microscopic wear particles can trigger an aseptic inflammatory response, leading to subsequent implant loosening.

Simplified stress-strain curves for bone tissue and the main types of prosthetic materials are shown in Figure 9.

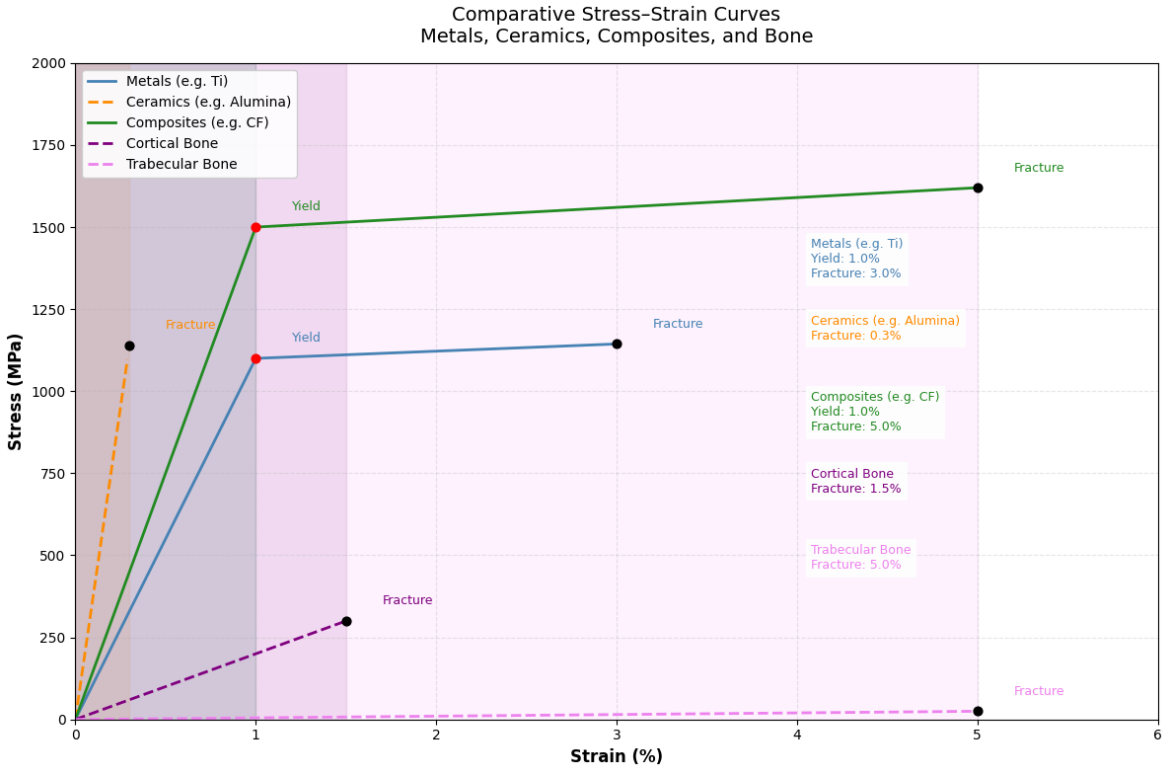

Figure 8. Simplified comparative stress–strain behaviour of bone tissues and prosthetic materials. Metals (titanium), ceramics (alumina), composites (carbon fibre), cortical bone, and trabecular bone are shown for comparison. Ceramics fail at ~0.3% strain abruptly, metals yield near ~1% and fracture around ~3%, while composites sustain the highest strains (~5%), most closely resembling trabecular bone. The pronounced stiffness mismatch between metallic implants and bone highlights the importance of modulus matching to mitigate stress shielding and subsequent bone resorption.

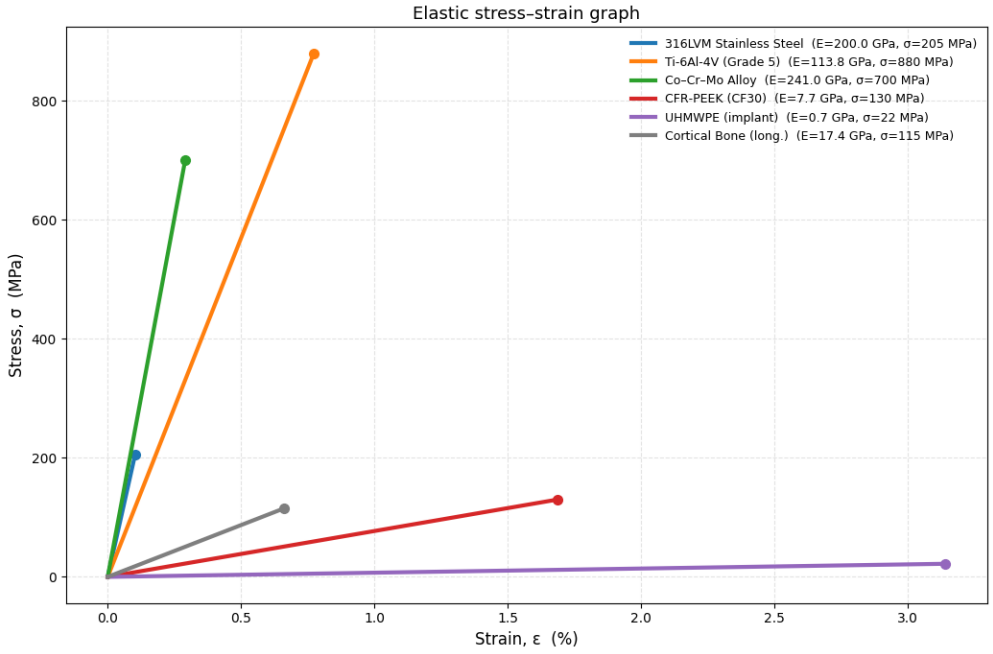

 doi:10.20944/preprints202605.0674.v1

Figure 9. Elastic stress–strain behavior of prosthetic materials compared with cortical bone. Metallic alloys (316LVM stainless steel, Ti-6Al-4V, Co-Cr-Mo) show high stiffness and strength but fracture at low strains (<1%), whereas CFR-PEEK and UHMWPE exhibit lower moduli and larger strain capacities, more closely approximating cortical bone ($E \approx 17.4$ GPa, $\sigma \approx 115$ MPa). These contrasts illustrate the trade-off between strength and modulus matching in implant material selection.

3.1.1. Metallic Alloys

Metallic alloy substrates provide high thermal and electromagnetic conductivity. Titanium alloys, such as Ti-6Al-4V, have a conductivity of 1.7×10^6 S/m [51], while 316SL steel exhibits 1.4×10^6 S/m [52]. They support rapid heat spreading and efficient DC and low-frequency AC conduction. However, alternating fields can induce surface currents in the implant. The current density decays rapidly with depth from the metal surface, and the decay rate depends on frequency, conductivity and magnetic permeability [53]. Metallic substrates can produce RF coupling, localized heating and variable signal attenuation. Frequency, Environment, Form and Surface (FEFS) determine these effects. Frequency sets induced current distribution and alloy surface depth. The environment, such as surrounding tissue permittivity and conductivity, controls EM absorption. Form, such as implant geometry, length and leads, creates antenna and resonance behaviour. Surface properties and coatings govern current confinement and contact losses [54]. The substrate is intended to be suitable for smart sensors and actuators, especially for the integration of smart alloys, but is limited by these effects.

Some alloys are adaptive, such as shape-memory alloys (e.g., NiTi with transformation temperatures of 0-100 °C) and magnetostrictive materials (e.g., Terfenol-D or Galfenol with magnetostriction of 1000-2000 ppm). They can be integrated directly into metallic matrices or applied as functional coatings 10-100 μm thick [55,56]. These systems can provide temperature-responsive stiffness adaptation with elastic modulus changes from 28 GPa (austenite) to 70 GPa (martensite), magnetic field-controlled actuation with strain rates up to 10^4 s^{-1}, or stress-responsive mechanical property modulation [57]. The metallic substrate provides structural stability while the smart component delivers responsive functionality. Smart components can be integrated as capsules and films, protected from direct contact with biological tissues and liquids due to biocompatibility and corrosion concerns.

Magnesium alloys are biodegradable with average corrosion rates of 0.1-1 mm/year. The biodegradability can be controlled through alloying and coatings [58]. Smart sensors embedded in biodegradable magnesium matrices can provide temporary monitoring capabilities with functional lifetimes of 3-12 months. In this time, the implant is dissolved and replaced by natural tissue [59]. This approach helps to avoid responses against long-term foreign body presence and can provide additional data [60].

However, there are identified challenges related to both the structural integrity of the prostheses and their sensor functionality. Sensor integration involves structural modification of prosthetic implants. Pin-socket sensor systems require drilling numerous holes in the implant surface to mount sensors, which may cause structural damage to the implant itself [61]. This mechanical alteration can potentially compromise the load-bearing capacity and long-term durability of the prosthesis. It raises questions about the trade-off and balance between monitoring capabilities and the structural integrity of smart metallic prostheses.

Beyond structural concerns, sensors themselves can undergo unwanted degradation in the biological environment. Sensors attached to standard implant surfaces experience debonding from the underlying substrate within a few weeks of implantation. Furthermore, sensors attached to porous tissue ingrowth surfaces can lose their original accuracy as tissue ingrowth progresses [61]. This degradation is a serious limitation for long-term monitoring. Sensor readings can become unreliable precisely when longitudinal data would be most valuable.

Material compatibility also poses significant issues, as direct bonding of sensing elements can be a biological irritant or hazard [62]. For long-term biocompatible implantation, common ferromagnetic

 doi:10.20944/preprints202605.0674.v1

materials such as cobalt and nickel, used in some sensor designs, are cytotoxic. They require careful attention to packaging quality, encapsulation and cover, as well as lifetime performance monitoring [63]. Mechanical tightening methods may damage the sensor patches themselves. A significant technical restriction is the size of the sensors and telemetry systems. They have to be sufficiently miniaturized to fit within standard bone grafts or prostheses without requiring significant structural modifications [61]. These changes can jeopardize implant performance and safety. Miniaturization also reduces the capabilities of sensors to function, to collect reliable information and to have the necessary range of parameters.

Metallic alloys are extensively used in load-bearing bone prosthetic replacements. They possess high tensile strength, ductility, and fatigue resistance (Figure 10).

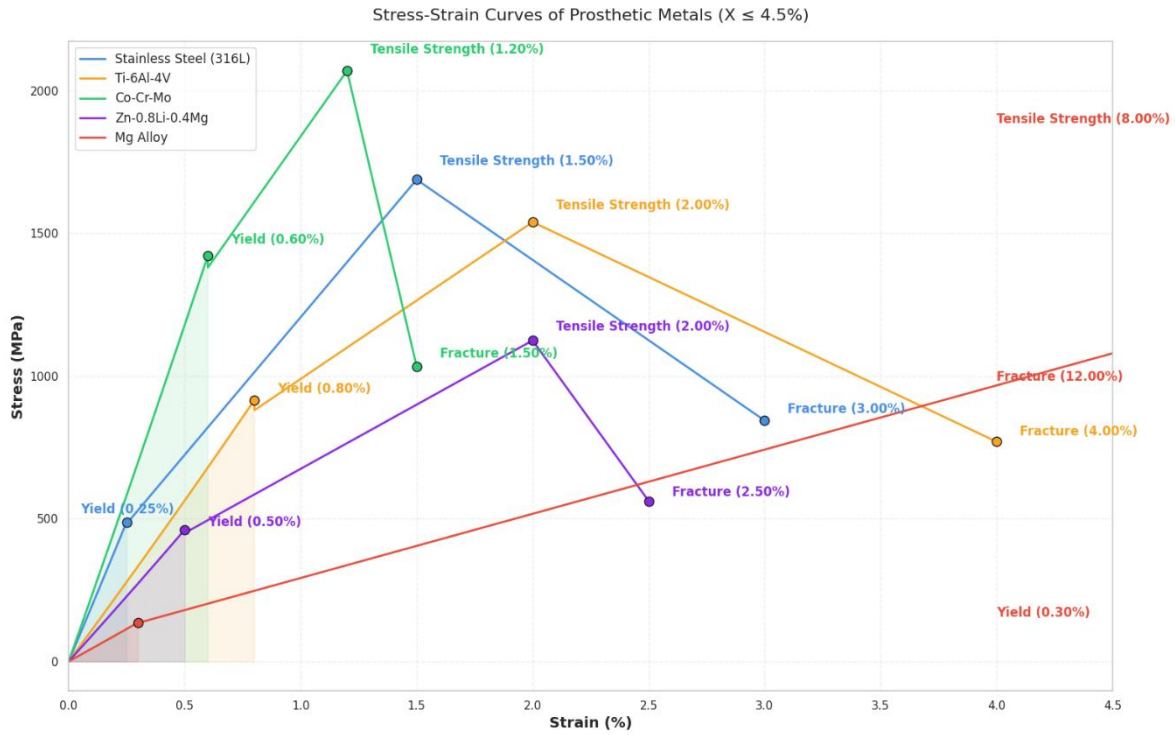

Figure 10. Stress–strain behavior of prosthetic metallic alloys. Stainless steel 316L, Ti-6Al-4V, Co-Cr-Mo, Zn-0.8Li-0.4Mg, and a Mg alloy are shown with their yield points, tensile strengths, and fracture strains. Co-Cr-Mo exhibits the highest strength (~2100 MPa) but limited ductility, whereas the Mg alloy reaches the greatest fracture strain (~12%), illustrating the strength–ductility trade-off among implant metals.

For example, stainless steel 316L is non-magnetic, with high corrosion resistance [64]. It has less than 0.03% of carbon, 16–18% of chromium, 10–14% of nickel, 2-3% of molybdenum and manganese, silicon, phosphorus, sulfur, nitrogen, and less than 2% each. Chromium forms a passive Cr_2O_3 oxide layer, which makes 316L steel corrosion-resistant [65]. Nickel stabilizes the austenitic 12-atoms Face-Centered Cubic (FCC) structure (Figure 11) at room temperature.

 doi:10.20944/preprints202605.0674.v1

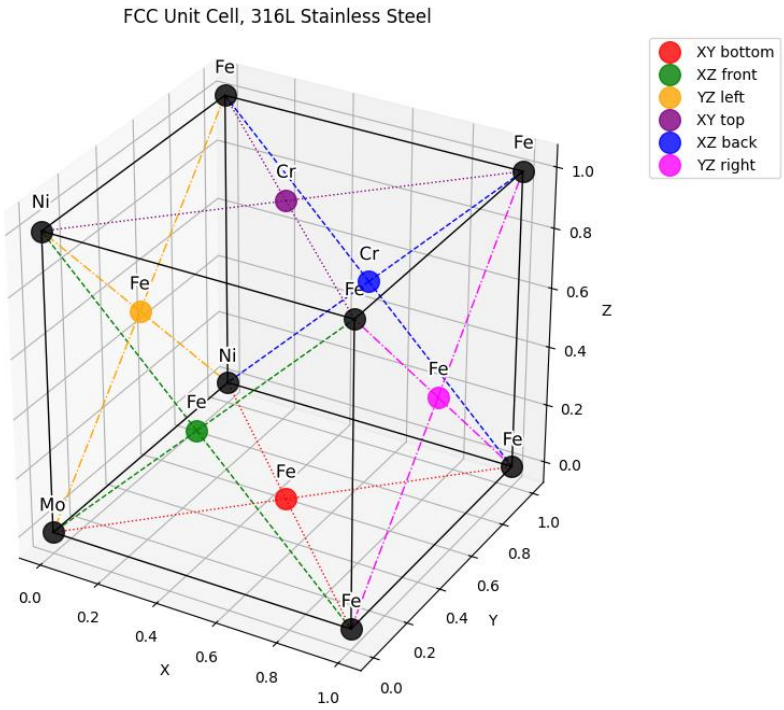

Figure 11. Face-centered cubic (FCC) unit cell of 316L stainless steel. The FCC lattice illustrates the distribution of Fe, Cr, Ni, and Mo atoms within the 12-atom austenitic structure. Nickel stabilizes the FCC phase at room temperature, enhancing the alloy's ductility and corrosion resistance.

Any main alloy atom can be in every position due to close atomic radii sizes: Fe ≈ 1.26 Å, Cr ≈ 1.28 Å, Ni ≈ 124 pm = 1.24 Å, Mo ≈ 139 pm = 1.39 Å. Molybdenum enhances pitting and crevice corrosion resistance, especially in chloride environments, which is important for tissue compatibility [66]. High strength and fatigue life (Table 8) make the material useful for long bone replacement. However, relatively high weight (density) and moderate wear resistance make it a suboptimal choice as a prosthetic alloy. The high Young's modulus typical of most prosthetic alloys can cause stress shielding [67]

Table 8. Physico-mechanical properties of alloys used for bone implants and grafts.

Property	316L Stainless Steel	Ti-6Al-4V	Co-Cr-Mo	Notes
Tensile strength (MPa)	500–1000	900–1100	800–1400	Determines the ability to withstand elongation in bones, tendons
Compressive strength (MPa)	500–1000	900–1100	800–1400	Supports weight-bearing sites (vertebrae, femoral condyles, tibial plateau)
Fatigue life	>10^6 cycles	>10^6 cycles	>10^6 cycles	Ensures durability under physiological cyclic loads
Young's modulus (GPa)	190–210	110–120	200–230	Compared to cortical bone (10–20 GPa), potential stress shielding
Fracture toughness (MPa·$m^{½}$)	40-60	50–100	30–60	Resists crack initiation and propagation

 doi:10.20944/preprints202605.0674.v1

Wear, abrasion resistance	Moderate	Moderate (enhanced with coatings)	High	Particle generation (<1 μm for Co-Cr-Mo) leads to inflammation and implant loosening
Density (g/cm³)	7.8–8.0	4.4–4.5	8.3–8.5	Influences of musculoskeletal energy expenditure
Vickers Hardness (HV)	150–200	300	300–400	Higher hardness, better for articulating surfaces, reduces cartilage wear

Titanium alloys, such as Ti-6Al-4V, are comparatively light and have relatively high strength, Young`s modulus and fatigue life. Ti-6Al-4V has alpha and beta phases (Figure 12). The proportion of the two phases in the alloy depends on the thermomechanical treatment [65].

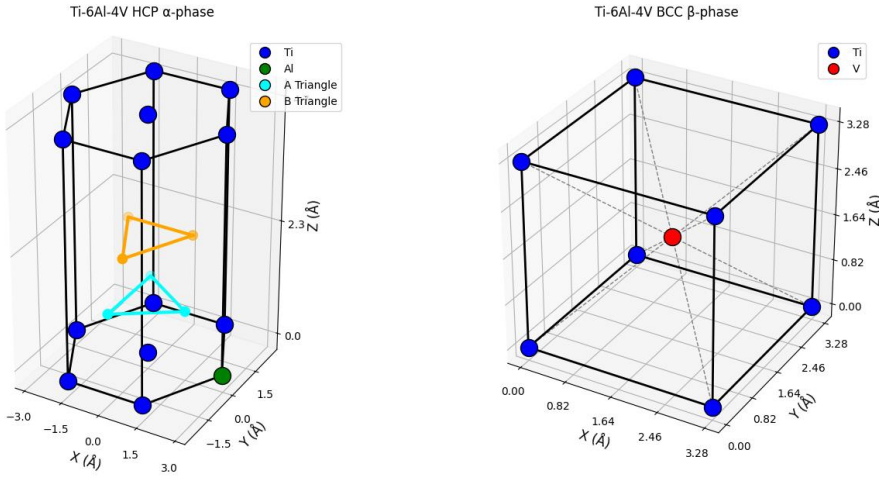

Figure 12. Crystal structures of the α- and β-phases in Ti-6Al-4V. The hexagonal close-packed (HCP) α-phase shows Ti and Al atoms arranged in alternating A- and B-layer stacking, while the body-centered cubic (BCC) β-phase is stabilized by V. The relative proportions of these phases depend on thermomechanical processing, which governs the alloy's mechanical properties.

The alpha phase is hexagonal close-packed (HCP) and is stabilized at room temperature by aluminium. Atoms in HCP are also packed in layered ABAB triangles, when A-level atoms occupy positions dissimilar to level B atoms. The beta phase is body-centered cubic (BCC) and is stabilized at room temperature by vanadium. Atoms are packed in a more complex ABC way, which is also characteristic of FCC. Another alpha-beta implant titanium alloy is Ti-6Al-7Nb. Nitinol, a nickel-titanium alloy, is used in monolithic and foam form and possesses superelastic and shape-memory effects [68].

Cobalt–Chromium–Molybdenum (Co–Cr–Mo) alloys are dense and hard. Due to these qualities, Co–Cr–Mo alloys are used for articulating surfaces in joint replacements [65]. Wear particles generated from these surfaces can elicit inflammatory responses and contribute to implant loosening [66].

3.1.2. Bioceramics

Bioceramics possess extremely high compressive strength (Table 9) but can be brittle under tensile stress (Figure 13), with a relatively low fatigue life of 10^3–10^4 cycles [69].

 doi:10.20944/preprints202605.0674.v1

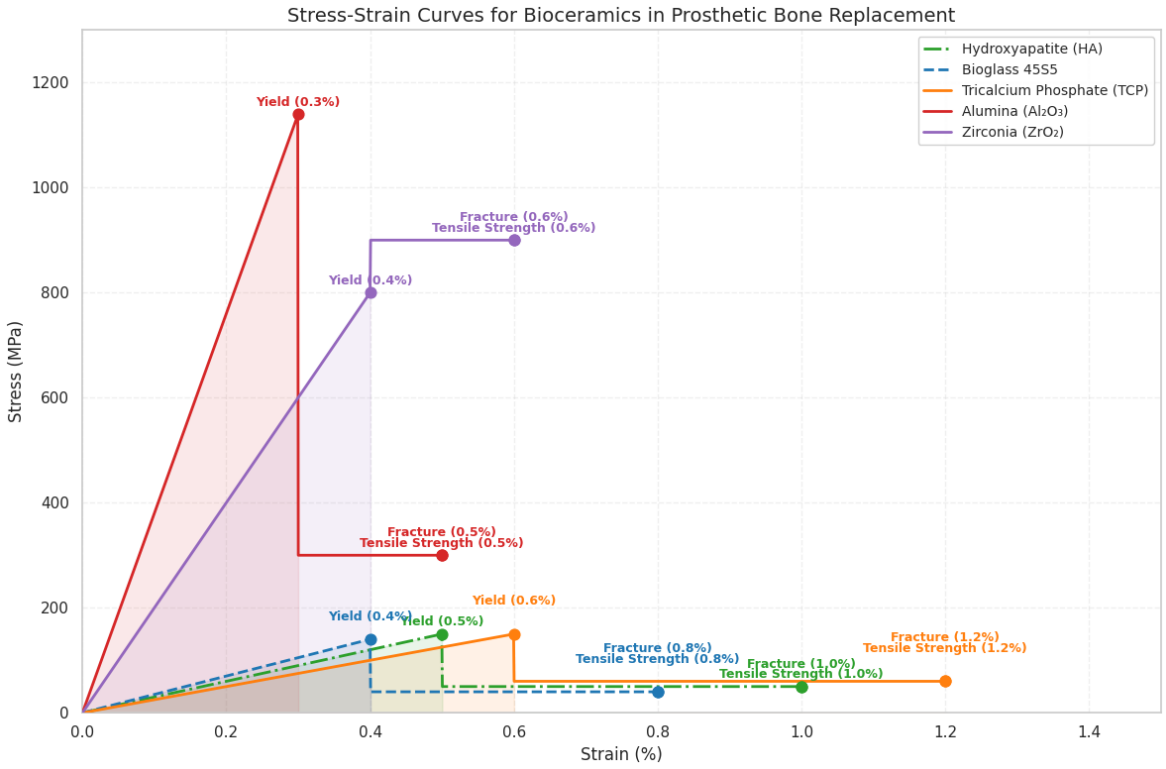

Figure 13. Stress–strain behaviour of bioceramic materials used in prosthetic applications. Hydroxyapatite (HA), Bioglass 45S5, tricalcium phosphate (TCP), alumina (Al_2O_3), and zirconia (ZrO_2) are shown for comparison. Alumina exhibits the highest strength (~1200 MPa) but fails abruptly at ~0.5% strain, while zirconia combines high strength (~900 MPa) with slightly greater fracture strain (~0.6%). Bioactive ceramics (HA, Bioglass 45S5, TCP) display lower strengths (50–150 MPa) and higher fracture strains (up to ~1.2%), more closely aligning with cortical bone. These trends highlight the trade-off between mechanical strength and bioactivity in bioceramic selection.

The hardness, structural stability, and high wear resistance make them effective for joint resurfacing, dental implants, and coating materials. Alumina (Al_2O_3), or corundum, has a fine-grained polycrystalline structure in which a hexagonal close-packed oxygen lattice with Al^{3+} ions in octahedral sites is formed. It has trigonal symmetry [70]. Strong ionic-covalent Al–O bonds are responsible for the properties of the material (Figure 14). It makes Alumina suitable for compression bearing, for example, in articulating surfaces and in joint prostheses, for wear resistance [71]. Usually not used alone, and combined with other materials, such as alloys. Due to the high Young's modulus can create stress shielding.

 doi:10.20944/preprints202605.0674.v1

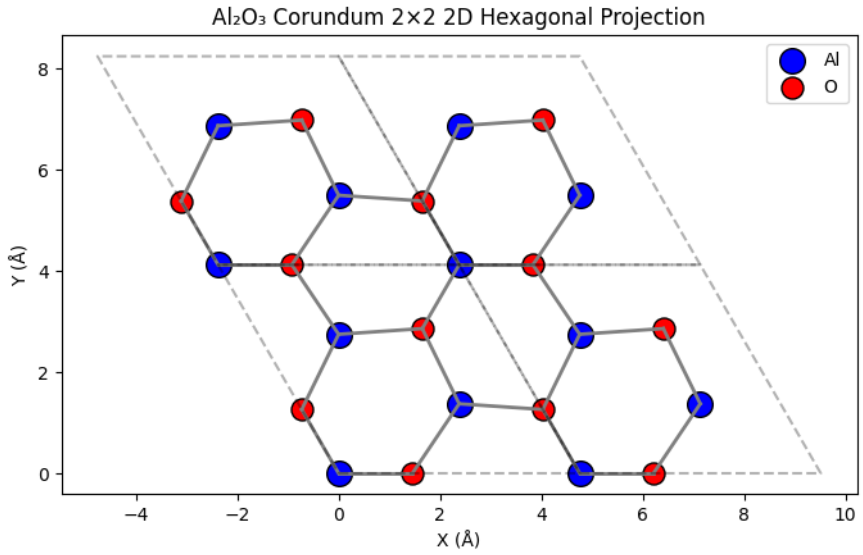

Figure 14. Corundum 2D hexagonal projection.

Zirconia (ZrO_2) is monoclinic at room temperature and has a stabilized tetragonal FCC structure with Y^{3+} doping [72]. It has strong ionic and covalent Zr–O bonds. Cations (Zr^{4+} and Y^{3+}) form a face-centered cubic (FCC) lattice (Figure 15). Anions (O^{2-}) occupy all the tetrahedral sites with possible vacancies. The monoclinic transformation under stress increases fracture toughness.

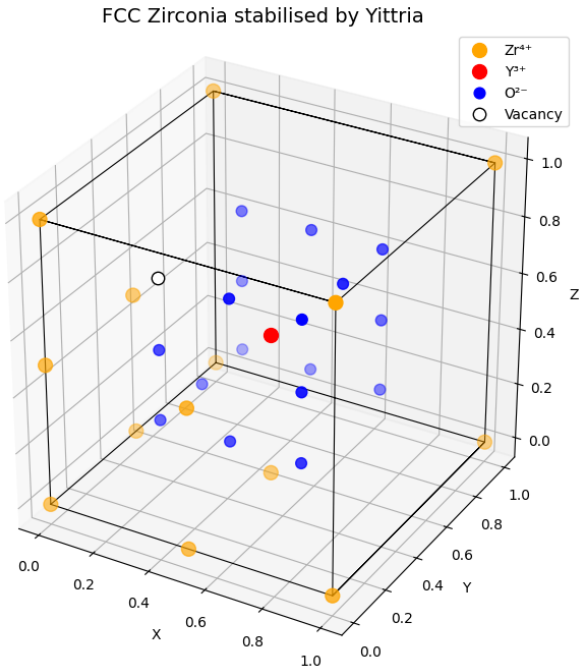

Figure 15. FCC Zirconia stabilized by Yittria.

Hydroxyapatite (HA, $Ca_{10}(PO_4)_6(OH)_2$) has ionic Ca–O and phosphate covalent bonds, which are weak compared to metals, and forms crystals with a hexagonal lattice. It can be porous or dense polycrystalline. Highly brittle, it is bioactive via the Ca–P framework and is often used as an osteoconductive scaffold or coating for other materials [73].

Bioglass (45S5) is one of the types of bioglass. It is an amorphous silicate network (Si–O–Si), partially disrupted by Na^+ and Ca^{2+} modifiers (Figure 16) [74]. It has mostly covalent Si–O bonds, and ionic modifiers disrupt the network [75]. The microstructure is non-crystalline glass. HA and bioglass

 doi:10.20944/preprints202605.0674.v1

have Young's moduli closer to those of cortical bone. It is bioactive due to surface ion exchange with body fluids [76]. Bioactivity will be discussed in one of the sections below.

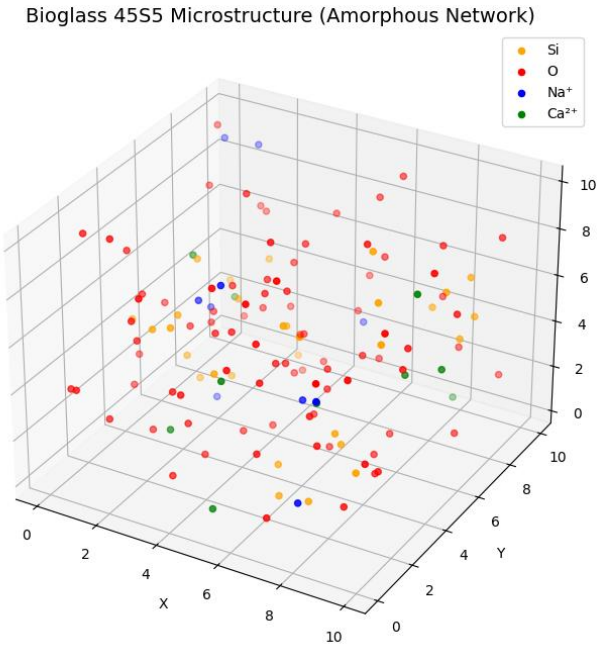

Figure 16. Bioglass microstructure.

The most frequently used bioceramics in medical implants are Alumina, Zirconia, Hydroxyapatite (HA), and Bioglass. They might differ in mechanical strength and biological compatibility. Alumina and Zirconia are the structural performers. They have high tensile and compressive strength, excellent wear resistance, and superior hardness, making them suitable for load-bearing applications such as joint prostheses. However, their high stiffness (Young's modulus) can lead to stress shielding, in which the bone surrounding the implant weakens due to reduced mechanical loading.

HA and Bioglass sit at the opposite end. Their modulus closely matches cortical bone, reducing stress shielding, and they offer superior bioactivity. However, they are significantly weaker in tension, fatigue, and fracture toughness, which makes them prone to catastrophic brittle failure under cyclic or tensile loading (see Table 9).

Table 9. Physico-mechanical properties of bioceramics used for bone implants and grafts.

Property	Alumina (Al_2O_3)	Zirconia (ZrO_2, Y-TZP)	Hydroxyapatite (HA)	Bioglass (45S5 type)	Notes
Tensile strength (MPa)	200–400	500–1000	40–100	40–100	Brittle fracture risk; ceramics generally poor in tension
Compressive strength (MPa)	2000–4000	1500–2000	300–1000	200–500	Suitable for compressive loads, but rarely used alone in load-bearing sites
Fatigue life	10^3–10^4 cycles	10^4–10^5 cycles	<10^3 cycles	<10^3 cycles	Brittle nature limits cyclic durability
Young's modulus (GPa)	380–400	200–210	80–110	35–40	Close to cortical bone in bioglass and

 doi:10.20944/preprints202605.0674.v1

Fracture toughness (MPa·m½)	3–5	5–10	0.7–1.2	0.5–0.8	HA; ceramics risk stress shielding Much lower than metals; prone to catastrophic fracture
Wear, abrasion resistance	High	High	Low	Low	Alumina/zirconia used in joint prostheses for wear resistance
Density (g/cm³)	3.9–4.0	5.8–6.1	3.1–3.2	2.6–2.8	Lower density than metals lighter implants
Vickers hardness (HV)	1800–2000	1200–1300	400–600	450–600	High hardness resists scratching but increases brittleness

3.1.3. Carbon-Based Materials

Carbon-based composite materials have adequate strength (Table 10), high fatigue life [77], Young's modulus comparable to those of bone tissue, significant fatigue life and low density. It can be used for vertebroplasty, micro- and macro-scaffolding [78].

Table 10. Physico-mechanical properties of carbon-based materials used for bone implants and grafts.

Property	CF-PMMA	PEEK	UHMWPE	PLLA/PDLA	CNT reinforced composites	Notes
Tensile strength (MPa)	90–150	90–100	40–50	50–70 / 40–60	200–1500	Determines ability to resist elongation; critical in fixation and structural implants
Compressive strength (MPa)	80–120	100–120	20–30	70–100 / 50–80	200–800	Important for weight-bearing applications (vertebrae, interbody cages)
Fatigue life	10^5 cycles	>10^6 cycles	>10^6 cycles	0.8–1×10^5/ 0.6–0.8×10^5 cycles	10^6–10^7 cycles	Ensures long-term durability under cyclic physiological loads
Young's modulus (GPa)	3–5	3–4	0.8–1.5	2–4 / 1–3	10–100	Compared to cortical bone (10–20 GPa), closer modulus reduces stress shielding

 doi:10.20944/preprints202605.0674.v1

Fracture toughness (MPa·m½)	1–2	3–4	2–6	2–4 / 1.5–3	5–15	Resists crack initiation and propagation, important for reliability
Wear, abrasion resistance	Poor, moderate	Moderate	Moderate	Moderate	High	Particle generation and wear debris
Density (g/cm³)	1.2–1.3	1.3–1.4	0.93	1.2–1.3/ 1.1–1.2	1.2–1.4	Lower density reduces musculoskeletal energy expenditure
Vickers hardness (HV)	20–30	20–25	10–20	20–25 / 15–20	50–200	Hardness improves surface durability and reduces scratching and wear

Pyrolytic carbon demonstrates high hemocompatibility. It is used in mechanical heart valves and orthopedic joint surfaces. It minimizes platelet adhesion, reduces thrombus formation, and avoids activation of the complement cascade. This limits systemic inflammatory responses. Clinical applications in orthopedics include pyrocarbon arthroplasty in acute unreconstructable radial head fractures [79].

Carbon nanotubes and graphene derivatives exhibit size- and dose-dependent cytotoxicity. Smaller nanoparticles are capable of penetrating cellular membranes. They can generate oxidative stress by disrupting mitochondrial function. Larger sheets tend to demonstrate lower cytotoxicity and improved stability. Functionalization strategies can include PEGylation, carboxylation, or peptide grafting [80]. They improve cytocompatibility by regulating protein corona formation and controlling cellular uptake. It shifts the biological response from an inflammatory to a regenerative response. At the organismic level, immune interactions are complex and can vary in accordance with the size, shape, and surface chemistry of the nanomaterial. Graphene oxide and carbon nanotubes may activate macrophages and dendritic cells. Biodistribution studies indicate potential accumulation in reticuloendothelial organs, including the liver, spleen, and bone marrow [81].

Most carbon-based materials, such as carbon fiber-reinforced PEEK (CF-PEEK) are inherently bioinert. It limits their ability to integrate directly with bone or soft tissues. Ultra-High-Molecular-Weight Polyethylene (UHMWPE) is also biologically inert. This limits immune responses and tissue irritation, as well as osseointegration, often resulting in fibrous tissue formation rather than direct bone bonding [82]. Plasma treatments and chemical functionalization can introduce oxygen, nitrogen, or hydroxyl groups, thereby improving wettability and facilitating protein adsorption. For example, oxygen plasma treatment of single-walled carbon nanotube films has been shown to enhance human osteoblast attachment and proliferation [83].

The application of bioactive coatings includes HA, calcium phosphates, and short peptide motifs such as arginine-glycine-aspartic (RGD) acid. It provides osteoconductivity and osteoblast adhesion [84]. Systems that combine carbon nanostructures with biodegradable polymers can provide load-bearing strength and the biological signals necessary for tissue integration. It improves osseointegration and stimulates vascularized bone formation. Porous carbons and carbon foams have been investigated as lightweight scaffolds with tunable porosity that can support osteoconduction and bone ingrowth [85].

 doi:10.20944/preprints202605.0674.v1

Polylactic acid (PLA) and polylactic-co-glycolic acid (PLGA) are biodegradable polymers used in temporary scaffolds and fixation devices, degrading safely without surgical removal [86]. Nanomaterials enhance surface bioactivity by increasing hydrophilicity and protein adsorption (fibronectin), upregulating osteogenic gene expression (RUNX2, ALP) and extracellular matrix mineralization. Degradation rates can be tuned by nanomaterial content, which balances scaffold resorption with tissue regeneration. These composites also modulate immune responses by reducing pro-inflammatory cytokines (IL-6, TNF-α), fostering a regenerative microenvironment [87].

Polymethyl methacrylate (PMMA) is widely used as bone cement for anchoring orthopedic implants due to its injectability and rapid setting. However, its brittleness and lack of bioactivity necessitate improvements. Incorporating CNTs or graphene enhances compressive and flexural strength, improving fatigue resistance under cyclic loading. These nanostructures confer antibacterial activity through the generation of reactive oxygen species and the physical disruption of bacterial cell walls, thereby reducing biofilm formation [88].

Polyetheretherketone (PEEK) composites with graphene oxide (GO) coating show osteogenic activity and antibacterial properties [89,90]. GO-decorated PEEK with specific properties demonstrates antibacterial activity [91]. It also accelerates cell proliferation and osteogenic differentiation.

Figure 17 demonstrates simplified stress-strain curves for carbon-based and polymer prosthetic materials.

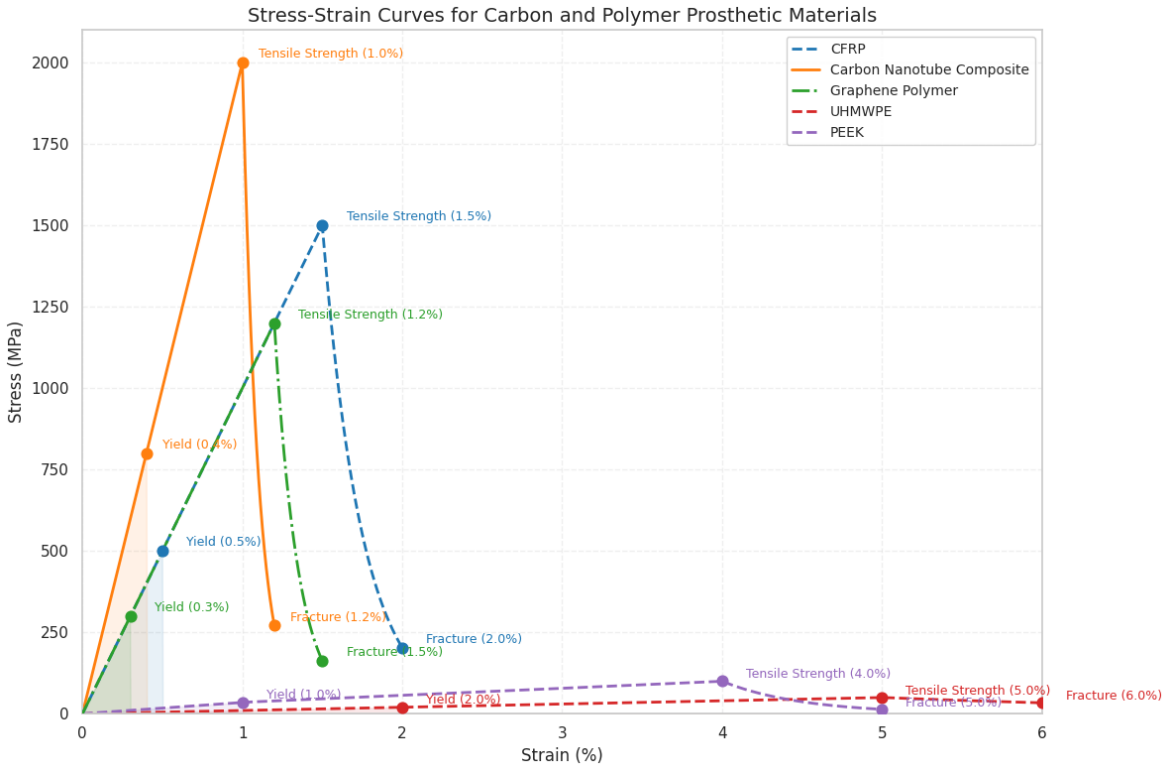

Figure 17. Stress–strain behavior of carbon-based and polymer prosthetic materials. CFRP, carbon-nanotube composites, and graphene-reinforced polymers achieve high strengths (1200–2000 MPa) but fail at low strains (<2%), whereas UHMWPE and PEEK exhibit lower strength yet markedly higher ductility (up to ~6%), more closely reflecting the deformation behavior of trabecular bone.

Carbon fibers in the polymethyl methacrylate (CF-PMMA) matrix (Figure 18) are chopped with a maximal length of 100–500 μm, sometimes up to 1 mm. Fibers are made of graphitic carbon with a diameter of 5–10. It is used as a bone void filler, in craniofacial reconstruction and vertebroplasty.

 doi:10.20944/preprints202605.0674.v1

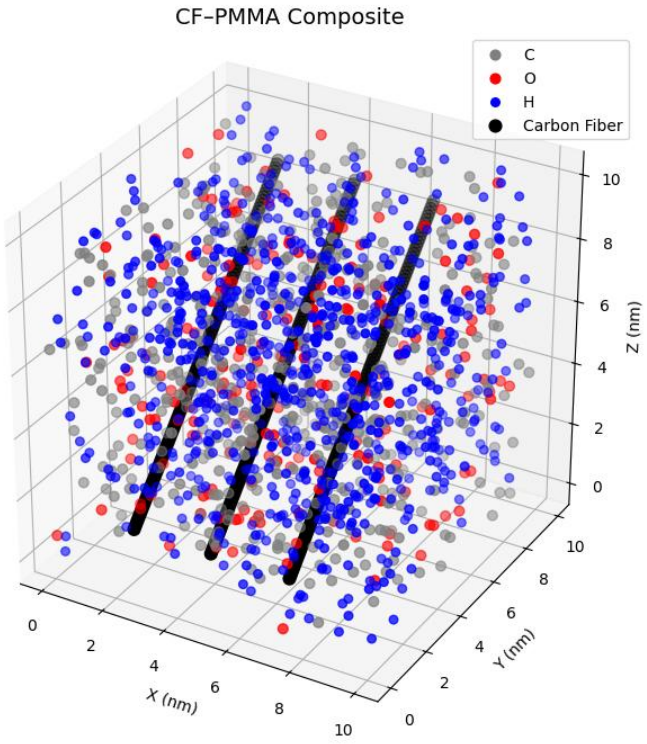

Figure 18. (CF-PMMA composite). Molecular structure of a carbon fiber–PMMA (CF-PMMA) composite, showing aligned carbon fibers embedded within a matrix of carbon (C), oxygen (O), and hydrogen (H) atoms across a 10 × 10 × 10 nm volume. The reinforcing carbon fibers provide structural stiffness within the compliant PMMA matrix, supporting its use as a bone void filler in craniofacial reconstruction and vertebroplasty.

Polyetheretherketone (PEEK) is a semicrystalline thermoplastic with a relationship of 30–35% crystalline and 65–70% amorphous (Figure 19) [92]. Crystalline regions form small lamellae with a thickness of 10–50 nm. They make fibers with a granular structure. This part provides stiffness, tensile strength, and thermal stability, while the amorphous part is non-granular and provides flexibility and impact resistance. It is used as rods and vertebral interbody fusion cervical, lumbar, and thoracic cages.

 doi:10.20944/preprints202605.0674.v1

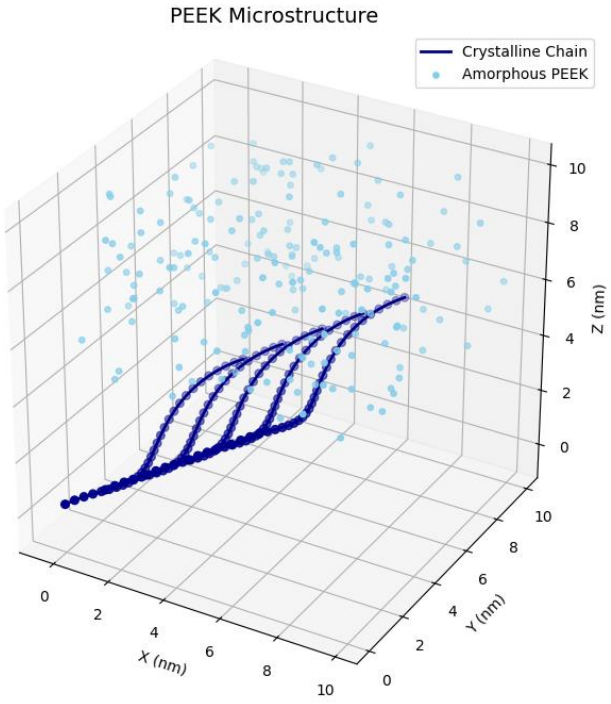

Figure 19. Microstructure of polyetheretherketone (PEEK). The molecular architecture shows crystalline lamellae (30–35%) embedded within an amorphous matrix (65–70%) in a 10 × 10 × 10 nm volume. The crystalline phase imparts stiffness and tensile strength, while the amorphous regions provide flexibility and impact resistance, supporting PEEK's use in spinal rods and interbody fusion cages.

Ultra-high molecular weight polyethylene (UHMWPE) is a semi-crystalline polymer with a higher level of crystallinity, from 40 to 60%. It is softer than CF-PMMA or PEEK but has high toughness and wear resistance [93]. It is suitable for articulating surfaces in joint replacements, such as a liner or tibial insert in the knee reconstruction.

Poly-L-lactic acid (PLLA) and poly-D-lactic acid (PDLA) are two stereoisomers of polylactic acid (PLA). While PLLA is semicrystalline, PDLA is mostly amorphous. They have specific biodegradation times: 1.5-5 years for PLLA and 6-12 months for PDLA. A mixture of both can help to regulate resorption time. While PLA is softer than other polymers and can be brittle, it is suitable for temporary supporting structures. 3D printing is applicable [92].

Carbon nanotubes are not a standalone material, but a reinforcement for a polymer matrix. Single-wall carbon nanotubes (SWCNTs) (Figure 20) have a hexagonal carbon layer as a wall, or multi-wall carbon nanotubes (MWCNTs). PMMA, PLLA, and PEEK can be reinforced with CNTs via dispersion at weight percentages below 5% to avoid agglomeration or brittleness. CNTs can be aligned to achieve maximum tensile strength along the axis or oriented randomly to achieve quasi-isotropic, uniform mechanical improvement. CNT-reinforced composites are used as spinal cages, orthopedic plates and screws, resorbable bone scaffolds, and joint-bearing surfaces [77,78].

 doi:10.20944/preprints202605.0674.v1

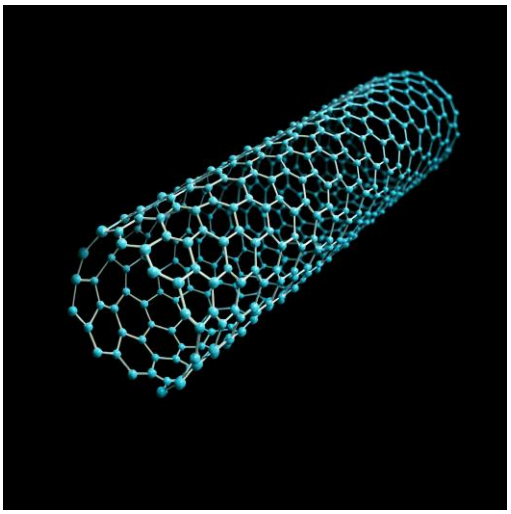

Figure 20. Single-Wall Carbon Nanotube (SWCNT).

3.1.4. Composite and Hybrid Material Combinations

The complexity of mechanical requirements, biocompatibility characteristics, and surface interactions may necessitate the creation of implants and grafts composed of more than one material and with a specific architectural composition (Table 11). Two or more components can have different types of relationships with different proportions, such as hybrid materials as molecular mixtures, composite materials as layered structures or macro mixtures, cores or bases with coating or more complex relationships (Figure 21).

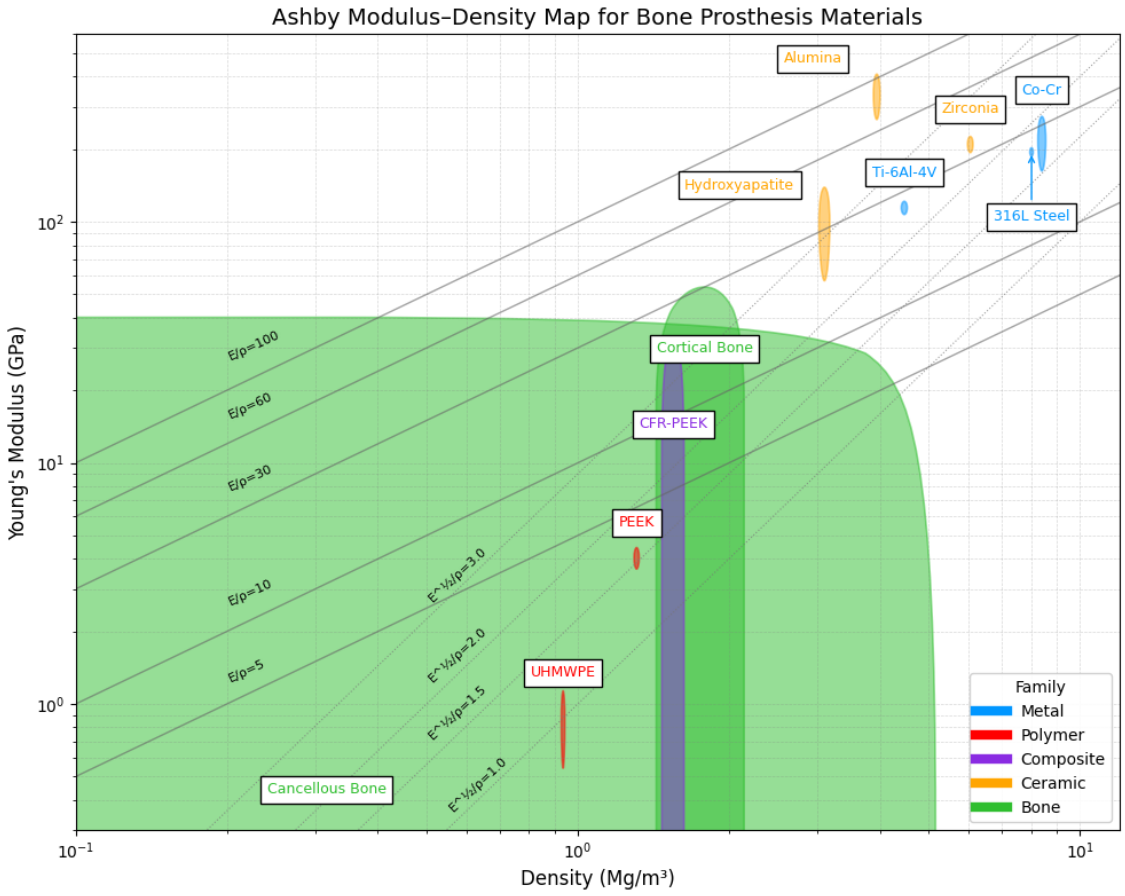

Figure 21. Ashby modulus–density map for prosthetic material families compared with bone. Metals (Co-Cr, Ti-6Al-4V, 316L steel) and bioceramics (alumina, zirconia, hydroxyapatite) exhibit moduli far above those of

 doi:10.20944/preprints202605.0674.v1

cortical and cancellous bone, while CFR-PEEK and PEEK plot closest to cortical bone in both stiffness and density. UHMWPE aligns with cancellous bone, highlighting the potential of polymers and composites to reduce modulus mismatch in advanced prosthetic designs.

Main components usually provide basic functionality, such as load-bearing, filling, or bioactivity. Metamaterials with specific mechanical or physical properties can be used as such a component (see Table 11). Sub-wavelength unit cells in metamaterials can focus different types of waves [94] to enhance osseointegration and regeneration [95]. Ultrasound at 1–10 MHz has wavelengths of approximately 0.15–1.5 mm and is often used to stimulate metamaterials with submillimeter structures (10–100 μm) [96]. Smart materials exhibit additional responsiveness to external environmental stimuli such as temperature, pressure, electric field, and pH [97]. Some smart materials can be designed as metamaterials.

Table 11. Composite and hybrid bone implant and graft materials.

Hybrid or composite type	Mechanical properties and components	Biological notes and anatomical applications
Metal with dispersed ceramic particles (Ti–HA, Ti–ZrO_2)	Metal component: High strength and stiffness; Ceramic component: Moderate stiffness, brittle	Strong load-bearing, osseointegrative; hip and knee prostheses, spinal fixation; joint arthroplasty surfaces
Metal core with bioglass coating (Ti–Bioglass)	Metal core: High strength; Bioglass coating: Lower stiffness, brittle	Bioactive, antibacterial; dental implants, craniofacial plates, articular surface coatings
Polymer–Ceramic composite (PEEK–HA, PLLA–HA)	Polymer matrix: Low-to-moderate strength; Ceramic filler: Moderate stiffness	Bioactive, degradable, osteoconductive; spinal cages, bone scaffolds, craniofacial scaffolds
Polymer–Bioglass composite (PLGA–Bioglass)	Polymer matrix: Low-to-moderate strength; Bioglass filler: Lower stiffness	Bioactive, degradable; spinal cages, craniofacial scaffolds, cartilage repair
Carbon fiber reinforced ceramic composite (CF–HA, CNT–HA)	Ceramic matrix: Moderate-to-high stiffness; Carbon fibers: Reinforcement	Osteoconductive, high fatigue life; craniofacial plates, spinal fixation plates, load-bearing joint implants
Carbon fiber reinforced bioglass composite (CF–Bioglass, CNT–Bioglass)	Bioglass matrix: Lower stiffness, brittle; Carbon fibers: Reinforcement	Osteoconductive, high fatigue life; craniofacial plates, spinal fixation plates, articular coatings
Biphasic ceramic–bioglass composite (HA–Bioglass, TCP–Bioglass)	Ceramic component: Moderate-to-high stiffness; Bioglass component: Lower stiffness, brittle	Highly bioactive, controlled degradation; bone defect fillers, dental scaffolds, joint surfaces
Metal core with ceramic and bioglass coatings (Ti–HA–Bioglass)	Metal core: High strength; Ceramic coating: Moderate stiffness; Bioglass coating: Lower stiffness	Load-bearing with bioactivity; hip/knee prostheses, spinal fixation, craniofacial plates
Polymer–Ceramic–Carbon hybrid (PEEK–HA–CF)	Polymer matrix: Low-to-moderate strength; Ceramic filler: Moderate stiffness; Carbon fibers: Reinforcement	Combines stiffness, toughness, fatigue resistance; spinal cages, craniofacial plates, articular surfaces

 doi:10.20944/preprints202605.0674.v1

Polymer–Ceramic–Carbon–Bioglass hybrid (PEEK–HA–CF–Bioglass)	Polymer matrix: Low-to-moderate strength; Ceramic filler: Moderate stiffness; Carbon fibers: Reinforcement; Bioglass filler: Lower stiffness	Combines stiffness, toughness, fatigue resistance, bioactivity; spinal cages, craniofacial plates, articular surfaces
Multicomponent polymer–ceramic–carbon–bioglass–metal/alloy (PEEK–HA–CF–Bioglass–Ti–Ni fibers	Polymer matrix: low-to-moderate strength (continuous 3D); Ceramic: moderate stiffness; Carbon fibers: reinforcement; Bioglass: bioactive filler; Metal/alloy fibers: high stiffness, functional -smart	Multifunctional: adaptive stiffness, bioactivity, fatigue resistance; spinal cages, craniofacial plates, load-bearing, stimuli-responsive implants

Two-component composites and hybrids: Metal alloys with dispersed ceramic particles (Ti–HA, Ti–ZrO_2) consist of a metal matrix reinforced with ceramic particles. The metal forms a continuous 3D component, while ceramic particles are dispersed. They are added for better osseointegration in load-bearing prostheses and spinal fixation [98]. Metal core with bioglass surface coating (Ti–Bioglass) combines a continuous titanium component with a thin bioglass outer layer. In addition to being surface-resistant to wear, it offers bioactivity and antibacterial properties. These properties are also used in dental implants and craniofacial plates [99]. Interpenetrating polymer–ceramic composites (PEEK–HA, PLLA–HA) integrate a strong polymer matrix with dispersed ceramic particles. Some scaffolds achieve partial 3D interpenetration at the microstructural level. They can form supportive, degradable, osteoconductive spinal cages and craniofacial scaffolds. However, modulus mismatch with bone can still occur [100]. Biphasic ceramic–bioglass composites (HA–Bioglass, TCP–Bioglass) are suitable as bioactive bone defect fillers and dental scaffolds. However, brittleness limits load-bearing use [99]. Carbon fibere-reinforced ceramic composites (CF–HA, CNT–HA) embed continuous or oriented carbon fibers into a ceramic matrix. They enhance tensile strength and fatigue life for osteoconductive craniofacial and spinal fixation plates [101]. Carbon fiber-reinforced bioglass composites (CF–Bioglass, CNT–Bioglass) similarly combine a bioglass matrix with reinforcing carbon fibers, improving fatigue resistance. The brittleness of bioglass can limit toughness [99].

Three-component composites and hybrids: Polymer–ceramic–carbon composites (PEEK–HA–CF) consist of a polymer matrix, dispersed ceramic fillers, and carbon fiber reinforcements. The polymer provides a continuous 3D component. Ceramics act as discrete stiffening fillers. Carbon fibers provide reinforcement in specific directions. These implants, grafts, and structures are osteoconductive and mechanically robust and can be used as scaffolds suitable for spinal cages and craniofacial plates [100,101].

Four or more-component composites hybrids: Multicomponent composites and hybrids (PEEK–HA–CF–Bioglass) can integrate polymers, ceramics, carbon, bioglass, and metals. The polymer forms a continuous matrix, ceramic and bioglass act as reinforcing or bioactive fillers, and carbon fibers provide high-strength reinforcement. These 3D structures balance stiffness, toughness, fatigue resistance, and bioactivity for spinal cages and craniofacial plates. Fabrication requires careful control of interface adhesion and component distribution to avoid delamination or mechanical instability [100,101]. Metal or alloy fibers can be added to provide high stiffness. They can also exhibit specific functional properties, such as shape memory or magnetostrictive responses. These multicomponent systems are often designed as lattices or interconnected cellular architectures. They can combine mechanical robustness, controlled energy absorption, bioactive signals, and adaptive response in a single implant. Composites can include layers. Proper component integration and interface engineering are important to prevent delamination or stress concentrations (Figure 22). They can be used in spinal, craniofacial, and load-bearing orthopedic applications.

 doi:10.20944/preprints202605.0674.v1

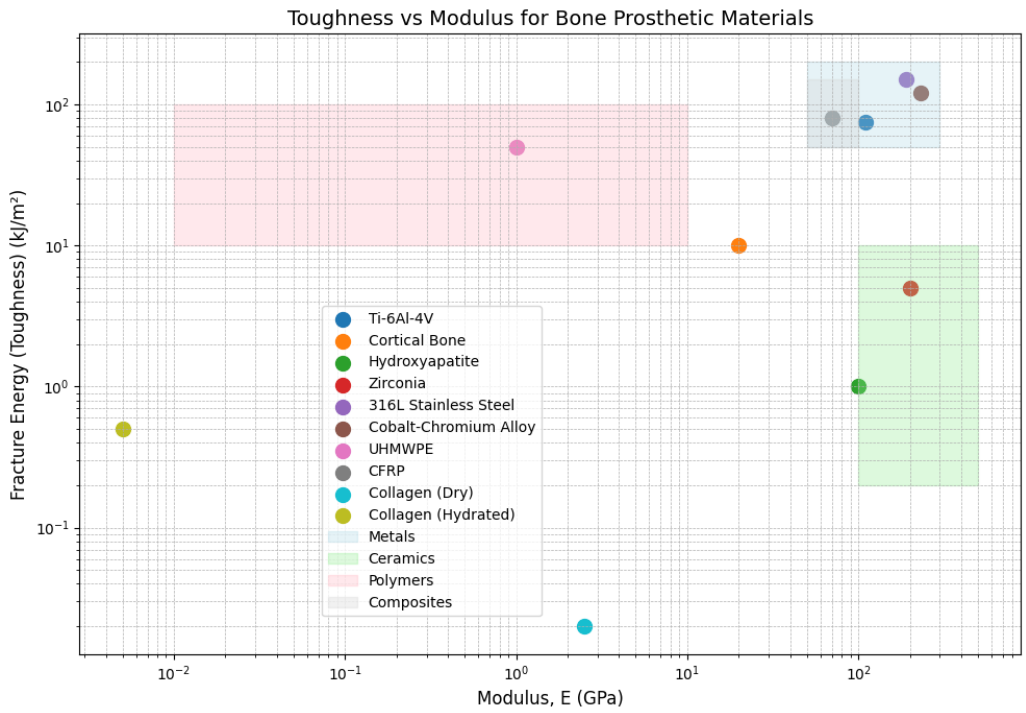

Figure 22. Toughness versus Young's modulus for prosthetic material families compared with bone. Metallic alloys (Ti-6Al-4V, 316L stainless steel, Co-Cr) combine high modulus with high fracture energy, whereas bioceramics (hydroxyapatite, zirconia) show high stiffness but low toughness, reflecting their brittleness. Cortical bone occupies an intermediate region, while polymers such as UHMWPE provide high toughness at low modulus. These contrasts underscore the need for careful interface engineering to avoid stress concentrations in load-bearing orthopedic applications.

3.2. Biocompatibility of Composite and Hybrid Systems

The biological compatibility of bone implants is evaluated across several domains (see Table 4). The main focus points can be grouped into the following categories: biological compatibility and cellular response; osseointegration and bone remodeling; surface and interfacial properties; and material stability and mechanical performance (Table 12). The ISO 10993 series provides a standardized framework for assessing cytotoxicity, immunogenicity, genotoxicity, and tissue compatibility (Food and Drug Administration (FDA), 2023). It employs both in vitro cellular assays and in vivo histopathological examination of peri-implant tissues (ISO 10993-1:2018). Initial material screening typically employs cytotoxicity testing using osteoblasts or mesenchymal stem cells. However, recent studies have revealed significant limitations in the standard ISO 10993-5 protocols, particularly concerning the cell variability in test conditions and the lack of specificity for certain biomaterials in direct contact with cells [102,103]. There are also ways to register septic and aseptic inflammatory reactions. The local inflammatory environment is characterized by cytokine release profiles. Levels of IL-6 and TNF-α are measured [104]. The balance between pro-inflammatory M1 and pro-regenerative M2 macrophage phenotypes influences whether the implant triggers chronic inflammation or productive tissue remodeling [105].

Osseointegration is the establishment of a direct structural connection between bone and implant. It represents the primary functional outcome for load-bearing implants [105]. Osseointegration and bone remodeling are evaluated in several ways. They are measured through alkaline phosphatase activity, mineralization patterns, and expression of RUNX2 and osteocalcin [106]. Osteogenic differentiation assays determine whether the material actively supports bone formation and osseointegration [107]. Osseointegration and overall biocompatibility can be affected by surface properties. Surface properties exert direct control over early biological events at the bone-implant interface. Microscale and nanoscale topography, surface roughness, wettability, and surface

 doi:10.20944/preprints202605.0674.v1

energy are modulating the initial protein adsorption layer. This layer dictates cell adhesion, spread and differentiation [108].

Material degradation and ion-release kinetics are also factors in biocompatibility. Excessive metal ion leakage can induce cytotoxic effects locally or on the organizmic level. It can also cause systemic accumulation [109]. Mechanical compatibility requires matching the implant's elastic modulus shielding [110]. It also has to be connected to cyclical loads. Wear resistance in a wet, corrosive biological environment can indicate surface particles detaching from the implant.

Table 12. Biocompatibility and Osseointegration Assessment Criteria for Bone Implants.

Metric	Description	Assessment Method(s)
Overall Biocompatibility (ISO 10993 Series)	Integrated evaluation of local and systemic biological responses to the implant, encompassing cytotoxicity, immunogenicity, genotoxicity, tissue compatibility.	In vitro: ISO 10993-5 (cytotoxicity), -10 (irritation), -11 (systemic toxicity). In vivo: subcutaneous or intramedullary implantation; histopathology of peri-implant tissue, inflammation, fibrosis, necrosis; systemic compatibility
Cytotoxicity (ISO 10993-5)	Measures the viability of osteogenic cells in contact with the material or its extract.	MTT, Alamar Blue, or Live/Dead assays using osteoblasts, MSCs, or MC3T3-E1 cells.
Inflammatory or Immune Response	Measures local immune reaction to the implant.	Cytokine assays (IL-6, TNF-α), macrophage polarization (M1/M2) by immunostaining.
Osteogenic Differentiation Potential	Evaluates the material's ability to induce osteoblast differentiation and mineralization.	ALP activity, Alizarin Red staining, qPCR or immunostaining for RUNX2, OCN, COL1A1.
Tissue Integration Osseointegration Score	Quantifies bone–implant interfacial bonding and tissue ingrowth.	Histomorphometry, BIC %, micro-CT, or histology.
In Vivo Bone Remodeling Response	Assesses new bone formation, remodeling, and resorption around the implant.	Histology, micro-CT, dynamic histomorphometry (fluorochrome labeling).
Surface Roughness and Topography	Characterizes micro- and nanoscale surface features that affect cell behavior.	AFM, profilometry, SEM.
Surface Energy and Wettability	Reflects hydrophilicity and surface chemistry influencing protein adsorption.	Contact-angle measurement, surface-free-energy calculation.
Protein Adsorption Profile	Identifies and quantifies proteins bound to the surface.	BCA assay, SDS-PAGE, LC-MS.
Biofilm Formation Potential	Evaluates bacterial adhesion and colonization on the implant surface.	Crystal-violet assay, SEM, or confocal microscopy with *S. aureus* / *S. epidermidis*.
Ion Release / Leaching	Quantifies release of metallic ions or degradation by-products.	ICP-MS, AAS of immersion media.
Corrosion / Degradation Rate	Assesses chemical breakdown under physiological conditions.	Potentiodynamic polarization, immersion in SBF or PBS, ICP-MS, gravimetric loss.

 doi:10.20944/preprints202605.0674.v1

Mechanical Compatibility (Elastic Modulus, Strength)	Comparable stiffness and strength with cortical or trabecular bone.	Compression, bending, or nanoindentation testing.
Fatigue and Wear Resistance	Evaluates resistance to cyclic mechanical loads and wear in wet environments.	Fatigue testing, fretting wear, cyclic compression in SBF.

Composite and hybrid systems integrate several material components. Interfaces are engineered using electrophoretic deposition, sol-gel processing, plasma spraying, sputtering, Chemical Vapor Deposition (CVD), Physical Vapor Deposition (PVD), dip coating, laser cladding, ion implantation, biomimetic mineralization, and 3D printing [111]. Complex compositions can synergize controlled biological interactions through the careful choice of components` order and contact surfaces. Levels of inflammatory cytokines IL-1β, IL-6, and TNF-α are reduced around HA-coated titanium in Ti–HA implants [112]. The HA layer releases calcium (Ca^{2+}) and phosphate (PO_4^{3-}) ions at biocompatible concentrations that upregulate osteogenic genes (ALP, OCN, RUNX2) through calcium-sensing receptor activation and MAPK pathway signaling [113,114]. In the HA-Ti system, ion scavenging effects reduce Reactive Oxygen Species (ROS) production and preserve mitochondrial function. This maintains cell viability 80-90% in direct-contact assays for cytotoxicity studies [115]. Surface energy modifications enhance the adsorption of fibronectin and vitronectin (Figure 19), stimulating integrin-mediated focal adhesion (FA) and mechanotransduction intracellular pathways [116]. Histological analysis shows reduced local fibrous encapsulation with capsule thickness below 50 μm. Histomorphometry demonstrates Bone-Implant Contact (BIC) reaching 80-95% at 12 weeks post-implantation [66]. Other positive effects have been observed in Diamond-Like Carbon (DLC) coatings. Levels of anti-inflammatory cytokines IL-10 and TGF-β1 are increased around DLC-coated titanium implants. It demonstrates enhanced anti-inflammatory and regenerative responses [117].

Carbon fiber-reinforced polymer composites have mechanical properties that more closely match those of natural bone. They have a reduced elastic modulus and lower stress-shielding effects. However, carbon components demonstrate inherent bioinertness. It limits direct osseointegration [118]. CF-PEEK composites with bioactive additives address it. Incorporation of HA or bioactive glass into the polymer matrix provides osteoconductivity. while preserving the mechanical advantages of carbon reinforcement. Surface energy modifications by surface plasma treatment or bioactive glass deposition increase implant wettability and fibronectin and vitronectin absorption, thereby improving osteoblast attachment [83]. These composites or hybrids achieve BIC percentages of 70-85% with thinner fibrous capsule formation if compared to untreated carbon-polymer systems. It also reduces activation of the complement system and improves hemocompatibility. It means lower occurrence of immune-mediated inflammation and clotting.

 doi:10.20944/preprints202605.0674.v1

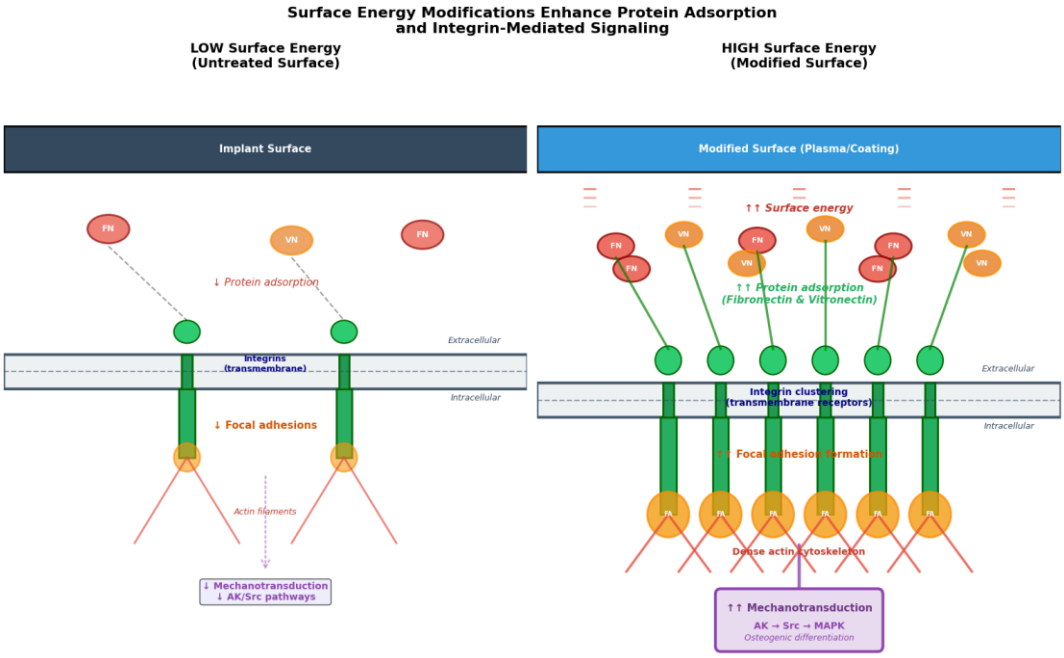

Figure 19. Influence of surface energy on protein adsorption and mechanotransduction at the implant interface. Low-energy untreated surfaces exhibit limited fibronectin and vitronectin adsorption, sparse integrin clustering, and weak focal adhesion formation, resulting in reduced AK/Src signalling. High-energy modified surfaces promote dense protein adsorption, integrin clustering, and robust focal adhesion assembly, activating the AK→Src→MAPK pathway and supporting osteogenic differentiation.

A biodegradable composite of the systems can be designed with control of degradation kinetics with preserved biocompatibility. Magnesium alloys with polymer-ceramic coatings can regulate Mg^{2+} ion release at a level (Cusanno et al., 2025) sufficient to activate Wnt signaling pathways for osteogenesis, but below the trigger level of hypermagnesemia. Protective coatings buffer local changes in tissue and fluid pH during degradation (Husak et al., 2018). They reduce ROS production. Coatings suppress pro-inflammatory cytokine expression. For example, IL-1β level is reduced (Frumento and Țălu, 2025). In vitro, studies demonstrate cell viability of 90-95%. In vivo tissue integration processes show BIC exceeds 85% with fibrous capsule thickness below 30 μm. Tantalum-infused bioactive glass combines tantalum's hemocompatibility and corrosion resistance with bioactive glass's osteoinductive ion release. It is suitable for load-bearing applications with direct bone contact (Wang, X., et al. 2022).

Carbon nanomaterials can catalyse the formation of ROS, such as superoxide, hydrogen peroxide and hydroxyl radicals. High ROS levels lead to oxidative stress with damage to molecules, lipids, proteins, and DNA. It can also trigger programmed cellular death or apoptosis and unprogrammed necrosis. The high aspect ratio of carbon nanotubes and the sharp edges of graphene sheets can physically disrupt cell membranes. It alters membrane integrity and potential and can damage the structure and functionality of integral membrane proteins, including ion channels and receptors. Inside the cell nanostructures can interfere with mitochondrial function, reduce ATP production, and disrupt cytoskeletal organization. Protein adsorption onto their surfaces may induce endoplasmic reticulum stress and activate inflammatory pathways.

Carbon nanomaterial-bioceramic hybrids can address the cytotoxicity concerns associated with native carbon nanostructures, such as graphene, graphene oxide, carbon nanotubes (CNTs), and carbon nanodots (CNDs). Carbon nanomaterial concentrations below 25 $\mu g \cdot mL^{-1}$ in composite formulations exhibit low cytotoxicity in vitro, with reductions in viability at higher levels attributable to apoptosis, particularly above 50 $\mu g \cdot mL^{-1}$ (Zhou et al., 2017). At 200 $\mu g \cdot mL^{-1}$, carboxyl and hydroxyl functionalized MWCNTs aggregate more than non-oxidized MWCNTs and cause necrosis and a

 doi:10.20944/preprints202605.0674.v1

higher level of DNA oxidation. Ceramic encapsulation and surface modification can reduce all these effects. HA and bioglass can also be incorporated. PEGylation and peptide grafting can further improve cytocompatibility by regulating protein corona formation and controlling cellular uptake. It can shift biological responses from inflammatory and cytotoxic toward regenerative (Spinelli et al., 2022).

Multicomponent composite or hybrid systems combine distinct biocompatibility mechanisms in a single implant construct. Titanium-CNT-HA composites or hybrids integrate HA for calcium and phosphate ion signaling carbon nanotubes for ROS scavenging and mechanical reinforcement. They can also incorporate RGD-like peptide motifs (Arg-Gly-Asp) for enhanced integrin binding. These systems demonstrate complex biocompatibility profiles. They include inflammatory cytokine levels` reduction, improved hemocompatibility through reduced platelet adhesion, and long-term tissue integration. Cell viability exceeds 85-95% and osseointegration has a BIC of 80-95% (Williams, 2021).

Table 13. Physico-mechanical properties of bones and materials ordered by Young's modulus.

Group	Young's Modulus (GPa)	Tensile Strength (MPa)	Compressive Strength (MPa)	Density (g/cm³)	Examples / Notes
Porous / Immature / Weak Bones	0.1–12	5–60	2–120	0.1–2.2	Cancellous, woven, osteomalacic, osteoporotic, Pagetic bones; very low stiffness; energy absorption; deformable
Mature Cortical / Load-Bearing Bones	15–25	50–150	100–250	1.8–2.1	Cortical, lamellar, Haversian, subchondral bone; main structural support
Dense Pathological Bones (Osteopetrotic)	25–35	50–100	200–400	2.5–3.0	Extremely stiff, brittle; low repair potential
Lightweight Metals & Composites	45–150	200–1500	200–950	1.6–4.5	Mg, Ti, CF, CF-reinforced Ti; high strength-to-weight, fatigue resistant, conductive
Bioactive / Hard Ceramics	80–500	100–1000	200–4000	3.1–5.6	HA, Al_2O_3, ZrO_2, SiC; extremely hard, brittle; coatings or articulating surfaces
Heavy Metals	210	700–1000	800–1200	6.5–8.3	Co-Cr, high stiffness, wear-resistant, heavy
Nanostructured Carbon Materials	500–1000	3000–5000	600–1000	1.3–1.5	CNTs, Graphene; ultra-high strength-to-weight; conductive; ideal for smart prosthetics

4. Integration of Smart Functionality Elements

4.1. Integration Problem

 doi:10.20944/preprints202605.0674.v1

Bone implants and grafts based on the biomedical materials discussed above have transitioned from passive implants to active, responsive systems capable of adapting to physiological conditions in real time (Hager et al., 2015). Smart materials and metamaterials possess biocompatibility and mechanical properties and can exhibit dynamic responses to mechanical, electrical, thermal, or chemical stimuli (Meng and Li, 2013). Multi-component composite or hybrid systems incorporating these materials can develop implants that adapt, sense, and respond to their biological environment (Jani et al., 2014).

Smart materials can change their properties in response to external stimuli. They include shape-memory effects, piezoelectric responses, magnetostrictive behavior, and conductivity modulation (Sun et al., 2012). Conventional biomaterials can be integrated with smart components. It provides a range of diagnostic and therapeutic functionalities, including controlled drug release, real-time clinical monitoring, adaptive mechanical capabilities, and active tissue integration via bioelectric stimulation (Mano, 2008). The constraint for smart component integration is ensuring structural integrity. The complexity of the problem rises in implants with multiple material components and several functionalities (Ratner et al., 2004).

The integration of smart functionality into biomedical implants has three primary categories. They include smart materials, sensors and actuators (Ponmozhi et al., 2009). Smart materials are stimuli-responsive and can autonomously adapt to environmental changes. Sensors are primarily used to monitor physiological parameters and implant performance. Actuators can provide mechanical and electrical stimulation, active peri-implant bioenvironmental response, or localised, precisely focused delivery of medication, bioactive substances, or cells.

Sensors embedded within specific implant parts enable real-time detection of mechanical loading, such as strain, stress or pressure. Sensitivity can be as little as from 0.01% for strain. Sensors can also detect and transmit chemical changes, such as pH, ion concentrations, and biomarker levels. Sensitivity can be 10^{-9} M for biochemical detection. Thermal variations registration, such as temperature gradients, may indicate aseptic inflammation or infection (Kim et al., 2011; Windmiller and Wang, 2013).

Actuators in smart bone implants can provide controlled therapeutic outputs through multiple modalities. Piezoelectric actuators enable mechanical stimulation with displacements at the nanometer to micrometer scale. It facilitates mechanotransduction and bone remodeling (Tandon et al., 2018). Electrical stimulation systems can produce current densities in the range of 5–20 $\mu A/cm^2$. They have been shown to enhance osteogenesis and accelerate bone healing (Griffin and Bayat, 2011). Smart materials can combine sensing and actuation capabilities within single-component or multi-component architectures. It enables closed-loop feedback systems in which detected stimuli trigger appropriate material responses without external intervention (Lendlein and Kelch, 2002). The integration of sensors, actuators, and smart materials into multi-component composite or hybrid systems enables complex implant functionalities. It can include self-monitoring for early problem detection, adaptive load distribution to prevent stress shielding, controlled drug delivery triggered by physiological needs, and bioelectric stimulation optimized through real-time feedback (Dvir et al., 2011).

4.2. Material-Specific Smart Integration Capabilities

The integration of sensing, actuation, and computational capabilities into orthopedic implants requires consideration of material-specific constraints on electronic functionality (Table 14). Sensor accuracy varies across material platforms due to their intrinsic mechanical and electrical properties. It is often defined as the precision of embedded force, strain, or electromyographic (EMG) signal acquisition, but is not limited to it. Metallic implants, particularly titanium and its alloys, provide rigid substrates. It enables accurate strain-gauge integration and force measurement. However, the electrical conductivity of alloys necessitates electromagnetic interference (EMI) shielding to prevent signal degradation (Ledet et al., 2018).

 doi:10.20944/preprints202605.0674.v1

Bioceramics such as hydroxyapatite and zirconia provide efficient electrical insulation. It minimizes interference, but the bioceramic brittle nature limits sensor embedding to surface-mounted configurations (Peres et al. 2022). Polymeric materials such as polyetheretherketone (PEEK) and polycaprolactone (PCL) facilitate conformal sensor integration through their flexibility. However, viscoelasticity can introduce time-dependent signal drift under sustained loading conditions (Klimm and Kwok, 2022). Composite materials architectures with carbon fiber reinforcement and polymer matrices offer tunable mechanical properties. They can balance the rigidity required for accurate sensing and the flexibility needed for patient-specific adaptation (Niinomi and Nakai, 2011).

Response latency, or the temporal delay between physiological input detection and adaptive actuation, is minimal in rigid metallic and ceramic systems. It increases marginally in polymeric platforms due to their viscoelastic compliance (Kumar et al. 2023). Signal-to-noise ratio (SNR) is significantly higher in electrically insulating ceramics and polymers compared to conductive metals. Metallic alloys generate electromagnetic artefacts, and active filtering or shielding strategies have to be applied (Ledet et al. 2018). Power efficiency is influenced by thermal management requirements. It is measured in milliwatts per sensing or actuation function. The high thermal conductivity of metals demands additional insulation to prevent tissue heating. Polymers have low thermal mass, supporting energy-efficient operation (Kumar et al. 2023).

Wireless data stability is important for remote monitoring and telemetry. It is material-specific. Metallic components attenuate radiofrequency (RF) signals and require strategic antenna placement. Bioceramics and polymers demonstrate RF transparency, which enhances wireless communication reliability (Huang et al. 2025). Rigid metallic systems provide consistent mechanical feedback. Flexible polymeric substrates or sensors can provide continuous strain monitoring (Burton et al., 2021).

Table 14. Material-dependent smart functionality criteria for bone implants and grafts.

Metric	Description	Relevance / Material Considerations
Sensor Accuracy (%)	Precision of embedded force, motion, or EMG sensors.	*Metals*: High stiffness allows accurate strain/force sensing; may need EMI shielding. *Bioceramics*: Brittle; limits embedded sensors, mainly surface-mounted. *Polymers*: Flexible substrates allow conformal sensors; minor drift under load.
Response Latency (ms)	Time from input to adaptive actuation.	*Metals*: Minimal latency due to rigidity. *Bioceramics*: Minimal latency; rigid but brittle. *Polymers*: Slightly higher latency due to viscoelastic compliance.
Signal-to-Noise Ratio (SNR)	Quality of biosignal acquisition vs. background noise.	*Metals*: Conductive; may generate EM interference; requires shielding. *Bioceramics*: Electrically insulating; naturally reduces interference. *Polymers*: Flexible; isolates sensors; low interference.
Power Efficiency (mW per function)	Energy consumption of embedded electronics.	*Metals*: High thermal conductivity; may require insulation. *Bioceramics*: Low conductivity; careful thermal design needed. *Polymers*: Low thermal mass; energy-efficient.
Wireless Data Stability (%)	Reliability of telemetry, remote monitoring, and wireless control.	*Metals*: May attenuate RF signals; antenna placement critical. *Bioceramics*: RF-transparent; good wireless signal propagation. *Polymers*: RF-transparent; stable wireless signals.

 doi:10.20944/preprints202605.0674.v1

Self-Adaptation; AI and ML Learning Rate	Speed and efficiency of ML-driven adjustments to tissue and usage patterns.	*Metals*: Rigid feedback supports predictable learning. *Bioceramics*: Limited deformation; mainly surface sensor adaptation. *Polymers*: Flexible; allows adaptive sensing and personalized calibration.

4.2.1. Bioceramic Implants and Grafts

Bioceramics present challenges for smart integration. It has insulating properties, with a resistivity of 10^8- 10^{14} Ω·cm for HA. It limits direct electrical functionality (Hench, 2006). These limitations can be overcome through coating, composite, and hybrid design strategies. Conductive coatings, such as CNTs, graphene, conductive polymers of 1-10 μm thick on ceramic substrates, can provide electrical functionality with sheet resistance 10^2-10^4 Ω/sq. Implants still maintain the bioactive properties of the ceramic core (Vallet-Regí and Ruiz-Hernández, 2011).

Sensors` functionality in bioceramic systems requires surface modifications or embedded conductive components. Carbon nanotube coatings with a thickness of 5-50 μm on bioceramic surfaces can provide strain sensing capabilities with gauge factors of 10-100. The configuration maintains biocompatibility, with cell viability exceeding 90% (Zhang et al., 2020). Another approach is the integration of conductive polymers, such as PEDOT: PSS or polyaniline, via infiltration into porous ceramic structures. The optimal porosity is 40-70%. In this way, it is possible to create composite and hybrid systems. They can be both bioactive and possess smart sensing properties, with conductivities of 1-100 S/cm (Balint et al., 2014).

An exception is piezoelectric hydroxyapatite with bioactivity and smart functionality. A single ceramic component has a piezoelectric coefficient d33 = 2-7 pC/N (Lang, 2011). The material can generate electrical charges in response to mechanical loads at physiological load stress levels of 1-10 MPa. The piezoelectric response can enhance bone formation by 30-50% through bioelectrical stimulation mechanizms, voltage-gated calcium channels activation (Sheikh et al., 2015).

4.2.2. Carbon-Based Smart Bone Prostheses

Carbon-based materials possess a number of useful qualities and high potential for sensory integration, either as part of the material or as standalone sensors. Some carbon-based materials not only have suitable mechanical properties (Popov, 2004; Lee et al., 2008) but also have inherent conductivity, such as 10^3-10^6 S/m for CNTs and 10^4-10^6 S/m for graphene and can be integrated into a suitable carbon-based matrix. CNTs and graphene demonstrate high capabilities for strain sensing with gauge factors of 10-1000, pressure detection with sensitivity 0.1-10 kPa^{-1}, and bioelectrical monitoring applications with impedance 10^3-10^6 Ω at 1 kHz [119,120]. CNTs have a high aspect ratio of length to diameter, bigger than 1000. They can enable the formation of percolation networks at loadings of 0.1-2 wt%. It can also provide sensing capabilities in composite structures [121].

Carbon nanomaterials can be integrated into composites used in bone prosthetics. The piezoresistivity properties make it capable of strain sensing through electrical resistance changes of $\Delta R/R$ = 1-10% per 1% strain under mechanical deformation [122]. These sensory systems can detect implant loading patterns with a resolution of 0.01% strain. Another possibility is to monitor tissue healing responses through changes in mechanical compliance. They can provide feedback for adaptive control of mechanical properties with response times under 10 ms [123]. The high sensitivity and fast response times of carbon-based sensors make them suitable for real-time monitoring applications, such as gait analysis and joint loading assessment [120].

Graphene-based systems can demonstrate multi-modal sensing capabilities. For example, mechanical sensing with a gauge factor of 2-200; thermal sensing with a temperature coefficient of resistance 10^{-3}-10^{-4} K^{-1}; chemical detection with limits of 10^{-9}-10^{-12} M for glucose and lactate [124,125]. Graphene-enriched materials can monitor multiple physiological parameters simultaneously. It enables comprehensive information on implant performance and tissue responses at sampling rates

 doi:10.20944/preprints202605.0674.v1

up to 1 kHz. The atomic-scale thickness of graphene, 0.34 nm per layer, enables its integration without affecting the overall material properties [126].

Polyetheretherketone (PEEK) composites with graphene oxide (GO) can support multimodal cellular- and tissue-focused therapeutic applications. It can be operated via synergistic photothermal and photodynamic effects, with temperature control for localized therapy [89]. GO-PEEK systems demonstrate electrical conductivity. It enables bioelectrical signal monitoring and electrical stimulation applications in orthopaedic implants [127,128].

Polymethylmethacrylate (PMMA) bone cement modified with graphene nanoplatelets (GnP) demonstrates electrical conductivity. This property enables real-time monitoring of the healing process via resistance measurements during polymerization [129]. Multi-Walled Carbon Nanotubes (MWCNTs) in PMMA at 0.1-0.5 wt% provide piezoresistive sensing capabilities. It can detect load and microdamage in cemented implants [130,131].

Thermoplastic polyurethane (TPU) composites with CNTs are capable of flexible strain sensing. It is applied for prosthetic monitoring. CNT-TPU composite yarns demonstrate gauge factors of 67.2 at strains below 50% and 51.7 at strains exceeding 150% [132]. It enables real-time implant load detection with fracture elongation up to 1066%. TPU-CNT composites can serve as multimodal sensors for comprehensive prosthetic monitoring [133]. It can detect strain in a 0-160% range, with GF = 12.88. It can also sense pressure in 0-55 kPa range, with sensitivity 0.08 kPa^{-1}.

Graphene-CNT-TPU fabric-based strain sensors have a broad strain range of 112%, high sensitivity with GF above 210, low detection limits (0.1‰), and stability over 3000 cycles and can be used for joint movement registration [134]. Polydimethylsiloxane (PDMS)-encapsulated CNT composites can create soft bioelectronic interfaces with low electrical impedance for electrical stimulation and recording from nervous and muscular systems in neural prostheses [135]. Porous fluororubber/TPU nanocomposites exhibit piezoresistive sensitivity, with a sensing range of 150 Pa for pressure detection [134].

4.3. Polycomponent Smart Systems

The combination of different material classes enables optimization of smart functionality while maintaining mechanical stability. Underlying material can be load-bearing and structure-forming, while sensing materials, systems, or actuators are integrated into or added to the substrate. Titanium substrates with 1-10 µm-thick CNT coatings can increase conductivity from 10^5 S/m in pure Ti to 10^6-10^7 S/m for sensor integration [136]. It also maintains biocompatibility with cell viability of more than 95% [137]. This combination helps overcome the conductivity limitations of pure titanium while maintaining good corrosion resistance [138].

Bioceramic–carbon fiber hybrids can combine smart sensor functionality with sufficient support and significant bioactive properties. The carbon fiber reinforcement is usually 10–30 vol%, which provides structural support and increases tensile strength by 100–300% [139]. At the same time, it provides electrical conductivity up to 2*107 S/m and comparable to that of silver, copper, gold, and aluminium [140]. Bioceramic components such as hydroxyapatite and bioactive glass with 30–50 wt% contribute bioactivity with apatite formation within 7–14 days and osseointegration capabilities [7,141]. Smart polymer components at 5–20 wt% can be integrated into a bioactive environment to provide a controlled drug release at regulated rates of 1–100 µg/day. It can also have adaptive mechanical properties with stiffness modulation of 50–200% [7,141]. The compatibility between different components has to be balanced with maximized synergistic effects. Interface design is important for maintaining mechanical integrity. Interfacial shear strength is an important system support with efficient bioelectronic sensing and wireless data transfer through the bone-implant interface [142]. It can include a monitoring system with minimized signal interference.

4.3.1. Two-Component Smart Composite and Hybrid Systems

Smart coating integration

 doi:10.20944/preprints202605.0674.v1

Two-component systems with coatings represent the straightforward approach to smart material integration. Smart coatings are applied to conventional metal or polymer matrices. The smart component typically forms a discrete or surface layer, enabling stimuli-responsive bioactivity, local mechanical adaptation, or controlled ion release without compromise of the continuous structural matrix [143]. This configuration allows the bulk material to provide mechanical support while the smart coating delivers functional capabilities. Coating thickness typically ranges from 1 μm to 100 μm [144]. Shape-memory alloy coatings on titanium substrates provide adaptability for the prostheses. The coating can undergo reversible component transformations in response to temperature changes with transformation temperatures between 37-45 °C, which matches physiological conditions [145]. These binary systems provide adaptive stiffness match to surrounding bone tissue, with elastic modulus variations of 20-80 GPa depending on component state It reduces stress shielding effects and maintains implant stability [55]. The shape-memory effect can be programmed to be activated at body temperature. It can gradually adapt to physiological load conditions over time, with recovery strains up to 8% [146]. Piezoelectric bioglass coatings can generate electrical charges in the range of 1-10 pC/N (Formula 4) in response to mechanical deformation [147]. These coatings can provide bioelectric stimulation to enhance bone tissue formation. Piezoelectric coefficients d33 range is 5-15 pC/N for bioactive glass-ceramics [148].

Piezoelectric charge coefficient d_{33}

$$d_{33} = \left(\frac{\partial S_3}{\partial E_3}\right)_T = \left(\frac{\partial D_3}{\partial T_3}\right)_E \quad (4)$$

where:

E is electric field applied voltage per unit distance inside the piezoelectric material (pC/N; V/m);

S is mechanical strain; relative deformation produced by the electric field or stress (m/m);

D is electric displacement; surface charge density generated by mechanical stress (C/m²);

T is mechanical stress; force applied per unit area of the material (N/m² or Pa).

The piezoelectric response of the prosthesis creates local electric fields of 10-100 mV/mm. It promotes osteoblast proliferation and mineral deposition by 30-50% [149]. Natural piezoelectric and flexoelectric biomaterials demonstrate high biocompatibility and biodegradability compared to conventional ceramic counterparts. Degradation rates can be controllable and range between 3 and 18 months [150,151].

Stimuli-responsive mechanisms

The integration of smart coatings enables multiple stimuli-responsive mechanisms. that can be tailored to specific clinical applications. The pH-responsive polymer coatings based on polymethacrylic acid (PMAA) or on chitosan can provide controlled drug release in response to infection-related acidosis, pH 5.5-6.5. The release rates increase 5-10-fold at acidic pH compared to physiological pH 7.4 [152,153].

Thermally responsive systems incorporating poly-N-isopropylacrylamide (PNIPAAM) can modulate drug delivery in response to temperature-related inflammatory signals. Local tissue temperature elevation to 38-40 °C and lower critical solution temperature (LCST) tunable between 32 and 42 °C are trigger-related boundaries [154]. Electroactive polymers integrated as surface layers can provide controlled mechanical stimulation to surrounding tissues with actuation strains of 2-5% at voltages of 1-5 V [155]. These systems can generate small-scale movements or vibrations at frequencies of 1-100 Hz. It promotes tissue vascularization and prevents fibrous encapsulation. The reduction of capsule thickness is significant, 40-60% compared to passive implants [118]. Electric stimulation can be programmed to deliver specific patterns of activation. It can be optimized for tissue integration without interfering with normal physiological function; stimulation amplitudes range from 10 to 100 μA/cm² [156].

4.3.2. Three-Component Hybrid Systems

 doi:10.20944/preprints202605.0674.v1

Three-component systems can combine polymer or ceramic matrices with carbon or metallic reinforcements and a smart functional component, such as magnetostrictive particles (10-30 vol%) or conductive polymers (5-15 wt%). This configuration allows simultaneous load- bearing, passive sensing and active feedback capabilities. These systems can modulate stiffness by 50-200%, provide vibration damping with loss factors of 0.1-0.3, or deliver bioelectric cues to cells and tissues [157,158].

The architecture of three-component systems can be designed as continuous-discrete hybrids, in which the smart component is intimately embedded within or along reinforcement pathways at volume fractions of 5-25%. This distribution ensures integration of smart functionality throughout the material structure. It also maintains efficient load transfer between components with interfacial shear strengths exceeding 20 MPa [159]. The continuous matrix gives structural stability, the discrete reinforcement enhances mechanical properties by 100-300%, and the smart component provides responsive functionality [203].

Carbon nanotube-reinforced polymer matrices with embedded piezoelectric ceramic particles are examples of three-component smart integration [161]. The particles have 10-40 vol% and are usually made of lead zirconate titanate, PZT, barium titanate, $BaTiO_3$. Another example is a polymer matrix with biocompatibility and processability, containing 0.5-3 wt% CNTs. which enhance mechanical properties by 50-150% and electrical conductivity by 5-10 orders of magnitude; and piezoelectric particles which enable mechanical-to-electrical energy conversion with coupling coefficients of 0.3-0.6 [162,163]. It can be used for self-powered sensing applications. There is an option to use shape-memory polymer composites incorporating CNTs. They demonstrate high sensitivity with gauge factors up to 20 at 5% strain. They can detect subtle physiological movements with a resolution of 0.1% strain [125].

Conductive polymer components, such as polyaniline, polypyrrole, and PEDOT:PSS, can be integrated into three-component systems. They enable electrical stimulation capabilities with conductivities of 1-1000 S/cm. It can be controlled externally or through embedded sensor feedback [164]. These systems can provide programmable electrical stimulation patterns at current densities of 1-100 $\mu A/cm^2$ that promote specific cellular responses and enhance nerve regeneration, increasing neurite outgrowth by 50-100%. They can also prevent bacterial adhesion through electrochemical mechanisms, reducing biofilm formation by 80-95% [165]. Advanced shape-memory alloys integrated into MEMS devices demonstrate their capability for precise mechanical actuation at microscale levels with displacement resolution of 1-10 nm and force outputs of 0.1-10 mN [166].

The multi-component architecture enables the integration of sensing capabilities to monitor implant performance and tissue responses in real time. It can have sensitivity up to 0.01% of strain and response times below 10 ms. Strain-sensitive carbon nanotube networks can detect mechanical loading patterns with gauge factors ranging from 1 to 50. The pH-sensitive polymer components can incorporate fluorescent indicators to monitor local tissue conditions with pH resolution of 0.1 units [123,167]. This information can be transmitted through conductive pathways with signal-to-noise ratios exceeding 40 dB to external monitoring systems [168].

Temperature-sensitive components that incorporate thermochromic materials or thermistors can detect inflammatory responses at the onset of infection with a temperature resolution of 0.1 °C. They can trigger appropriate therapeutic responses through controlled drug release or enhanced antimicrobial activity when temperatures exceed 38 °C [153]. The integration of multiple sensing modalities within a single system creates comprehensive monitoring capabilities with chemical detection limits of 10^{-6} M for relevant biomarkers that can significantly enhance implant safety and effectiveness [169].

4.3.3. Four and Multi-Component Complex Systems

Four or more component systems represent a sophisticated approach to integrating smart materials. They can combine polymer, ceramic, carbon, bioglass, and smart elements. They are able to produce mechanically robust systems, with compressive strength 50-200 MPa, fatigue-resistant, with more than 10^6 cycles at 50% of ultimate strength, bioactive, with apatite formation within 7 days

 doi:10.20944/preprints202605.0674.v1

in simulated body fluid, and adaptive materials [170,171]. In these systems, metamaterial design principles are applied. These principles include unit-cell geometry optimization, negative-Poisson's-ratio structures with ν = -0.2 to -0.8, and auxetic architectures. These systems can achieve tailored anisotropic stiffness with Ex/Ey ratios in the range of 2-10, energy absorption of 10-50 J/g, and mechanical wave-guiding capabilities [172].

Metamaterials are structures with properties not found in natural materials. They have optimized geometry with design of unit cell shape, connectivity, and angles of cells` struts, beams, or voids between these elements [76]. The main goal of these microscopic changes is to achieve the desired mechanical properties in macroscopic materials. A combination of metamaterials` properties with smart properties gives bone prostheses high functionality and effectiveness. For example, auxetic structures with a negative Poisson ratio expand laterally when stretched and can provide enhanced energy absorption by 50-200%. They can also improve interfacial bonding with surrounding tissues by increasing the contact area by 30-50% compared to conventional materials [173]. These structures can be designed with specific directionality to match the anisotropic properties of bone tissue (Ex = 10-20 GPa longitudinal, 5-10 GPa transverse), with incorporation of smart functionality throughout the architecture. Negative-Poisson's-ratio materials can provide enhanced fracture resistance. The fracture toughness increases by 40-70%, and improved load distribution with stress concentrations is reduced by 30-50% compared to conventional materials [174]. When combined with smart components, these structures can adapt their mechanical response based on loading conditions. They provide enhanced protection against fatigue failure with S-N curve improvements of 50-100%.

Complex multi-component systems can simultaneously address several clinical requirements. It includes mechanical support with compressive strength greater than 100 MPa, biological integration with 80% bone-implant contact, infection resistance with bacterial adhesion reduced by 90%, and real-time monitoring with a strain resolution of 0.01% [142]. The integration of bioglass components at 10-30 wt% [99] provides bioactive ion release of Ca^{2+}, PO_4^{3-}, and Si^{4+} at concentrations of 50-200 ppm. It enhances osseointegration with bone apposition rates of 1-3 μm/day. Conductive components at 5-15 wt% enable electrical stimulation at 10-100 μA/cm² and add sensing capabilities [156].

Polymer components with 30-60 wt% can provide controlled drug release with zero-order kinetics over 1-12 weeks [175]. Ceramic components of 20-40 wt% contribute to mechanical stability with an elastic modulus of 10-50 GPa and wear resistance with wear rates less than 10^{-6} mm³/Nm (Katti, 2004). The spatial distribution of different components can be optimized to match specific anatomical requirements. In spinal applications, stiffer components with E = 5-20 GPa can be concentrated in load-bearing regions (E = 0.1-1 GPa). More compliant smart components can be positioned to interface with neural tissues. Young's modulus for the spinal cord is 0.5-1 kPa.

5. Design and Optimization Principles

5.1. Structural Compatibility Requirements

Smart and metamaterial components must be structurally compatible with load-bearing components to prevent interface failure and ensure long-term implant stability for 10-20 years. The mechanical properties of different components should be matched to minimize stress concentrations at interfaces with stress concentration factors less than 2. At the same time, they have to maintain efficient load transfer throughout the structure with interfacial shear strengths of more than 20 MPa. Porous multilateral structures can offer variants for solutions for complex bone replacements, with possible inclusions of biomaterials [176]. Thermal expansion coefficients should be similar, with minimal mismatch prevent interface stresses during temperature cycling. Physical mismatch in thermal material properties between different materials in bone implants can lead to inconsistent thermal expansion or contraction under the same thermal loads [177].

The bonding strength between components is critical to maintaining structural integrity under cyclic loading. It is typical in bone prostheses applications with 10^6-10^7 cycles over the implant

 doi:10.20944/preprints202605.0674.v1

lifetime. Chemical bonding via silane coupling agents or mechanical interlocking via surface texturing with a roughness Ra = 1-10 μm can enhance interfacial strength by 50-200% [178]. The interface design has to accommodate differential expansion and contraction. Thermal strains are typically 10^{-4}- 10^{-3} K^{1}, while electrical continuity is maintained with a contact resistance of less than 10 Ω·cm². Mechanical continuity and crack deflection at interfaces are essential [179].

Compatibility of processing stages, parameters, and conditions is essential for creating effective multi-component systems [180]. There is a significant difference in the range of processing temperatures. Polymers are usually processed at temperatures between 20 °C and 200 °C. For ceramics, it often exceeds 1000 °C, while for metals the range is commonly 600–1200 °C. The chemical processing environments can vary from strongly oxidizing to reducing. It typically covers a pH range of 1–14 [181].

Mechanical stresses during fabrication can also span quite broad ranges. During polymer molding, composite consolidation or thin-film formation, typical compressive stresses are 1–100 MPa, and shear or interlayer stresses are around 0.1–10 MPa [182]. During ceramic sintering and metal alloy formation, localized stresses can exceed 100 MPa and, in extreme cases, approach the material yield strength. Higher transient stresses have to remain compatible across all components to avoid delamination, cracking, or warping during thermal cycling and cooling. Sequential processing may also be necessary to prevent degradation of temperature-sensitive smart components during high-temperature processing of ceramic or metallic components. The maximum temperature exposures are limited to 100-200 °C for most smart polymers and 400-600 °C for shape-memory alloys [183].

5.2. Component Distribution

The spatial distribution of different components usually determines the mechanical, biological, and functional performance of smart hybrid systems. Coating configurations with a thickness of 1-100 μm and surface coverage of more than 95% provide maximum surface functionality while maintaining bulk mechanical properties. This approach is effective for applications with surface-specific responses, for example, in coating with a thickness of 2.5-10 μm and controlled drug release rates of 7-10 μg over 90 days [184]. It is also effective for bioelectrical stimulation with a current density of 1-100 μA/cm². Filler distributions throughout the matrix provide volume-based functionality. It maintains processability at a viscosity below 10^4 Pa·s for injection molding. This configuration is suitable for sensing applications with distributed detection. It requires a spatial resolution of 1-10 mm. It can also be used for adaptive mechanical properties with response throughout the material volume. The response times are less than 1 s [185]. In composites, the filler concentration has to be optimized for functional percolation thresholds. Typically, these materials contain 0.1-5 wt% CNTs and 1-10 vol% conductive particles [121].

Lattice architectures provide control over local material properties. Spatial resolution of 0.1–1 mm with complex geometries is adjusted to match anatomical requirements [186]. 3D printing technologies, such as fused deposition modeling, stereolithography, and selective laser sintering, can create lattice structures with varying relative density from 10% to 90%, fiber angles orientation range of 0–90° and material composition throughout the implant volume with feature resolution of 50–500 μm [187]. This approach allows optimization of mechanical properties with stiffness variation 0.5–10 GPa [186] and biological properties with pore sizes 100–500 μm for bone ingrowth [188]. Functional properties are provided by sensor density 1–100 per cm³ [189]. 4D printing techniques, when combined with smart materials, enable the fabrication of lattices that can dynamically respond to external stimuli. Responses to temperature, humidity, and electric fields can enable adaptive changes in shape or mechanical properties over time [186].

5.3. Performance Requirements and Optimization

The optimization of smart hybrid systems requires consideration and balance of multiple competing requirements. For example, it can be listed as mechanical tensile strength of more than 100 MPa, mechanical compressive strength of more than 200 MPa; biocompatibility with cell viability

 doi:10.20944/preprints202605.0674.v1

of more than 85%; inflammatory response with grade less than 2; functional responsiveness with response time less than 10 s, normalized sensitivity output above 1 [189]. The range of requirements is much longer and addressed in the tables above. Multi-objective production optimization approaches using genetic algorithms or particle swarm optimization can identify designs that provide acceptable performance across all requirements while maximizing critical performance parameters, typically requiring 100-1000 iterations [190].

Finite element modeling can predict mechanical behavior under physiological loading conditions such as 1-10 MPa stress, 0.1-1% strain, and 1-10 Hz frequency. At the same time, it accounts for different material properties of each component, such as the elastic modulus, which ranges from 0.1 MPa to 200 GPa [50,191] These models can identify potential failure modes with stress concentration factors above 3 and strains above 5%. They can guide interface design to ensure long-term durability with safety factors above 2. The models must include fatigue considerations, given the cyclic loading environment in biomedical applications, with load cycles of 10^6-10^7 over the implant lifetime. They can use S-N curves and cumulative damage models in accordance with Miner's rule.

Biological tests have to evaluate the biocompatibility of the complete multi-component system rather than individual components according to ISO 10993 standards. The interaction between different components may create unexpected biological responses such as cytotoxicity, sensitization, and irritation that are not predicted from single-component testing [66]. Long-term clinical studies, 6-12 months in vitro, 1-2 years in vivo, are essential to ensure that smart functionality does not compromise biocompatibility over extended implantation periods. Cell viability has to be steadily maintained above 85%, and inflammatory markers such as IL-6, TNF-α, on levels below 2 baselines [118].

Functional tests must evaluate complex, smart material responses under realistic physiological conditions. The appropriate mechanical load is in the range of 1-10 MPa, 1-10 Hz (human walking range is 1-3 Hz), chemical environments with pH 7.4, ionic strength 0.15 M, temperature 37 °C, with variations 35-39 °C [192]. The testing protocols have to assess both immediate responses, such as response time less than 10 s and sensitivity above 1, and long-term stability of smart functionality: performance degradation less than 20% over 6-12 months. Accelerated testing methods with increased temperatures 45-60 °C, pH extremes of pH 5-9 or mechanical cycling of 10 Hz for weeks to simulate years may be necessary to evaluate performance over clinically relevant time scales of 5-15 years [193].

6. Clinical Applications

Clinical and functional outcome metrics are used to evaluate the effectiveness of bone implants and prosthetic systems (Table 15). Mobility improvement is quantified by comparing patient movement before and after implantation using gait speed, stride length, and joint range of motion [194]. Functional mobility tests such as the Timed Up and Go or six-minute walk test [195]. Load distribution efficiency is assessed through pressure mapping or force-sensing in weight-bearing prosthetics to determine how loads are transmitted through bone, soft tissue, or prosthetic interfaces. Proper load distribution reduces the risk of tissue damage, implant overload, and stress shielding and is an important determinant of long-term implant usage.

Patient comfort and ergonomics are captured via the Visual Analogue Scale (VAS, 1–10) to evaluate comfort, fit, and ease of daily use. user-centred research shows that these patient-reported measures predict daily wear and long-term adherence better than isolated laboratory metrics [196]. Activity adaptation reflects the implant or prosthetic system's ability to support a range of activities, such as walking on uneven terrain, climbing stairs, or lifting. It is increasingly assessed through multimodal protocols that combine wearable inertial sensors, portable force plates, and task-specific performance tests. Device longevity is measured as operational lifespan before replacement, revision, or significant performance degradation. Complication rate tracks the incidence of adverse clinical events, including infection, implant loosening, fracture, or peri-implant bone resorption [197].

 doi:10.20944/preprints202605.0674.v1

Smart prostheses have demonstrated significant improvements across multiple clinical and functional metrics. By integrating sensors, actuators, and adaptive ML and AI algorithms, these devices enhance mobility, allowing more natural gait patterns, improved stride length, and greater joint range of motion. Embedded load-sensing technology distributes forces efficiently, reducing tissue stress and the risk of implant overload [197]. Patient comfort and ergonomics are increased through real-time adaptive adjustments, reflected in higher VAS scores. Activity adaptation is optimized as the prosthesis dynamically responds to terrain changes or varying loads. Additionally, continuous monitoring and adaptive control contribute to device longevity by reducing mechanical wear and preventing overloading, while complication rates are lowered through precise biomechanical alignment and feedback-driven adjustments [194]. Collectively, smart prosthetic systems provide a measurable enhancement in functional efficacy, safety, and user satisfaction [197].

Table 15. Clinical outcome metrics for the orthopedic prostheses.

Metric	Description	Relevance / Clinical Significance
Mobility Improvement (%)	Quantitative assessment of patient movement compared to pre- and post-implant/prosthesis. Includes gait speed, stride length, joint range of motion, and functional mobility tests (e.g., Timed Up and Go, 6-minute walk).	Measures functional efficacy and recovery; indicates how well the implant restores natural biomechanics.
Load Distribution Efficiency (%)	Pressure mapping or force-sensing evaluation in weight-bearing implants or prosthetics, assessing how loads are transmitted through bone, soft tissue, or prosthetic interfaces.	Ensures even load sharing, reducing the risk of tissue damage, implant overload, or stress shielding.
User Comfort / Ergonomics (VAS 1–10)	Subjective patient-reported scoring for comfort, fit, and ease of daily use using visual analogue scales or structured questionnaires.	Evaluates daily usability, compliance, and patient satisfaction. Critical for long-term adherence.
Activity Adaptation	Ability of the implant/prosthetic system to support varied activities (walking on uneven terrain, stair climbing, lifting, or dynamic load adjustment).	Measures real-world applicability and the system's capability to adapt to patient lifestyle and activity demands.
Device Longevity (years)	Operational lifespan before implant replacement, revision, or significant performance degradation.	Indicates durability and cost-effectiveness, guiding clinical decision-making and long-term planning.
Complication Rate (%)	Incidence of adverse clinical events including infection, implant loosening, fracture, peri-implant bone resorption, or other complications.	Primary safety metric; essential for regulatory evaluation and risk-benefit analysis.

6.1. Application Concepts

Smart, multi-component systems in load-bearing orthopedic applications can provide adaptable mechanical stability, with compressive strengths of 120–250 MPa and a gradual transfer of loads to the bone. Smart implants with embedded Fiber Bragg Grating (FBG) sensors with a strain resolution of 0.005–0.02% and biochemical assays, for example, osteocalcin, with detection limits of 10^{-10} M, can monitor healing progress. They dynamically adjust stiffness via shape-memory polymers, achieving 15–35% monthly reductions. In this manner, they optimize mechanotransduction and reduce stress shielding [198,199].

 doi:10.20944/preprints202605.0674.v1

The integration of antimicrobial components confers infection resistance through the controlled release of agents. Silver nanoparticles with a diameter of 0.5–15 ppm, vancomycin 5–150 μg/mL or low-intensity electrical stimulation with a range of 1–15 μA/cm² can disrupt biofilm formation and reduce bacterial viability by 85–99% [200–202]. These mechanisms are activated in response to early indicators: pH 5.8–6.7, temperature 37.5–39 °C. The pH-responsive NO-releasing coatings achieve MRSA eradication [203]. These systems can lower periprosthetic joint infection rates from 2–5% to less than 1% and enhance implant longevity by 50–80% in high-risk cohorts.

6.2. Current Clinical Implementations

Piezoelectric osseointegration enhancers can be embedded in uncemented implants to stimulate bone ingrowth. PZT nanofiber coatings harvest micromotion of less than 100 μm to generate electric energy of 1–20 μA/cm² at 1–10 kHz. Osteoblast differentiation is boosted without batteries [5]. Preclinical trials show 20–40% faster integration with stability at 6–8 weeks vs standard 10–12 and 50–70% higher pull-out strength of 1.5 kN vs 1.0 kN versus controls. Capacitance stability holds less than 5% of annual drift over 5–10 years, supporting more than 10-year durability via impedance checks.

In load-sensing total hip arthroplasties (THA) prostheses can include strain gauge arrays with a resolution of 1 N and a range of 0–5 kN, and accelerometers with a sensitivity of 50–100 mV/g and a bandwidth of 0–100 Hz. They can track in vivo forces during physical activities such as gait, with peak forces up to 5 kN, and register falls [204,205]. Another early example demonstrates improvement in reoperation rates. In cohorts of 1000 patients, sensors achieve 80–90% sensitivity in detecting aseptic loosening via load asymmetry when it exceeds 20% deviation. It reduces reoperations by 40–60% through early interventions [205].

Sensor-enabled Total Knee Arthroplasties (TKA) incorporate embedded strain gauges with a resolution of 1 N and a range of 0–5 kN, accelerometers with a sensitivity of 50–100 mV/g and a bandwidth of 0–100 Hz. Wireless telemetry is used to monitor in vivo forces during walking, stair climbing, and other dynamic activities [204,205]. These devices detect abnormal load distributions, optimize surgical alignment, guide rehabilitation, and enable early detection of loosening or wear. Sensor feedback allows real-time post-operative adjustments to reduce complications and improve implant performance.

Sensor-integrated spinal fusion cages use a number of measurements. PH with ΔpH of 0.1, temperature with ΔT of 0.2 °C, and impedance sensors with levels above 5 kΩ for infection vigilance. Triggers such as pH below 6.8 or temperature activate medication release at a specific rate from polymer matrices [206]. Trials' reports cite 85–95% sensitivity and specificity for early osteomyelitis; a reduction in surgical site infections (SSIs) from 3–5% to less than 1% in monitored cases [207,208]. NFC telemetry is used for postoperative decision-making, with no device failures. Spinal fusion cages and fixation systems can integrate piezoelectric and impedance-based sensors that measure micromotion of less than 100 μm, local electrical changes, and early signs of hardware loosening [209,210]. Wireless telemetry transmits data on osseointegration, device stability, and bone healing, enabling timely clinical interventions. Early studies report improved post-operative monitoring, faster detection of complications, and enhanced patient-specific management.

Adaptive SMA fixation in Nitinol plates and nails modulates stiffness in the range of 28–90 GPa [36,211]. It uses fiber Bragg grating (FBG) sensors with a resolution of 1 με and a range of 0–5,000 με [212]. Dynamization trials reduce the non-union rate from 10–15% to 3–5% by ramping up load transfer during weeks 6–12 [213].

In craniofacial reconstructions, multi-component smart materials show significant promise. Complex geometries and diverse tissue interfaces require sophisticated material responses. 3D-printed prostheses have hierarchical scaffolds incorporating polycaprolactone (PCL) and hydroxyapatite (HA) gradients. They adapt their mechanical properties to match those of hard tissues (E = 10–18 GPa for cortical bone) and soft tissues (E = 0.5–5 MPa for periosteum and cartilage). They facilitate vascular ingrowth and gradient osseointegration over 4–8 months in critical-sized calvarial

 doi:10.20944/preprints202605.0674.v1

defects [214,215]. These bioresorbable composites can be enhanced with stimuli-responsive polymers. They achieve 70–90% bone volume regeneration in preclinical models, outperforming static autografts by reducing donor site morbidity and enabling patient-specific designs via additive manufacturing [216,217].

6.3. Emerging Applications

Smart orthopedic implants with integrated sensors enable precise, real-time assessment of bone healing [218]. Wireless metamaterial platforms can provide strain resolution of 0.005–0.02% and sample at 20–2000 Hz [219], often being electronic-free. Loosening detection via micromotion, with a threshold of 5–40 μm, is possible, with load distribution or force resolution of 0.5–5 N [209]. These devices can provide predictive alerts 2–5 months before first symptoms are detected by standard methods. They register load asymmetry of more than 15%, micromotion spikes of more than 120 μm, elevated biomarkers such as IL-6, and TNF-α, elevated more than 1.5 times above baseline. AI-driven protocols can optimize rehabilitation, achieving 30–60% faster union rates for tibial fractures [199,220].

4D-printed smart scaffolds can dynamically direct tissue formation via tunable mechanical cues. They have a strain of 0.05–8% with frequency 0.05–15 Hz, provide spatiotemporal growth factors, elution of 0.5–150 ng/mL over 2–16 weeks and form bioelectric signals with current density of 0.5–150 μA/cm² and voltage 0.05–1.5 V/cm) [216,217]. Often, they utilize hybrid PCL-HA with shape-memory responses, which modulate stiffness from 15–120 MPa initially to 0.5–8 MPa by weeks 6–10. They promote seamless scaffold resorption over 4–24 months and vascularized tissue ingrowth [214,215]. In vivo models show more than 92% cell viability, proliferation rates 2-4 times higher versus static scaffolds, and infiltration depths of 1.5–6 mm within 3–10 weeks. They also accelerate functional recovery in cartilage and neural defects [202].

6.4. Future Outlook

Smart implants are increasingly integrating biomaterials, becoming fully autonomous, bioadaptive systems with AI. 4D printing and closed-loop bioelectronics are extensively used for precise drug delivery and regenerative medicine. The merging of nanomaterials utilization with machine learning can help to develop personalized, focused therapeutic approaches and potentially halve revision rates with the extension of smart implant lifespans beyond 15 years [208,221]. It is envisaged that by 2030, hybrid scaffolds with embedded nanosensors could enable real-time modulation of the microenvironment. It will reduce infection risk to less than 0.5% and boost osseointegration by 60–80%, including for complex craniofacial and neural repairs. There are still challenges of scalability, long-term biocompatibility, and ethical data governance.

Author Contributions: Conceptualization, D.J.H. and A.Z.; writing—original draft preparation, D.J.H.; writing—review and editing, N.J.H.; visualization, D.J.H..; supervision, A.Z.; project administration, N.J.H.. All authors have read and agreed to the published version of the manuscript." Please turn to the CRediT taxonomy for the term explanation. Authorship must be limited to those who have contributed substantially to the work reported.

Funding: This research received no external funding.

Data Availability Statement: Not applicable.

Conflicts of Interest: The authors declare no conflicts of interest.

References

1. Raschke, S.U. Limb prostheses: Industry 1.0 to 4.0: Perspectives on technological advances in prosthetic care', *Frontiers in Rehabilitation Sciences*, **2022**; 3, p.854404. https://doi.org/10.3389/fresc.2022.854404.

 doi:10.20944/preprints202605.0674.v1

2. Eschweiler, J., Greven, J., Rath, B., Kobbe, P., Modabber, A., Hildebrand, F., Migliorini, F. and Hofmann, U.K. 'High-performance ceramics in musculoskeletal surgery: Current use and future perspectives', *Ceramics*, **2024**; 7(1), pp. 310–328. https://doi.org/10.3390/ceramics7010020.
3. Ohashi, H., Morita, K., Yamana, S., Tsuchida, K., Furuta, Y., Mizushima, T., Hishinuma, Y., Katsumi, S., Shinohara, A., Tani, S., & Murayama, Y. Proposal of a method for evaluating the bone affinity of pedicle screws and considering differences between carbon fiber reinforced plastic and titanium alloy. *Discover Applied Sciences*, **2025**; 7, Article 1347. https://doi.org/10.1007/s42452-025-07888-0.
4. Kim, H., Jang, S., Do, P.T., Lee, C.K., Ahn, B., Kwon, S., Chang, H. and Kim, Y. Development of wearable finger prosthesis with pneumatic actuator for patients with partial amputations. *Actuators*, **2023**; 12(12), p.434. https://doi.org/10.3390/act12120434.
5. Ledet, E.H., Liddle, B., Kradinova, K. and Harper, S. Smart orthopedic implants: A review of current technology and future directions. *Innovation and Entrepreneurship in Health*, **2018**; 5, pp.41–51. https://doi.org/10.2147/IEH.S133518.
6. Resendes, T., Freitas Rodrigues, P., Cruz, F., Gatões, D., Santos, V.M., Ramos, A.S. and Vieira, M.T. 'Advanced medical monitoring: 3D printed prosthetics with integrated strain sensor', *Progress in Additive Manufacturing*, 2025; 10(1), pp.219–229. https://doi.org/10.1007/s40964-024-00615-y.
7. Kim, C.-H.; Lee, S.-Y.; Rhee, K. Y.; Park, S.-J. Carbon-based composites in biomedical applications: a comprehensive review of properties, applications, and future directions. *Advanced Composites and Hybrid Materials*, *2024*; 7(2), 55. https://doi.org/10.1007/s42114-024-00846-1.
8. Krepsky, Daniel Victor, João Pedro Da Silva Cardoso, Gustavo Cézar GT, Daniel Hermann Lickfeld, Leonardo Mejia Rincon, and Ebrahim Samer El Youssef. "Development of a low-cost biomechanical hand prosthesis prototype." In 2025 Brazilian Conference on Robotics (CROS), vol. 1, pp. 1-6. IEEE, 2025. https://doi.org/10.1109/CROS66186.2025.11066149.
9. Marin, E. and Lanzutti, A.'History of metallic orthopedic materials', *Metals*, **2025**; 15(4), p.378. https://doi.org/10.3390/met15040378.
10. Ceddia, M. and Trentadue, B. 'A review of carbon fiber-reinforced polymer composite used to solve stress shielding in total hip replacement', *AIMS Materials Science*, **2024**; 11(3). https://doi.org/10.3934/matersci.2024023.
11. Piconi, C. and Sprio, S. 'Oxide bioceramic composites in orthopedics and dentistry', *Journal of Composites Science*, **2021**; 5(8), p.206. https://doi.org/10.3390/jcs5080206.
12. Sánchez-Alfonso, A.L., Gaytán-Tocavén, L., Alcantara-Quintana, L.E., Paredes, R.G. and Ruiz-Aguilar, C. (2025) 'Characterization and In Vivo Evaluation of Phosphate-Based Glass/TiO_2 for Skull Prosthetic Application', IRBM, 46(4), p.100899. https://doi.org/10.1016/j.irbm.2025.100899.
13. Domínguez-Ruiz, A., López-Caudana, E.O., Lugo-González, E., Espinosa-García, F.J., Ambrocio-Delgado, R., García, U.D., López-Gutiérrez, R., Alfaro-Ponce, M. and Ponce, P. 'Low limb prostheses and complex human prosthetic interaction: A systematic literature review', *Frontiers in Robotics and AI*, **2023;** 10, pp. 1032748. https://doi.org/10.3389/frobt.2023.1032748.
14. Bousch, J. F., Beyersdorf, C., Schultz, K., Windolf, J., Suschek, C. V., & Maus, U. Proinflammatory cytokines enhance the mineralization, proliferation, and metabolic activity of primary human osteoblast like cells. *International Journal of Molecular Sciences*, **2024;** 25(22), 12358. https://doi.org/10.3390/ijms252212358.
15. Castro, F., Ferreira, J., Oliveira, M., Santos, R., Almeida, P., Correia, A., Lopes, C., Martins, D., Silva, T., Rodrigues, L., Pereira, H. and Costa, R. 'An update on hydroxyapatite/collagen composites: What is there left to say about these bioinspired materials?', *Biomaterials Advances*, **2024**; 158, pp.112–124. https://doi.org/10.1002/jbm.b.34976.
16. Dalle Carbonare, L., Cominacini, M., Trabetti, E., Bombieri, C., Pessoa, J., Romanelli, M.G. and Valenti, M.T. (2025) 'The bone microenvironment: new insights into the role of stem cells and cell communication in bone regeneration', Stem Cell Research & Therapy, 16, 169. https://doi.org/10.1186/s13287-025-04288-4.
17. Buck, H.V. and Stains, J.P., Osteocyte-mediated mechanical response controls osteoblast differentiation and function. *Frontiers in physiology*, **2024**; 15, p.1364694. https://doi.org/10.3389/fphys.2024.1364694.

 doi:10.20944/preprints202605.0674.v1

18. Freeman, C., Diana, A.S. and Priscilla, A.S. 'Unraveling the intricacies of OPG/RANKL/RANK biology and its implications in neurological disorders—A comprehensive literature review', *Molecular Neurobiology*, **2024;** 61, pp.10656–10670. https://doi.org/10.1007/s12035-024-04227-z.
19. Florencio-Silva, R., Sasso, G.R., Sasso-Cerri, E., Simões, M.J. and Cerri, P.S. 'Biology of bone tissue: structure, function, and factors that influence bone cells', *BioMed Research International*, **2015**, article ID 421746. https://doi.org/10.1155/2015/421746.
20. Schaffler, M.B. and Kennedy, O.D. 'Osteocyte signaling in bone', *Current Osteoporosis Reports*, **2012;** 10(2), pp.118–125. https://doi.org/10.1007/s11914-012-0105-4.
21. Hubert, M. and Wellik, D. 'Hox genes in development and beyond', *Development*, **2023;** 150(1), pp. dev192476. https://doi.org/10.1242/dev.192476,
22. Wu, M., Wu, S., Chen, W. and Li, Y. 'The roles and regulatory mechanisms of TGF-β and BMP signalling in bone and cartilage development, homeostasis, and disease', *Cell Research*, **2024;** 34(2), pp. 101–123. https://doi.org/10.1038/s41422-023-00918-9.
23. Hu, L., Chen, W., Qian, A. and Li, Y. Wnt/β-catenin signaling components and mechanisms in bone formation, homeostasis, and disease. *Bone Research*, **2024;** 12(39). https://doi.org/10.1038/s41413-024-00342-8.
24. López, J.M. 'Bone development and growth', International Journal of Molecular Sciences, **2024;** 25(12), 6767. https://doi.org/10.3390/ijms25126767.
25. Simon, A. 'Delaying the growth plate closure to augment height', Journal of Pediatric Endocrinology and Diabetes, **2024;** 4(1), pp.7–8. https://doi.org/10.25259/JPED_22_2024.
26. Clarke, B. 'Normal bone anatomy and physiology', Clinical Journal of the American Society of Nephrology, **2008;** 3(Supplement 3), pp. S131–S139. https://doi.org/10.2215/CJN.04151206.
27. Morgan, E.F., Unnikrisnan, G.U. and Hussein, A.I. Bone mechanical properties in healthy and diseased states. *Annual Review of Biomedical Engineering*, **2018;** 20, pp.119–143. https://doi.org/10.1146/annurev-bioeng-062117-121139.
28. Baleani, M., Erani, P., Acciaioli, A. and Schileo, E. 'Tensile yield strain of human cortical bone from the femoral diaphysis is constant among healthy adults and across the anatomical quadrants', *Bioengineering*, **2024;** 11(4), 395. https://doi.org/10.3390/bioengineering11040395.
29. Roohani-Esfahani, S.-I., Newman, P. and Zreiqat, H. 'Design and Fabrication of 3D printed Scaffolds with a Mechanical Strength Comparable to Cortical Bone to Repair Large Bone Defects', *Scientific Reports*, **2016;** 6, 19468. https://doi.org/10.1038/srep19468.
30. Bittner Frank, M., Reisinger, A.G., Andriotis, O.G., Pahr, D.H. and Thurner, P.J. 'Cortical and trabecular mechanical properties in the femoral neck vary differently with changes in bone mineral density', *JBMR Plus*, **2024;** 8(6). https://doi.org/10.1093/jbmrpl/ziae049.
31. Belluzzi, E., Todros, S., Pozzuoli, A., Ruggieri, P., Carniel, E.L. and Berardo, A. 'Human cartilage biomechanics: Experimental and theoretical approaches towards the identification of mechanical properties in healthy and osteoarthritic conditions', *Processes*, **2023;** 11(4), 1014. https://doi.org/10.3390/pr11041014.
32. Krakowski, P., Rejniak, A., Sobczyk, J. and Karpiński, R. 'Cartilage integrity: A review of mechanical and frictional properties and repair approaches in osteoarthritis', *Healthcare*, **2024;** 12(16), 1648. https://doi.org/10.3390/healthcare12161648.
33. Levy, M. and Yosibash, Z., Heterogeneous fracture toughness of human cortical bone tissue. *International Journal of Fracture*, **2025;** 249(1), p.17. https://doi.org/10.1007/s10704-024-00836-w.
34. Granke, M., Makowski, A.J., Uppuganti, S., Does, M.D. and Nyman, J.S. 'Identifying Novel Clinical Surrogates to Assess Human Bone Fracture Toughness', *Journal of Bone and Mineral Research*, **2015;** 30(7), pp.1290–1300. https://doi.org/10.1002/jbmr.2452.
35. Ehnert, S. and Histing, T. 'Advances in fracture healing research', Bioengineering, 11(1), Article 67. https://doi.org/10.3390/bioengineering11010067.
36. Zhang, J., Wei, S., Liu, C., Shang, C., He, Z., Duan, Y. and Peng, Z., (2024). Porous nanocomposites with enhanced intrinsic piezoresistive sensitivity for bioinspired multimodal tactile sensors. *Microsystems & Nanoengineering*, **2024;** 10, p.19. https://doi.org/10.1038/s41378-023-00630-z

 doi:10.20944/preprints202605.0674.v1

37. Cusanno, A. and Piccininni, A. 'Embedding a controlled layer of hydroxyapatite on a Ti-6Al-4V substrate in superplastic condition', *The International Journal of Advanced Manufacturing Technology*, **2025;** 137, pp. 6123–6138. Available at: https://doi.org/10.1007/s00170-025-15504-z
38. Homa, K., Zakrzewski, W., Dobrzyński, W., Piszko, P.J., Piszko, A., Matys, J., Wiglusz, R.J. and Dobrzyński, M. 'Surface functionalization of titanium-based implants with a nanohydroxyapatite layer and its impact on osteoblasts: a systematic review', *Journal of Functional Biomaterials*, **2024;** 15(2), Article 45. https://doi.org/10.3390/jfb15020045.
39. Goriainov, V., Cook, R., Latham, J.M., Dunlop, D.G. and Oreffo, R.O.C. 'Bone and metal: an orthopaedic perspective on osseointegration of metals', *Acta Biomaterialia*, **2014;** 10(10), pp. 4043–4057. https://doi.org/10.1016/j.actbio.2014.06.004.
40. Niinomi, M. Mechanical biocompatibilities of titanium alloys for biomedical applications. *Journal of the Mechanical Behavior of Biomedical Materials*, **2008;** 1(1), pp.30–42. https://doi.org/10.1016/j.jmbbm.2007.07.001.
41. Katti, K.S. Biomaterials in total joint replacement. *Colloids and Surfaces B: Biointerfaces*, **2004;** 39(3), pp.133–142. https://doi.org/10.1016/j.colsurfb.2003.12.002.
42. Food and Drug Administration (FDA) Use of International Standard ISO 10993-1, "Biological evaluation of medical devices - Part 1: Evaluation and testing within a risk management process": Guidance for Industry and Food and Drug Administration Staff. Silver Spring, MD: FDA, Center for Devices and Radiological Health, 2023.
43. Sharma, D.K., Pattnaik, G., Behera, A., Deshmukh, K. and Moharana, S. 'Functionalized carbon nanostructures for smart medical implants', in Handbook of Functionalized Carbon Nanostructures. *Springer*, **2024;** pp.2211–2255.
44. Daniel, A.S., Anand, S.P., Naveen, J., Khan, T. and Khahro, S.H. 'Advancement in biomedical implant materials—a mini review', *Frontiers in Bioengineering and Biotechnology*, **2024;** 12, Article 1400918. https://doi.org/10.3389/fbioe.2024.1400918.
45. Ellakwa, D.E.S., Abu-Khadra, A.S. and Ellakwa, T.E. 'Insight into bioactive glass and bio-ceramics uses: unveiling recent advances for biomedical application', *Discover Materials*, **2025;** 5, Article 78. https://doi.org/10.1007/s43939-025-00254-2.
46. Brochu, B.M., Sturm, S.R., Goncalves, J.A.K.D.Q., Mirsky, N.A., Sandino, A.I., Panthaki, K.Z., Panthaki, K.Z., Nayak, V.V., Daunert, S., Witek, L. and Coelho, P.G. 'Advances in bioceramics for bone regeneration: a narrative review', *Biomimetics*, **2024;** 9(11), Article 690. https://doi.org/10.3390/biomimetics9110690.
47. Chen, M., Luo, C., Yuan, Y., Zhou, H., Li, Z., Wang, Q., Gong, B., Li, Z. and Sun, H. 'Modification of PEEK for implants: strategies to improve mechanical, antibacterial, and osteogenic properties', Reviews on Advanced Materials Science, **2024;** 63(1). https://doi.org/10.1515/rams-2024-0025.
48. Liu, X., Wang, C., Wang, H., Wang, G., Zhang, Y. and Zhang, Y. Calcium phosphate-based anti-infective bone cements: Recent trends and future perspectives. *Frontiers in Pharmacology*, **2025;** 16, Article 1522225. https://doi.org/10.3389/fphar.2025.1522225.
49. Seraji, A., Ghaffari, M., Shamsabadi, A.A., Ghasemi, A., Ghasemi, M., Ghasemi, A. and Ghasemi, M. 'Finite element analysis and in vitro tests on endurance life and durability of composite bone substitutes', *Frontiers in Bioengineering and Biotechnology*, **2024;** 12, Article 1417440. https://doi.org/10.3389/fbioe.2024.1417440.
50. Baroni, S., Oliviero, S., La Mattina, A. A., Maglio, M., Martini, L., Fini, M., & Viceconti, M. Calibration of Aseptic Loosening Simulation for Coatings Osteoinductive Effect. *Annals of Biomedical Engineering*, **2025** 53, 34–47. https://doi.org/10.1007/s10439-024-03588-9.
51. Boivineau, M., Cagran, C., Doytier, D., Eyraud, V., Nadal, M-H., Wilthan, B. and Pottlacher, G. 'Thermophysical Properties of Solid and Liquid Ti-6Al-4V (TA6V) Alloy', *International Journal of Thermophysics*, **2006;** 27(2), pp. 507–529. https://doi.org/10.1007/PL00021868.
52. Mitchell, B.S. An Introduction to Materials Engineering and Science: For Chemical and Materials Engineers. Hoboken, NJ: Wiley, 2004. ISBN: 978-0-471-43623-2.
53. Ida, N. and Bastos, J.P. Electromagnetics and calculation of fields. Springer Science & Business Media, 2013.
54. Winter, L., Seifert, F., Zilberti, L., Murbach, M. and Ittermann, B. 'MRI Related Heating of Implants and Devices: A Review', *Journal of Magnetic Resonance Imaging*, **2021;** 53(6), pp.1646–1665. https://doi.org/10.1002/jmri.27194

 doi:10.20944/preprints202605.0674.v1

55. Duerig, T., Pelton, A. and Stöckel, D.J.M.S., An overview of nitinol medical applications. *Materials Science and Engineering*, **1999;** A, 273, pp.149-160. https://doi.org/10.1016/S0921-5093(99)00294-4
56. Olabi, A.G. and Grunwald, A. 'Design and application of magnetostrictive materials', *Materials & Design*, **2008;** 29(2), pp.469–483. 10.1016/j.matdes.2006.12.016
57. Morgan, N.B. Medical shape memory alloy applications—the market and its products. *Materials Science and Engineering*, **2004;** A, 378(1–2), pp.16–23. https://doi.org/10.1016/j.msea.2003.10.326
58. Witte, F., Hort, N., Vogt, C., Cohen, S., Kainer, K.U., Willumeit, R. and Feyerabend, F. 'Degradable biomaterials based on magnesium corrosion', *Current Opinion in Solid State and Materials Science*, **2008;** 12(5–6), pp.63–72. https://doi.org/10.1016/j.cossms.2009.04.001
59. Staiger, M.P., Pietak, A.M., Huadmai, J. and Dias, G. 'Magnesium and its alloys as orthopedic biomaterials: a review', *Biomaterials*, **2006;** 27(9), pp.1728–1734. https://doi.org/10.1016/j.biomaterials.2005.10.003
60. Witte, F. 'The history of biodegradable magnesium implants: a review', *Acta Biomaterialia*, **2010;** 6(5), pp.1680–1692. https://doi.org/10.1016/j.actbio.2010.02.028
61. D'Lima, D. D., Townsend, C. P., Arms, S. W., Morris, B. A., & Colwell, C. W. An implantable telemetry device to measure intra-articular tibial forces. *Journal of Biomechanics*, **2005;** 38(2), 299-304. https://doi.org/10.1016/j.jbiomech.2004.02.011
62. Kim, H., Kim, D., Kim, J., Lee, Y., Shin, M., Kim, J., Bossuyt, F.M., Lee, G.H., Lee, B., Taylor, W.R. and Lee, J., Advances and perspectives in fiber-based electronic devices for next-generation soft systems. npj *Flexible Electronics*, **2025;** 9(1), p.84. https://doi.org/10.1038/s41528-025-00465-w
63. Hannon, P., A brief review of current orthopedic implant device issues: biomechanics and biocompatibility. *Biol End Med*, **2016;** 1(1), p.1κ2. https://doi.org/10.15761/BEM.1000102
64. Ahuir-Torres, J.I., Al-Mahdy, A., Sharp, M.C., Opoz, T.T., Zhu, G., Bashir, M. and Kotadia, H.R. 'The influence of texture density and free surface energy on corrosion in 316L stainless steel', *npj Materials Degradation*, **2025;** 9(1), p. 115. https://doi.org/10.1038/s41529-025-00622-6
65. Manaka, T., Tsutsumi, Y., Takada, Y., Chen, P., Ashida, M., Doi, K., Katayama, H. and Hanawa, T. 'Galvanic Corrosion among Ti–6Al–4V ELI Alloy, Co–Cr–Mo Alloy, 316L-Type Stainless Steel, and Zr–1Mo Alloy for Orthopedic Implants', *Materials Transactions*, **2023;** 64(1), pp. 131–137. https://doi.org/10.2320/matertrans.MT-MLA2022001
66. Williams, D.F., Assessing the triad of biocompatibility, medical device functionality and biological safety. *Medical Devices & Sensors*, **2021;** 4(1), p.e10150. https://doi.org/10.1002/mds3.10150
67. Shimizu, J., & Nagoya, S. Bone Remodeling and Stress Shielding. In: *Advances in Total Hip Arthroplasty* **2024**; (pp. 343–362). Springer, Singapore.
68. Filip, P., Titanium-nickel shape memory alloys in medical applications. In: Brunette, D.M., Tengvall, P., Textor, M. and Thomsen, P., eds. Titanium in Medicine. *Springer*, Berlin, Heidelberg, **2001;** pp. 113–124.
69. D'Andrea, L. and Vena, P. Mechanical properties of porous bioceramics: a methodological overview. *Porous Bioceramics for Biomedical Applications*, **2026**; pp.237-272. doi.org/10.1016/B978-0-443-30130-8.00026-5
70. Lachowicz, M., Stępniewski, Z., Morawska-Kochman, M. and Lachowicz, M., The use of porous alumina bioceramics to repair bone defects in the aspect of long-term success of hip arthroplasty. *Orthopedic Reviews*, **2025;** 17, p.144080. https://doi.org/10.52965/001c.144080
71. Piconi, C., Maccauro, G., Muratori, F. and Brach del Prever, E., Alumina and zirconia ceramics in joint replacements. Journal of Applied Biomaterials & Biomechanics, **2003;** 1(1), pp.19–32.
72. Piconi, C. and Porporati, A.A., Bioinert ceramics: zirconia and alumina. In: I.V. Antoniac, ed. Handbook of Bioceramics and Biocomposites. *Springer, Cham*, **2016;** pp.59–87.
73. Fiume, E., Magnaterra, G., Rahdar, A., Verné, E. and Baino, F., Hydroxyapatite for biomedical applications: A short overview. *Ceramics*, **2021;** 4(4), pp.542-563. https://doi.org/10.3390/ceramics4040039
74. Vukajlovic, D., Novakovic, K. and Bretcanu, O., . Self-crystallisation, an unexpected property of 45S5 Bioglass®. *Chemical Communications*, **2021**;57(99), pp.13558-13561. https://doi.org/10.1039/D1CC04847C
75. Moghanian, A., Mehrjardi, L.D. and Safaee, S., Ion substitution in bioactive glass: A comprehensive review of structural modifications and functional effects. *Next Materials*, **2025;** 8, p.100598. https://doi.org/10.1016/j.nxmate.2025.100598

 doi:10.20944/preprints202605.0674.v1

76. Nogueira, D.M.B., Rosso, M.P.d.O., Buchaim, D.V., Zangrando, M.S.R. and Buchaim, R.L. Update on the use of 45S5 bioactive glass in the treatment of bone defects in regenerative medicine. *World Journal of Orthopedics*, **2024;** 15(3), pp.204–214. https://doi.org/10.5312/wjo.v15.i3.204
77. Perkins, B.L. and Naderi, N., Carbon nanostructures in bone tissue engineering. The Open Orthopaedics Journal, **2016;** 10, p.877. https://doi.org/10.2174/1874325001610010877
78. Shar, A., Shar, A. and Joung, D., Carbon nanotube nanocomposite scaffolds: advances in fabrication and applications for tissue regeneration and cancer therapy. Frontiers in Bioengineering and Biotechnology, **2023;** 11, p.1299166. https://doi.org/10.3389/fbioe.2023.1299166
79. Ricon, F.J., Lajara, F., Fuentes, A., Aguilar, M.L., Boix, A. and Lozano, J.A., Pyrocarbon arthroplasty in acute unreconstructable radial head fractures: mid-term to long term results. *Journal of Orthopaedics and Traumatology*, **2018;** 19, p.13. https://doi.org/10.1186/s10195-018-0499-6
80. Fisher, C., E. Rider, A., Jun Han, Z., Kumar, S., Levchenko, I. and Ostrikov, K., Applications and nanotoxicity of carbon nanotubes and graphene in biomedicine. *Journal of Nanomaterials*, **2012;** 2012(1), p.315185. https://doi.org/10.1155/2012/315185
81. Miyawaki, J., Matsumura, S., Yuge, R., Murakami, T., Sato, S., Tomida, A., Tsuruo, T., Ichihashi, T., Fujinami, T., Irie, H. and Tsuchida, K., Biodistribution and ultrastructural localization of single-walled carbon nanohorns determined in vivo with embedded Gd2O3 labels. *ACS nano*, **2009;** 3(6), pp.1399-1406. https://doi.org/10.1021/nn9004846
82. Kurtz, S.M. and Devine, J.N., PEEK biomaterials in trauma, orthopedic, and spinal implants. Biomaterials, 28(32), pp.4845-4869., S.M. and Devine, J.N., 2007. PEEK biomaterials in trauma, orthopedic, and spinal implants. Biomaterials, 28(32), pp.4845-4869. https://doi.org/10.1016/j.biomaterials.2007.07.013
83. Kalbacova, M., Broz, A., Kromka, A., Babchenko, O. and Kalbac, M., Controlled oxygen plasma treatment of single-walled carbon nanotube films improves osteoblastic cells attachment and enhances their proliferation. *Carbon*, **2011;** 49(9), pp.2926-2934. https://doi.org/10.1016/j.carbon.2011.02.069
84. Szwed-Georgiou, A., Płociński, P., Kupikowska-Stobba, B., Urbaniak, M.M., Rusek-Wala, P., Szustakiewicz, K., Piszko, P., Krupa, A., Biernat, M., Gazińska, M. and Kasprzak, M., Bioactive materials for bone regeneration: biomolecules and delivery systems. *ACS biomaterials science & engineering*, **2023;** 9(9), pp.5222-5254. https://doi.org/10.1021/acsbiomaterials.3c00609
85. Darie-Niță, R.N. and Frąckowiak, S., An Overview of Potential Applications of Environmentally Friendly Hybrid Polymeric Materials. *Polymers*, **2025;** 17(2), p.252. https://doi.org/10.3390/polym17020252
86. Castañeda-Rodríguez, S., González-Torres, M., Ribas-Aparicio, R.M., Del Prado-Audelo, M.L., Leyva-Gómez, G., Gürer, E.S. and Sharifi-Rad, J. 'Recent advances in modified poly (lactic acid) as tissue engineering materials', *Journal of Biological Engineering*, **2023**; 17, p. 21. https://doi.org/10.1186/s13036-023-00338-8
87. Lamparelli, E.P., Ciardulli, M.C., Giudice, V., Scala, P., Vitolo, R., Dale, T.P., Selleri, C., Forsyth, N.R., Maffulli, N. and Della Porta, G., 3D in-vitro cultures of human bone marrow and Wharton's jelly derived mesenchymal stromal cells show high chondrogenic potential. *Frontiers in Bioengineering and Biotechnology*, **2022;** 10, p.986310. https://doi.org/10.3389/fbioe.2022.986310
88. Butler, J., Handy, R.D., Upton, M. and Besinis, A., Review of antimicrobial nanocoatings in medicine and dentistry: mechanisms of action, biocompatibility performance, safety, and benefits compared to antibiotics. *ACS nano*, **2023;** 17(8), pp.7064-7092. https://doi.org/10.1021/acsnano.2c12488
89. Xu, X., Li, Y., Wang, L., Li, Y., Pan, J., Fu, X., Luo, Z., Sui, Y., Zhang, S., Wang, L., Ni, Y., Zhang, L. and Wei, S. 'Triple-functional polyetheretherketone surface with enhanced bacteriostasis and anti-inflammatory and osseointegrative properties for implant application', *Biomaterials*, **2019;** 212, pp.98–114. https://doi.org/10.1016/j.biomaterials.2019.05.014
90. Truong, T. and Kim, J. A wearable strain sensor utilizing shape memory polymer/carbon nanotube composites measuring respiration movements. *Polymers*, **2024**; 16(3), p.373. **doi.org/10.3390/polym16030373**
91. Ouyang, L., Deng, Y., Yang, L., Shi, X., Dong, T., Tai, Y., Yang, W. and Chen, Z.G., Graphene-oxide-decorated microporous polyetheretherketone with superior antibacterial capability and in vitro osteogenesis for orthopedic implant. *Macromolecular bioscience*, **2018;** 18(6), p.1800036. https://doi.org/10.1002/mabi.201800036

 doi:10.20944/preprints202605.0674.v1

92. Alonso-Fernández, I., Haugen, H.J., López-Peña, M., González-Cantalapiedra, A. and Muñoz, F., Use of 3D-printed polylactic acid/bioceramic composite scaffolds for bone tissue engineering in preclinical in vivo studies: A systematic review. *Acta Biomaterialia*, **2023;** 168, pp.1-21. https://doi.org/10.1016/j.actbio.2023.07.013
93. Hasegawa, M., Tone, S., Naito, Y. and Sudo, A., 2023. Ultra-high-molecular-weight polyethylene in hip and knee arthroplasties. Materials, 16(6), p.2140. doi.org/10.3390/ma16062140
94. Tsukerman, I. Effective parameters of metamaterials: A rigorous homogenization theory via Whitney interpolation. Journal of the Optical Society of America B, **2011;** 28(2), 577-586. https://doi.org/10.1364/JOSAB.28.000577
95. Qin, Y., Jing, Z., Zou, D., Wang, Y., Yang, H., Chen, K., Li, W., Wen, P. and Zheng, Y., A metamaterial scaffold beyond modulus limits: enhanced osteogenesis and angiogenesis of critical bone defects. *Nature communications*, **2025;** 16(1), p.2180. doi.org/10.1038/s41467-025-57609-9
96. Ake, B., Yang, H., Yang, H., Liu, H., Gui, X., Liu, T., Chen, J., Liu, J., Zhou, W., Qu, B. and Zeng, Z., Ultrasound-responsive smart biomaterials for bone tissue engineering. *Journal of Materials Chemistry B*, **2025;** 13(15), pp.4527-4543. https://doi.org/10.1039/d5tb00109a
97. Neto, A.S., Gaddam, A., Stan, G.E. and Ferreira, J.M. Multifunctional cuttlefish bone–derived scaffolds: smart biomimetic solutions for bone tissue repair and regeneration. *Journal of the American Ceramic Society*, **2025;** 108(11), p.e70044. doi.org/10.1111/jace.70044
98. Bose, S., Roy, M. and Bandyopadhyay, A. 'Recent advances in bone tissue engineering scaffolds', *Trends in Biotechnology*, **2012;** 36(10), pp. 546-554. https://doi.org/10.1016/j.tibtech.2012.07.005
99. Hench, L.L. The story of Bioglass®. Journal of Materials Science: *Materials in Medicine*, **2006**; 17(11), pp.967–978. https://doi.org/10.1007/s10856-006-0432-z
100. Sheikh, Z., Najeeb, S., Khurshid, Z., Verma, V., Rashid, H. and Glogauer, M. 'Biodegradable materials for bone repair', *Materials*, **2015;** 8(9), pp.5744–5794. https://doi.org/10.3390/ma8095273
101. Ramakrishna, S., Mayer, J., Wintermantel, E. and Leong, K.W. 'Biomedical applications of polymer-composite materials', *Composites Science and Technology*, **2001;** 61(9), pp.1189–1224. https://doi.org/10.1016/S0266-3538(00)00241-4
102. Kovrlija, I., Menshikh, K., Abreu, H., Cochis, A., Rimondini, L., Marsan, O., Rey, C., Combes, C., Locs, J. and Loca, D., Corrigendum to "Challenging applicability of ISO 10993-5 for calcium phosphate biomaterials evaluation: Towards more accurate in vitro cytotoxicity assessment"[Biomater. Adv. 160 (2024) 213866]. *Biomaterials Advances*, **2025,** p.214386. doi.org/10.1016/j.bioadv.2025.214386
103. Gruber, S. and Nickel, A. 'Toxic or not toxic? The specifications of the standard ISO 10993-5 are not explicit enough to yield comparable results in the cytotoxicity assessment of an identical medical device', *Frontiers in Medical Technology*, **2023;** 5, article 1195529. https://doi.org/10.3389/fmedt.2023.1195529
104. Chocholata, P.K., Dvorakova, J., Babuska, V. and Cedikova, M. 'Biomaterial strategies of macrophage behaviour in bone regeneration', *Regenerative Engineering and Translational Medicine*, **2025;** pp. 1–15. https://doi.org/10.1007/s40883-025-00443-8
105. Balasubramani, G., Premkumar, J. and Paul Pradeep, J. 'Optimizing bone-metal implant interfaces: the role of bio-ceramic coatings in improving stability and tissue metabolism', *Frontiers in Materials*, **2025;** 11 (1514559). https://doi.org/10.3389/fmats.2024.1514559
106. Frigério, P.B., de Moura, J., Pitol-Palin, L., Monteiro, N.G., Mourão, C.F., Shibli, J.A. and Okamoto, R., Combination of a Synthetic Bioceramic Associated with a Polydioxanone-Based Membrane as an Alternative to Autogenous Bone Grafting. *Biomimetics*, **2024;** 9(5), p.284. https://doi.org/10.3390/biomimetics9050284
107. Lim, S., Park, J., Kim, H. and Lee, J. Biocompatibility and dimensional stability through the use of 3D-printed scaffolds made by polycaprolactone and bioglass-7: An in vitro and in vivo study. *Clinical Implant Dentistry and Related Research*, **2024;** 26(5), pp.892–905. https://doi.org/10.1111/cid.13378
108. Kumar, A. and Singh, G. Surface modification of Ti6Al4V alloy via advanced coatings: Mechanical, tribological, corrosion, wetting, and biocompatibility studies. *Journal of Alloys and Compounds*, **2024;** 989, article 174418. https://doi.org/10.1016/j.jallcom.2024.174418

 doi:10.20944/preprints202605.0674.v1

109. Bijukumar, D.R., Segu, A., Souza, J.C.M., Li, X., Barba, M., Mercuri, L.G., Jacobs, J.J. and Mathew, M.T. 'Systemic and local toxicity of metal debris released from hip prostheses: A review of experimental approaches', *Nanomedicine: Nanotechnology, Biology and Medicine*, **2018;** *14(3), pp.951-963.* doi.org/10.1016/j.nano.2018.01.001
110. Niinomi, Mitsuo, and Masaaki Nakai. "Titanium-based biomaterials for preventing stress shielding between implant devices and bone." *International journal of biomaterials* **2011**.1 (2011): 836587. https://doi.org/10.1155/2011/836587
111. Nikam, N., Shenoy, B.S., K.N., C., Keni, L.G., Shetty, S. and Bhat, N.S. Advancements in surface coatings for enhancing longevity in hip implants: A review. *Prosthesis*, **2025;** 7(1), p.21. https://doi.org/10.3390/prosthesis7010021
112. Radulescu, R., Meleșcanu Imre, M., Ripszky, A., Rus, F., Popa, A., Moisa, M., Funieru, C., Ene, R. and Pituru, S., Exploring the Broad Spectrum of Titanium–Niobium Implants and Hydroxyapatite Coatings—A Review. *Materials*, **2024;** 17(24), p.6206. https://doi.org/10.3390/ma17246206
113. Margiotta, A., Coupling of Intracellular Calcium Homeostasis and Formation and Secretion of Matrix Vesicles: Their Role in the Mechanism of Biomineralization. *Cells*, **2025;** 14(10), p.733. https://doi.org/10.3390/cells14100733
114. Matsuzaka, T., Matsugaki, A., Ishihara, K. and Nakano, T., Osteogenic tailoring of oriented bone matrix organization using on/off micropatterning for osteoblast adhesion on titanium surfaces. *Acta Biomaterialia*, **2025;** 192, pp.487-500. https://doi.org/10.1016/j.actbio.2024.12.017
115. Kowalski, S., Gonciarz, W., Belka, R., Góral, A., Chmiela, M., Lechowicz, Ł., Kaca, W. & Żórawski, W. Plasma-Sprayed Hydroxyapatite Coatings and Their Biological Properties. *Coatings*, **2022;** 12(9), 1317. https://doi.org/10.3390/coatings12091317
116. Cantini, M., Gomide, K., Moulisova, V., González-García, C. and Salmerón-Sánchez, M., Vitronectin as a micromanager of cell response in material-driven fibronectin nanonetworks. *Advanced biosystems*, **2017;** 1(9), p.1700047. https://doi.org/10.1002/adbi.201700047
117. Kazimierczak, P. and Przekora, A., Osteoconductive and osteoinductive surface modifications of biomaterials for bone regeneration: A concise review. *Coatings*, **2020;** 10(10), p.971. https://doi.org/10.3390/coatings10100971
118. Anderson, J.M., Rodriguez, A. and Chang, D.T. 'Foreign body reaction to biomaterials', *Seminars in Immunology*, **2008;** 20(2), pp. 86–100. https://doi.org/10.1016/j.smim.2007.11.004
119. Baughman, R.H., Zakhidov, A.A. and de Heer, W.A. 'Carbon nanotubes--the route toward applications', *Science*, **2002;** 297(5582), pp. 787–792. https://doi.org/10.1126/science.1060928
120. Amjadi, M., Kyung, K.U., Park, I. and Sitti, M. 'Stretchable, skin-mountable, and wearable strain sensors and their potential applications: A review', *Advanced Functional Materials*, **2016;** 26(11), pp. 1678–1698. https://doi.org/10.1002/adfm.201504755
121. Bauhofer, W. and Kovacs, J.Z. 'A review and analysis of electrical percolation in carbon nanotube polymer composites', *Composites Science and Technology*, **2009;** 69(10), pp. 1486–1498. https://doi.org/10.1016/j.compscitech.2008.06.018
122. Dharap, P., Li, Z., Nagarajaiah, S., & Barrera, E. V. Nanotube film based on single-wall carbon nanotubes for strain sensing. *Nanotechnology*, **2004;** 15(3), 379-382. https://doi.org/10.1088/0957-4484/15/3/026
123. Zhang, X., Xiang, D., Zhu, W., Zheng, Y., Harkin-Jones, E., Wang, P., Zhao, C., Li, H., Wang, B. and Li, Y., Flexible and high-performance piezoresistive strain sensors based on carbon nanoparticles polyurethane sponges. *Composites Science and Technology*, **2020;** 200, p.108437. DOI: 10.1016/j.compscitech.2020.108437
124. Pumera, M., Ambrosi, A., Bonanni, A., Chng, E.L.K. and Poh, H.L. 'Graphene for electrochemical sensing and biosensing', *TrAC Trends in Analytical Chemistry*, **2010;** 29(9), pp.954–965. https://doi.org/10.1016/j.trac.2010.05.011
125. Liu, Y., Dong, X. and Chen, P. Biological and chemical sensors based on graphene materials. *Chemical Society Reviews*, **2012;** 41(6), pp.2283–2307. https://doi.org/10.1039/C1CS15270J
126. Novoselov, K.S., Geim, A.K., Morozov, S.V., Jiang, D., Zhang, Y., Dubonos, S.V., Grigorieva, I.V., Firsov, A.A., Electric field effect in atomically thin carbon films. *Science*, **2004,** 306(5696), pp.666-669. https://doi.org/10.1126/science.1102896

 doi:10.20944/preprints202605.0674.v1

127. Chen, Z., Sang, L., Liu, Y. and Bai, Z., Sono-Piezo Dynamic Therapy: Utilizing Piezoelectric Materials as Sonosensitizer for Sonodynamic Therapy. *Advanced Science*, **2025;** 12(12), p.2417439. doi.org/10.1002/advs.202417439
128. Wang, R., Sui, J. and Wang, X., Natural piezoelectric biomaterials: a biocompatible and sustainable building block for biomedical devices. *ACS nano*, **2022;** 16(11), pp.17708-17728. https://doi.org/10.1021/acsnano.2c08164
129. Dubey, U., Kesarwani, S., & Verma, R. K. Incorporation of graphene nanoplatelets/hydroxyapatite in PMMA bone cement for characterization and enhanced mechanical properties of biopolymer composites. *Journal of Thermoplastic Composite Materials*, **2023**; *36(5),* pp.1978-2008. doi.org/10.1177/08927057221086833
130. Ormsby, R., McNally, T., Mitchell, C., Halley, P., Martin, D., Nicholson, T. and Dunne, N. 'Effect of MWCNT addition on the thermal and rheological properties of polymethyl methacrylate bone cement', *Carbon*, **2011;** 49(9), pp.2893–2904. https://doi.org/10.1016/j.carbon.2011.02.039
131. Marrs, B., Andrews, R., Rantell, T. and Pienkowski, D. Augmentation of acrylic bone cement with multiwall carbon nanotubes. *Journal of Biomedical Materials Research Part* A, **2006;** 77(2), pp.269–276. https://doi.org/10.1002/jbm.a.30581
132. Nie, Z., Wang, Y., Li, X., Lei, M., Liu, N., Liu, X., Zhao, S., Niu, B. and Chen, Y. Strain sensor based on polyurethane/carbon nanotube elastic conductive spiral yarn with high strain range and sensitivity. *Polymer Composites*, **2024;** 45(6), pp.5522–5531. https://doi.org/10.1002/pc.28144
133. Wang, Z., Huang, Y., Sun, J., Huang, Y., Hu, H., Jiang, R., Gai, W., Li, G. and Zhu, C. 'Thermoplastic Polyurethane/Carbon Nanotube Composites for Stretchable Flexible Pressure Sensors', *ACS Applied Nano Materials*, **2023;** 6(8), pp.7220–7231. https://doi.org/10.1021/acsanm.3c01543
134. Zhao, W., He, P., Ling, K., Gao, C., Wang, K., Wu, L. and Yang, J., Printed graphene/CNTs/TPU-fabric wearable strain sensor for healthcare monitoring. *Soft Science*, **2025;** 5(1), pp.N-A. https://doi.org/10.20517/ss.2024.61
135. Wiranata, A., Ishii, Y., Hosoya, N. and Maeda, S. 'Simple and reliable fabrication method for PDMS dielectric elastomer actuators using CNT electrodes', *Advanced Engineering Materials*, **2021;** 22(12), p. 2001181. https://doi.org/10.1002/adem.202001181
136. McIntyre, D.J., Hirschman, R.K., Puchades, I. and Landi, B.J. 'Enhanced copper–carbon nanotube hybrid conductors with titanium adhesion layer', *Journal of Materials Science*, **2020;** 55(15), pp. 6610–6622. https://doi.org/10.1007/s10853-020-04457-1
137. Mahendran Logesh, Nguyen, K.T., Ahn, S.-G. and Choe, H.-C. 'Engineering bioactive MWCNT-reinforced hydroxyapatite coatings on Ti29Nb5Zr alloy by plasma electrolytic oxidation method: A comprehensive approach to dental implant surface optimization', *Journal of Alloys and Compounds*, **2024**, 176339. https://doi.org/10.1016/j.jallcom.2024.176339
138. Geetha, M., Singh, A.K., Asokamani, R. and Gogia, A.K. 'Ti based biomaterials, the ultimate choice for orthopaedic implants–A review', *Progress in Materials Science*, **2009;** 54(3), pp. 397–425. https://doi.org/10.1016/j.pmatsci.2008.06.004
139. Denk, J., Liao, X., Dulle, M., Schafföner, S., Förster, S., Greiner, A., Motz, G. and Agarwal, S. 'Synergistic enhancement of thermomechanical properties and oxidation resistance in aligned co-continuous carbon–ceramic hybrid fibers', *Materials Horizons*, **2024;** 11(22), pp. 4567–4581. https://doi.org/10.1039/D4MH00956H
140. Okolo, C., Rafique, R., Iqbal, S.S., Subhani, T., Saharudin, M.S., Bhat, B.R. and Inam, F., Customizable ceramic nanocomposites using carbon nanotubes. *Molecules*, **2019,** 24(17), p.3176. https://doi.org/10.3390/molecules24173176
141. Pádua, A.S., Martins, M.A., Cruz, R. and Gomes, M.E. 'Polycaprolactone/doped bioactive glass composite scaffolds for bone regeneration', *International Journal of Molecular Sciences*, **2025;** 26(2), p.2440. https://doi.org/10.3390/ijms26022440.
142. Peres, I., Rolo, P., Soares dos Santos, M.P. and Ferreira, J.A.F. 'Bioelectronic multifunctional bone implants: recent trends', *Bioelectronic Medicine*, **2022;** 8, p.15. https://doi.org/10.1186/s42234-022-00097-9
143. Yao, X., Peng, R. and Ding, J. 'Cell–material interactions revealed via material techniques of surface patterning', *Advanced Materials*, **2013;** 25(37), pp.5257–5286. https://doi.org/10.1002/adma.201301762

 doi:10.20944/preprints202605.0674.v1

144. Kumar, A., Sharma, K. and Dixit, A.R. A review on the mechanical properties of polymer composites reinforced by carbon nanotubes and graphene. *Carbon Letters*, **2021;** 31(2), pp.149–165. https://doi.org/10.1007/s42823-020-00161-x
145. Chen, X., Liu, Y., Miao, G., Lu, Y., Lin, C., Deformation behavior of a Ni-Ti-Nb shape memory alloy. *Journal of Materials Engineering and Performance,* **2022;** 31(3), pp.2205-2211. https://doi.org/10.1007/s11665-021-06192-1
146. Otsuka, K. and Ren, X. 'Physical metallurgy of Ti–Ni-based shape memory alloys', *Progress in Materials Science*, **2005;** 50(5), pp.511–678. https://doi.org/10.1016/j.pmatsci.2004.10.001
147. Jarkov, V., Allan, S.J., Bowen, C. and Khanbareh, H. Piezoelectric materials and systems for tissue engineering and implantable energy harvesting devices for biomedical applications. *International Materials Reviews* **2022***; vol. 67(7), pp. 683–733. https://doi.org/*10.1080/09506608.2021.1988194
148. Baino, F., Hamzehlou, S., Kargozar, S., Bioactive glasses: Where are we and where are we going? *Journal of Functional Biomaterials*, **2018;** 9(1), p.25. https://doi.org/10.3390/jfb9010025
149. Khare, D., Basu, B. and Dubey, A.K. Electrical stimulation and piezoelectric biomaterials for bone tissue engineering applications. *Biomaterials*, **2020;** 258, p.120280. https://doi.org/10.1016/j.biomaterials.2020.120280
150. Wang, X., Liu, W., Yu, X., Wang, B., Xu, Y., Yan, X. and Zhang, X., . Advances in surface modification of tantalum and porous tantalum for rapid osseointegration: A thematic review. *Frontiers in Bioengineering and Biotechnology*, **2022**; 10, p.983695. doi.org/10.3389/fbioe.2022.983695
151. Ribeiro, C., Sencadas, V., Correia, D.M. and Lanceros-Méndez, S. 'Piezoelectric polymers as biomaterials for tissue engineering applications', *Colloids and Surfaces B: Biointerfaces*, **2015;** 136, pp.46–55. https://doi.org/10.1016/j.colsurfb.2015.08.043
152. Schmaljohann, D. 'Thermo- and pH-responsive polymers in drug delivery', *Advanced Drug Delivery Reviews*, **2006;** 58(15), pp.1655–1670. https://doi.org/10.1016/j.addr.2006.09.020
153. Gao, W., Emaminejad, S., Nyein, H.Y.Y., Challa, S., Chen, K., Peck, A., Fahad, H.M., Ota, H., Shiraki, H., Kiriya, D., Lien, D.H. and Wang, J. 'Fully integrated wearable sensor arrays for multiplexed in situ perspiration analysis', *Nature*, **2016;** 529(7587), pp. 509–514. https://doi.org/10.1038/nature16521
154. Ward, M.A. and Georgiou, T.K. 'Thermoresponsive polymers for biomedical applications', *Polymers*, **2011;** 3(3), pp.1215–1242. https://doi.org/10.3390/polym3031215
155. Bar-Cohen, Y. Electroactive Polymer (EAP) Actuators as Artificial Muscles: Reality, Potential, and Challenges. 2nd edn. Bellingham, WA: SPIE Press, 2004.
156. Balint, R., Cassidy, N.J. and Cartmell, S.H. 'Conductive polymers: Towards a smart biomaterial for tissue engineering', Acta Biomaterialia, **2014;** 10(6), pp. 2341–2353. https://doi.org/10.1016/j.actbio.2014.02.015
157. Huang, C. and Chen, L. Negative Poisson's ratio in modern functional materials. *Advanced Materials,* **2016;** 28(37), pp.8079–8096. https://doi.org/10.1002/adma.201601363
158. Lendlein, A. and Kelch, S. Shape-memory polymers. *Angewandte Chemie International Edition*, **2002;** 41(12), pp.2034–2057. https://doi.org/10.1002/1521-3773(20020617)41:12<2034::AID-ANIE2034>3.0.CO;2-M
159. Coleman, J.N., Khan, U., Blau, W.J. and Gun'ko, Y.K. 'Small but strong: A review of the mechanical properties of carbon nanotube–polymer composites', *Carbon*, **2006;** 44(9), pp. 1624–1652. DOI: 10.1016/j.carbon.2006.02.038
160. Ajayan, P.M., Schadler, L.S. and Braun, P.V. Nanocomposite Science and Technology. Weinheim: Wiley-VCH, 2003. https://doi.org/10.1002/3527602127
161. Ramoso, J.P., Rasekh, M. and Balachandran, W. Graphene-based biosensors: Enabling the next generation of diagnostic technologies—A review. Biosensors, **2025;** 15(9), p.586. doi.org/10.3390/bios15090586
162. Priya, S. and Inman, D.J. Energy Harvesting Technologies. New York: Springer, 2009. https://doi.org/10.1007/978-0-387-76464-1.
163. Spitalsky, Z., Tasis, D., Papagelis, K. and Galiotis, C. 'Carbon nanotube–polymer composites: chemistry, processing, mechanical and electrical properties', *Progress in Polymer Science*, **2010,** 35(3), pp.357–401. https://doi.org/10.1016/j.progpolymsci.2009.09.003
164. Guimard, N.K., Gomez, N. and Schmidt, C.E. 'Conducting polymers in biomedical engineering', *Progress in Polymer Science*, **2007,** 32(8-9), pp. 876–921. https://doi.org/10.1016/j.progpolymsci.2007.05.012

 doi:10.20944/preprints202605.0674.v1

165. Gomes, M.E. and Reis, R.L. 'Biodegradable polymers and composites in biomedical applications: from catgut to tissue engineering. Part 1 Available systems and their properties', *International Materials Reviews*, **2004;** 49(5), pp. 261–273. https://doi.org/10.1179/095066004225021605
166. Velmurugan, C., Senthilkumar, V. and Dinesh, S. 'Shape memory alloys and polymers for MEMS/NEMS applications: review on recent findings and challenges in design, preparation, and characterization', *Metals*, **2021,** 11(3), p.415. https://doi.org/10.3390/met11030415
167. Stassi, S., Cauda, V., Canavese, G. and Pirri, C.F. 'Flexible tactile sensing based on piezoresistive composites: A review', *Sensors*, **2014;** 14(3), pp.5296–5332. https://doi.org/10.3390/s140305296
168. Kim, D.H., Lu, N., Ma, R., Kim, Y.S., Kim, R.H., Wang, S., Wu, J., Won, S.M., Tao, H., Islam, A. and Yu, K.J. Epidermal electronics. *Science*, **2011,** 333(6044), pp.838–843. https://doi.org/10.1126/science.1206157
169. Windmiller, J.R. and Wang, J. 'Wearable electrochemical sensors and biosensors: a review', Electroanalysis, **2013,** 25(1), pp.29–46. https://doi.org/10.1002/elan.201200349
170. Kazim, M., Pal, A. and Goswami, D., Mechanical metamaterials for bioengineering: in vitro, wearable, and implantable applications. *Advanced Engineering Materials*, **2025,** 27(7), p.2401806. DOI: 10.1002/adem.202401806
171. Jones, J.R. 'Review of bioactive glass: from Hench to hybrids', *Acta Biomaterialia*, **2013;** 9(1), pp. 4457–4486. https://doi.org/10.1016/j.actbio.2012.08.023
172. Rahimi-Lenji, A., Heidari-Rarani, M., Mirkhalaf, M. and Mirkhalaf, M., On the internal architecture of lightweight negative Poisson's ratio (auxetic) metastructures: a review. *Materials & Design*, **2025;** p.115225. doi.org/10.1016/j.matdes.2025.115225
173. Yang, L., Harrysson, O., West, H. and Cormier, D., Compressive properties of Ti–6Al–4V auxetic mesh structures made by electron beam melting. *Acta Materialia*, **2012;** 60(8), pp.3370-3379. doi.org/10.1016/j.actamat.2012.03.015
174. Evans, K.E. and Alderson, A. 'Auxetic materials: Functional materials and structures from lateral thinking!', *Advanced Materials*, **2000;** 12(9), pp. 617–628. https://doi.org/10.1002/(SICI)1521-4095(200003)12:9<617::AID-ADMA617>3.0.CO;2-3
175. Siepmann, J. and Peppas, N.A., Modeling of drug release from delivery systems based on hydroxypropyl methylcellulose (HPMC). *Advanced drug delivery reviews*, **2012;** 64, pp.163-174. https://doi.org/10.1016/j.addr.2012.09.028 (supplement volume)
176. Koushik, T.M., Miller, C.M. and Antunes, E. Bone tissue engineering scaffolds: function of multi-material hierarchically structured scaffolds. *Advanced healthcare materials*, **2023**; 12(9), p.2202766. https://doi.org/10.1002/adhm.202202766
177. Griffis, J.C., Shahed, K., Meinert, K., Yilmaz, B., Lear, M. and Manogharan, G., Multi-material laser powder bed fusion: effects of build orientation on defects, material structure and mechanical properties. npj *Advanced Manufacturing*, **2025;** 2(1), p.5. https://doi.org/10.1038/s44334-025-00020-5
178. Xie, Y., Hill, C.A., Xiao, Z., Militz, H. and Mai, C. 'Silane coupling agents used for natural fiber/polymer composites: A review', *Composites Part A: Applied Science and Manufacturing*, **2010;** 41(7), pp.806–819. DOI: 10.1016/j.compositesa.2010.03.005
179. Fischer, J P., Schleifenbaum, S., Gelberg, F., Barth, T., Wendler, T. and Löffler, S. 'Novel approach to assessing the primary stability of dental implants under functional cyclic loading in vitro: a biomechanical pilot study using synthetic bone', *Journal of Periodontal & Implant Science*, **2024;** 54(3), pp. 189–204. https://doi.org/10.5051/jpis.2301780089
180. Boccaccini, A.R. and Blaker, J.J. 'Bioactive composite materials for tissue engineering scaffolds', *Expert Review of Medical Devices*, **2005;** 2(3), pp. 303–317. https://doi.org/10.1586/17434440.2.3.303
181. KRC, S.R., R, S. and K, S.R. Ceramic–polymer hybrid coatings for diverse applications. *Frontiers in Coatings, Dyes and Interface Engineering*, **2024**, 2, p.1386920. https://doi.org/10.3389/frcdi.2024.1386920
182. Huff, M., Residual stresses in deposited thin-film material layers for micro-and nano-systems manufacturing. *Micromachines*, **2022;** 13(12), p.2084. https://doi.org/10.3390/mi13122084
183. Ratner, B.D., Hoffman, A.S., Schoen, F.J. and Lemons, J.E., Biomaterials science: an introduction to materials in medicine. San Diego, *California*, **2004;** 5, pp.162-4.

 doi:10.20944/preprints202605.0674.v1

184. Wulf, K., Goblet, M., Raggl, S., Teske, M., Eickner, T., Lenarz, T., Grabow, N. and Paasche, G. 'PLLA Coating of Active Implants for Dual Drug Release', *Molecules*, **2022;** 27(4), p.1417. https://doi.org/10.3390/molecules27041417
185. Jordan, J., Jacob, K.I., Tannenbaum, R., Sharaf, M.A. and Jasiuk, I. Experimental trends in polymer nanocomposites—a review. *Materials science and engineering: A*, **2005**, *393*(1-2), pp.1-11. https://doi.org/10.1016/j.msea.2004.09.044
186. Polo, S., García-Domínguez, A., Rubio, E.M. and Claver, J., Lattice structures in additive manufacturing for biomedical applications: A systematic review. *Polymers*, **2025,** 17(17), p.2285. https://doi.org/10.3390/polym17172285
187. Distefano, F., Pasta, S. and Epasto, G. Titanium lattice structures produced via additive manufacturing for a bone scaffold: a review. *Journal of Functional Biomaterials*, **2023**, *14*(3), p.125. https://doi.org/10.3390/jfb14030125
188. Toosi, S., Javid-Naderi, M.J., Tamayol, A., Ebrahimzadeh, M.H., Yaghoubian, S. and Mousavi Shaegh, S.A. Additively manufactured porous scaffolds by design for treatment of bone defects. *Frontiers in bioengineering and biotechnology*, **2024**, *11*, p.1252636. https://doi.org/10.3389/fbioe.2023.1252636
189. Park, J., Lee, H., Kim, S., Choi, Y., Jung, W., Han, D. and Lim, J. 'Fabrication of a lattice structure with periodic open pores through three-dimensional printing for bone ingrowth', *Scientific Reports*, **2022;** 12, p.17223. https://doi.org/10.1038/s41598-022-22292-z
190. Deb, K., Pratap, A., Agarwal, S. and Meyarivan, T. 'A fast and elitist multiobjective genetic algorithm: NSGA-II', IEEE Transactions on Evolutionary Computation, 2002; 6(2), pp. 182–197. https://doi.org/10.1109/4235.996017
191. Viceconti, M., Bellingeri, L., Cristofolini, L. and Toni, A. 'A comparative study on different methods of automatic mesh generation of human femurs', *Medical Engineering & Physics*, **1998;** 20(1), pp.1–10. https://doi.org/10.1016/s1350-4533(97)00049-0
192. Wagner, W.R., Sakiyama Elbert, S.E., Zhang, G. and Yaszemski, M.J. (eds.) Biomaterials Science: An Introduction to Materials in Medicine. 4th edn. Cambridge, MA: Academic Press, 2020.
193. Pruitt, L. and Chakravartula, A.M. Mechanics of Biomaterials: Fundamental Principles for Implant Design. Cambridge: Cambridge University Press, 2011.
194. Manz, S., Valette, R., Damonte, F., Gaudio, L.A., Gonzalez Vargas, J., Sartori, M., Dosen, S. and Rietman, J. 'A review of user needs to drive the development of lower limb prostheses', *Journal of NeuroEngineering and Rehabilitation*, **2022;** 19, article 119. https://doi.org/10.1186/s12984-022-01097-1
195. Capsi-Morales, P., Piazza, C., Sjoberg, L., Catalano, M.G., Grioli, G., Bicchi, A. and Hermansson, L.M., Functional assessment of current upper limb prostheses: An integrated clinical and technological perspective. *Plos one*, **2023;** 18(8), p.e0289978. https://doi.org/10.1371/journal.pone.0289978
196. Baldock, M., Pickard, N., Prince, M., Kirkwood, S., Chadwell, A., Howard, D., Dickinson, A., Kenney, L., Gill, N. and Curtin, S. 'Adjustable prosthetic sockets: a systematic review of industrial and research design characteristics and their justifications', Journal of NeuroEngineering and Rehabilitation, 2023, 20, article 147. https://doi.org/10.1186/s12984-023-01270-0
197. Chadwell, A., Diment, L., Micó-Amigo, M., Morgado Ramírez, D.Z., Dickinson, A., Granat, M., Kenney, L., Kheng, S., Sobuh, M., Ssekitoleko, R. and Worsley, P., Technology for monitoring everyday prosthesis use: a systematic review. *Journal of neuroengineering and rehabilitation*, **2020;** 17(1), p.93. https://doi.org/10.1186/s12984-020-00711-4
198. Li, S., Man, Z., Zuo, K., Zhang, L., Zhang, T., Xiao, G., Lu, Y., Li, W. and Li, N. Advancement in smart bone implants: the latest multifunctional strategies and synergistic mechanisms for tissue repair and regeneration. *Bioactive Materials*, **2025**; *51*, pp.333-382. https://doi.org/10.1016/j.bioactmat.2025.05.004
199. Cong, B. and Zhang, H., Innovative 3D printing technologies and advanced materials revolutionizing orthopedic surgery: current applications and future directions. *Frontiers in Bioengineering and Biotechnology*, **2025**; *13*, p.1542179. https://doi.org/10.3389/fbioe.2025.1542179
200. Kontakis, M.G., Carlsson, E., Palo-Nieto, C. and Hailer, N.P., Ionic silver coating of orthopedic implants may impair osteogenic differentiation and mineralization. *Experimental and Therapeutic Medicine*, **2025;** 29(3), p.51. https://doi.org/10.3892/etm.2025.12801

 doi:10.20944/preprints202605.0674.v1

201. Spoelstra, G.B., Elsinga, P.H., van Dijl, J.M., van Snick, J.H., Feringa, B.L., Glaudemans, A.W.J.M., Keizers, B., Kruijff, S., Szymanski, W., van Oosten, M. and IJpma, F.F.A. Vancomycin-based tracers guiding in situ visualization of bacteria on osteosynthesis devices and surgical debridement. *European Journal of Nuclear Medicine and Molecular Imaging*, **2025;** 52, pp.3877–3890. https://doi.org/10.1007/s00259-025-07249-4
202. Fang, J., Han, Y., Wang, L., Ai, J.L., Zhai, J.X., Ge, Z.G., Wang, Z.G. and Ning, C.Y. The development of electroactive materials for metal implant surface antimicrobial treatment and antibacterial adhesion: J. Fang et al. *Rare Metals*, **2025**; *44*(10), pp.6986-7010. doi.org/10.1007/s12598-025-03406-8
203. Anastasio, A.T., Paniagua, A., Diamond, C., Ferlauto, H.R. and Fernandez-Moure, J.S., Nanomaterial nitric oxide delivery in traumatic orthopedic regenerative medicine. *Frontiers in bioengineering and biotechnology*, **2021;** 8, p.592008. https://doi.org/10.3389/fbioe.2020.592008
204. Donyaparastlivari, L. and Ibrahim, A., 2025. A smart hip implant with embedded multidirectional sensing and wireless load monitoring for enhanced orthopedic care. *Biosensors and Bioelectronics: X*, *26*, p.100648. doi.org/10.1016/j.biosx.2025.100648
205. Giardini, M., Arcolin, I., Arcobelli, V.A., Picardi, M., Mellone, S. and Godi, M., Reliability and Discriminant Ability of an Instrumented Timed Up and Go Test in People With Postsurgical Orthopedic Conditions: Quantitative Study. *JMIR Rehabilitation and Assistive Technologies*, **2026;** *13*, p.e82632. DOI: 10.2196/82632
206. Fiore, L., Mazzaracchio, V., Gosti, C., Duranti, L., Vitiello, R., Maccauro, G. and Arduini, F. Functionalized orthopaedic implant as pH electrochemical sensing tool for smart diagnosis of hardware infection. Analyst, **2024;** 149, pp.3085–3096. https://doi.org/10.1039/D4AN00253A
207. Klevens, R.M., Morrison, M.A., Nadle, J., Petit, S., Gershman, K., Ray, S., Harrison, L.H., Lynfield, R., Dumyati, G., Townes, J.M. and Craig, A.S. Invasive methicillin-resistant Staphylococcus aureus infections in the United States. *Jama*, *298*(15), **2007**; pp.1763-1771. https://doi.org/10.1001/jama.298.15.1763
208. Cheng, J., Xue, N., Zhou, W., Qin, B., Qiu, B., Fang, G. and Sun, X. Recent Progress in Flexible Wearable Sensors for Real-Time Health Monitoring: Materials, Devices, and System Integration. *Micromachines*, **2025**; *16*(10), p.1124. doi.org/10.3390/mi16101124
209. Schumacher, N., Geiger, F., Spors, S., Bader, R., Haubelt, C. and Kluess, D. 'Detection of total hip replacement loosening based on structure-borne sound: influence of the position of the sensor on the hip stem', *Sensors*, **2024,** 24(14), p.4594. doi.org/10.3390/s24144594
210. Seibold, M., Sigrist, B., Götschi, T., Müller, R., Weber, M., Huber, M. and Langer, M. 'A new sensing paradigm for the vibroacoustic detection of pedicle screw loosening', *Medical & Biological Engineering & Computing*, **2025;** 63, pp.1001–1011. https://doi.org/10.1007/s11517-024-03235-4
211. Jahadakbar, A., Nematollahi, M., Safaei, K., Bayati, P., Giri, G., Dabbaghi, H., Dean, D. & Elahinia, M., Design, modeling, additive manufacturing, and polishing of stiffness-modulated porous Nitinol bone fixation plates. *Metals*, **2020;** 10(1), p.151. https://doi.org/10.3390/met10010151
212. Najafzadeh, A., Gunawardena, D.S., Liu, Z., Tran, T., Tam, H.Y., Fu, J. & Chen, B.K., Application of Fibre Bragg Grating sensors in strain monitoring and fracture recovery of human femur bone. *Bioengineering*, **2020**; 7(3), Article 98. https://doi.org/10.3390/bioengineering7030098
213. Krämer, M., Pfeifer, R., Müller, C.W., Wesling, V. & Hurschler, C., Stiffness properties of a shape-changing implant for fracture fixation: a preliminary study. *Biomedizinische Technik/Biomedical Engineering*, **2013;** 58(Suppl. 1). https://doi.org/10.1515/bmt-2013-4078
214. Kirmanidou, Y., Chatzinikolaidou, M., Michalakis, K. and Tsouknidas, A. Clinical translation of polycaprolactone-based tissue engineering scaffolds, fabricated via additive manufacturing: A review of their craniofacial applications. *Biomaterials Advances*, **2024;** 162, p.213902. https://doi.org/10.1016/j.bioadv.2024.213902
215. Khorasani, E. and Vahidi, B., 3D-Printed Scaffolds for Cranial Bone Regeneration: A Systematic Review of Design, Materials, and Computational Optimization. Biotechnology and Bioengineering, 2025. https://doi.org/10.1002/bit.28994
216. Jiamin, Jiaying, Chen, T., Luo, L. and Wenhua. Engineering Smart 3D-Printed Antibacterial Bone Scaffolds: Stimuli-Responsive Release and Personalized Therapy for Infected Bone Defects. *Journal of Biomedical Materials Research Part B: Applied Biomaterials*, **2026;** *114*(4), p.e70057. https://doi.org/10.1002/jbm.b.70057

 doi:10.20944/preprints202605.0674.v1

217. Taori, T., Borle, A., Maheshwari, S. and Reche, A., An insight into the biomaterials used in craniofacial tissue engineering inclusive of regenerative dentistry. *AIMS Bioengineering*, **2023,** 10(2). https://doi.org/10.3934/bioeng.2023011
218. Abhinav Rohan, K., Sindhwani, N.A., Nikitha, R., Kondayya, D. and John Rozario Jegaraj, J. 'Development of IoT Enabled 3D Printed Smart Prosthetic Leg', in Advances in Forming, Machining and Automation: Select Proceedings of AIMTDR 2021. Singapore: *Springer Nature Singapore*, **2022;** pp. 501–513. https://doi.org/10.1007/978-981-19-3866-5_41
219. Luo, J., Lu, W., Jiao, P., Jang, D., Barri, K., Wang, J., Meng, W., Kumar, R.P., Agarwal, N., Hamilton, D.K. and Wang, Z.L., Wireless electronic-free mechanical metamaterial implants. *Materials Today*, **2025;** 83, pp.145-156. https://doi.org/10.1016/j.mattod.2024.12.018
220. Parashar, B., Malviya, R., Sridhar, S.B., Wadhwa, T. and Shareef, J., 2025. IoT-enabled medical advances shaping the future of orthopaedic surgery and rehabilitation. *Journal of Clinical Orthopaedics and Trauma*, *68*, p.103113. https://doi.org/10.1016/j.jcot.2025.103113
221. Huang, J., Li, Q., Ding, X. and Dong, Y. 'Sensor-enabled orthopedic implants for musculoskeletal monitoring', *Advanced Sensor Research*, **2025;** 4(2), article 2400138. https://doi.org/10.1002/adsr.202400138